A 56-year-old woman with no significant past medical history presented to the emergency department with worsening shortness of breath over 8 months. She had no prior history of tobacco use. Physical examination was notable for bronchial breath sounds in both lungs with oxygen saturation of 93% on 3 liters of supplemental oxygen. A computed tomographic angiogram noted innumerable pulmonary nodules in a diffuse pattern. What is the most likely diagnosis for this presentation?

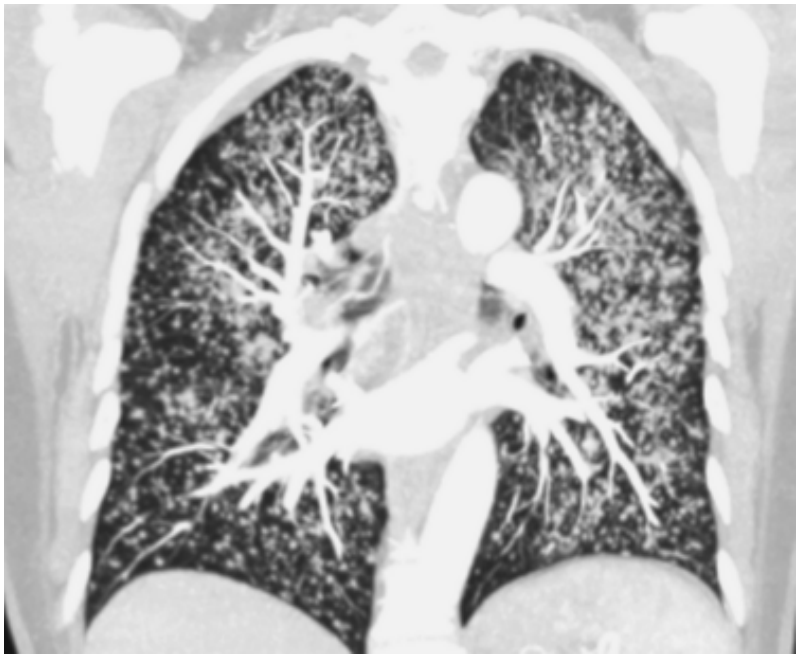

Non-small cell lung cancer

Sarcoidosis

Langerhans cell histiocytosis

Histoplasmosis

Septic embolization

The correct answer is non–small-cell lung cancer. This patient had hepatic lesions on subsequent imaging, and core biopsy confirmed primary lung adenocarcinoma. Next-generation sequencing revealed EGFR mutation. Miliary metastases have been reported in cases of non–small-cell lung cancer with EGFR mutations. The patient was started on treatment with erlotinib with partial response after 1 year.

Miliary metastases are associated with epidermal growth factor receptor mutations in non-small cell lung cancer: a population-based study

Miliary metastases are characterized by metastatic nodules that are diffuse, innumerable and small. The purpose of this study was to examine the incidence, prognostic significance and impact of epidermal growth factor receptor (EGFR) mutations for miliary metastases from non-small cell lung cancer (NSCLC).

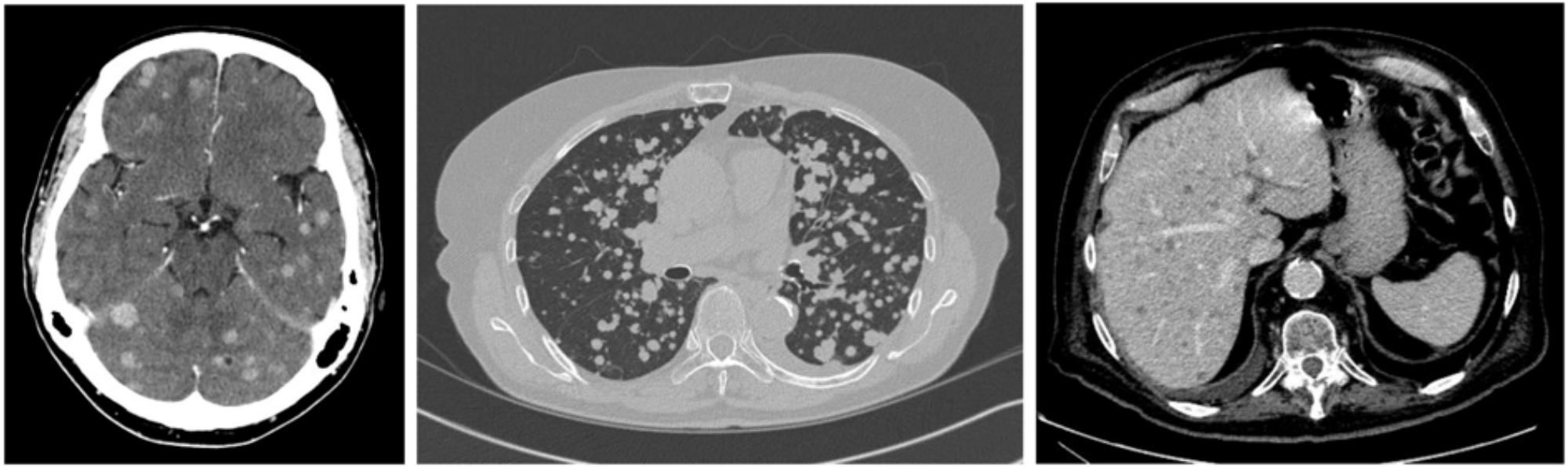

For 543 patients, the total number of brain, lung and liver metastases were 165 (30.4%), 290 (53.4%) and 67 (12.3%), respectively. The EGFR mutation positive (EGFR+) subgroup had a significantly higher 3-year cumulative incidence of miliary brain (4.1 vs. 0.5%, $p = .015$) and miliary lung (11.6 vs. 3.3%, $p < .001$) metastases compared to EGFR wild type (WT). A greater proportion of metastases from EGFR + cancers were miliary for brain (8.5 vs. 1.7%, $p = .035$) and lung (18.9 vs. 6.9%, $p = .003$) sites. Only non-miliary brain (HR = 1.45) and liver (HR = 1.70) metastases predicted for poor overall survival.

Mutations in EGFR were associated with a higher rate of miliary brain and lung metastases. The presence of miliary metastases did not predict for poor overall survival.

Sarcoidosis

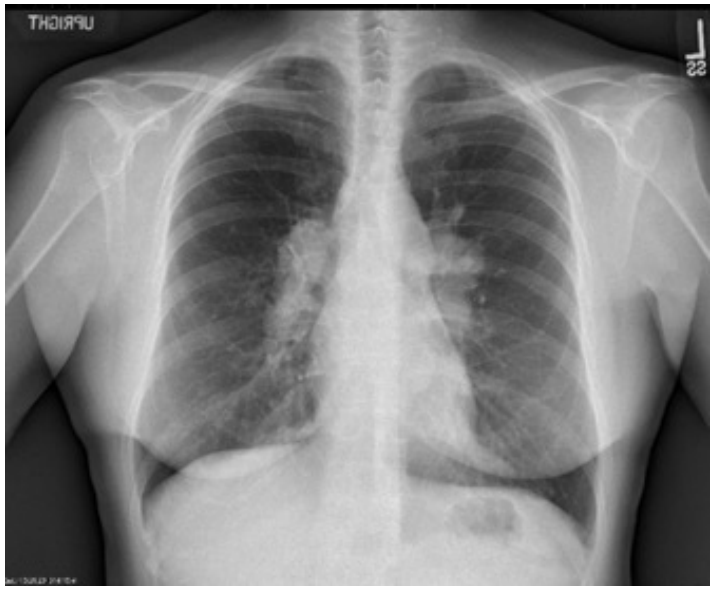

Langerhans cell histiocytosis was previously known as histiocytosis X. Essentially any part of the body can be affected and as such clinical presentation will depend on specific involvement. The course of the disease ranges from those that spontaneously regress to those that have a rapidly progressive course (the latter is especially common in young children with multi-system disease).
A more useful and less controversial classification, which roughly correlates to the eponymous diseases above, is as follows:
multiple organ systems, multiple sites involved
single-organ system, multiple sites involved
single lesion.

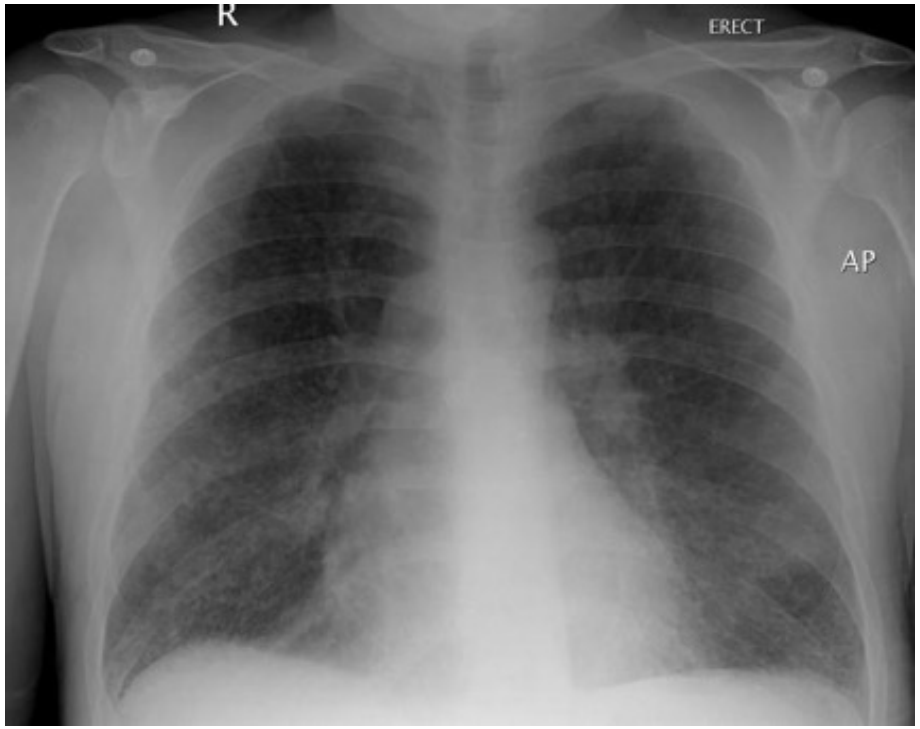

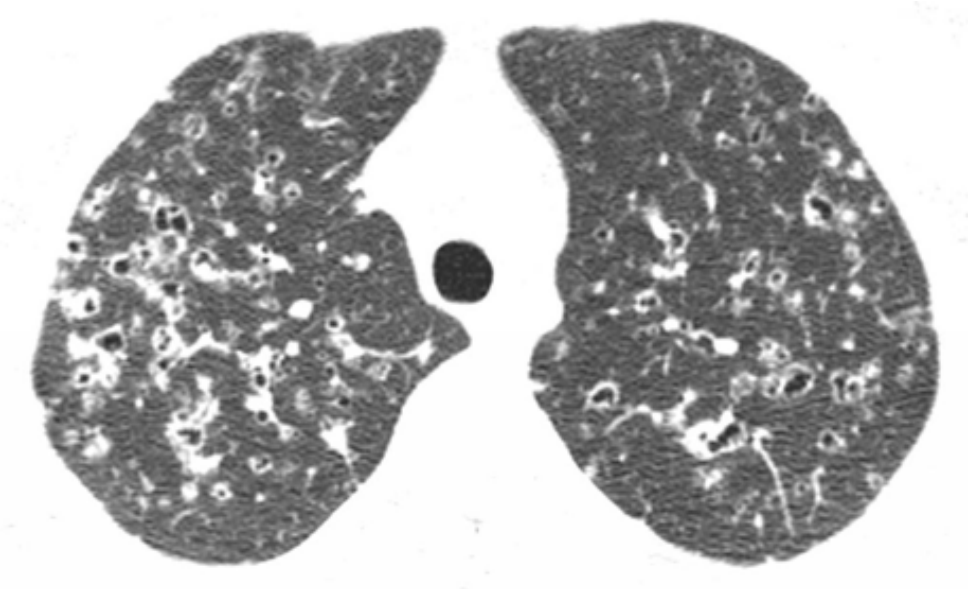

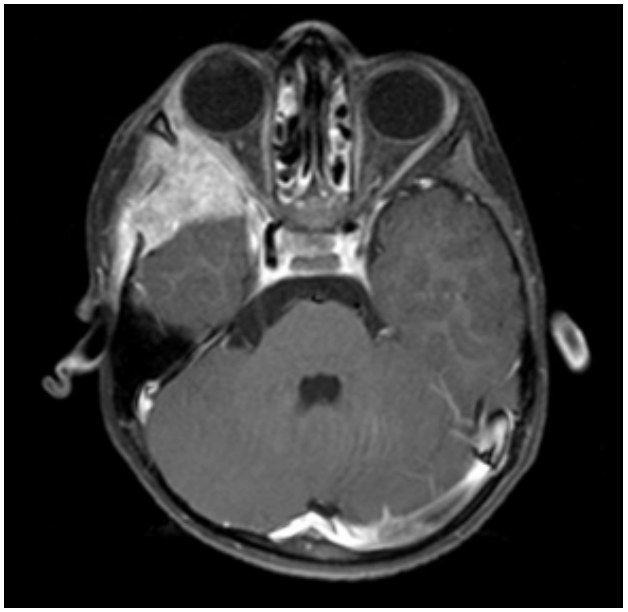

Histoplasmosis

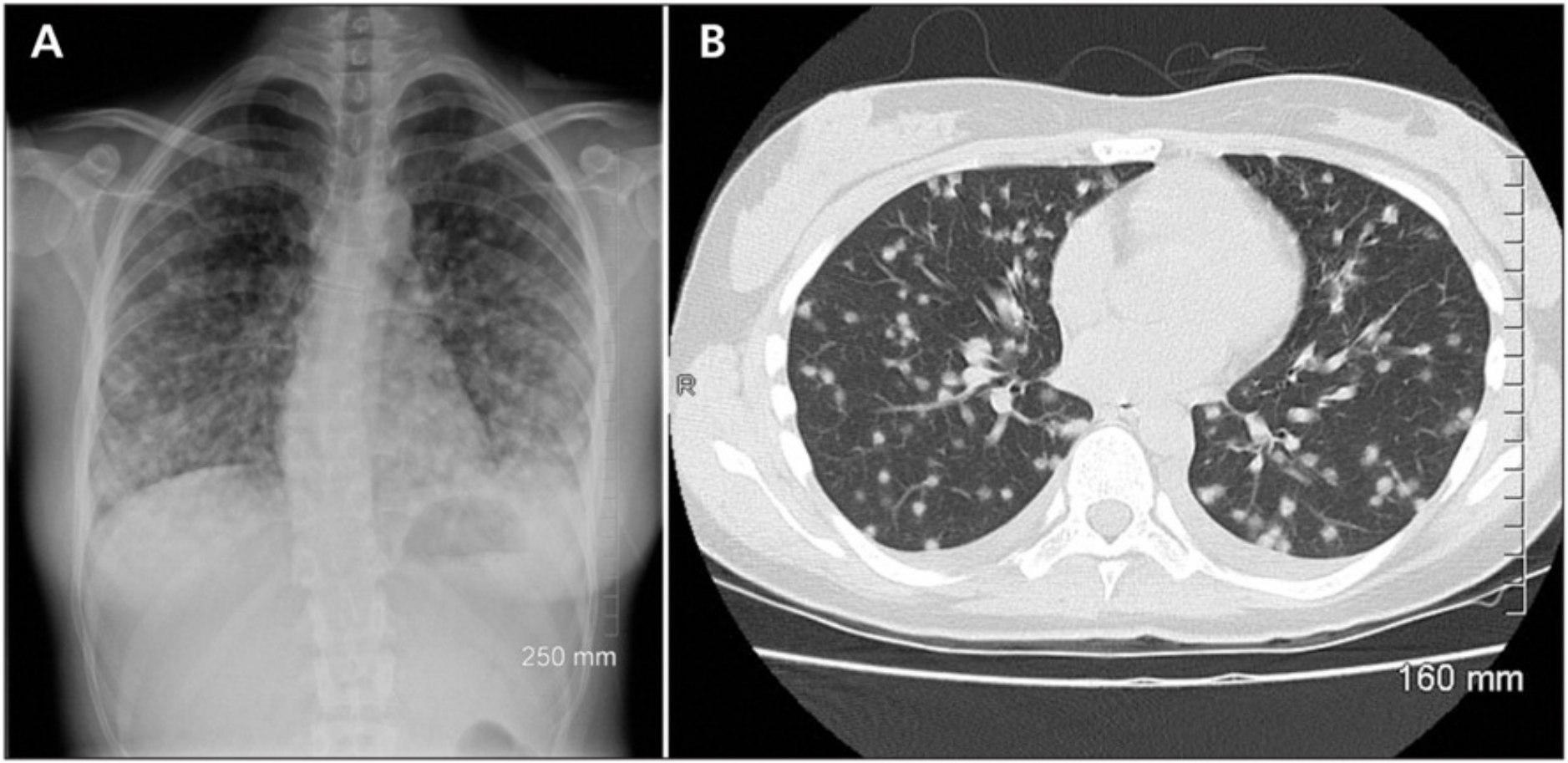

Septic emboli

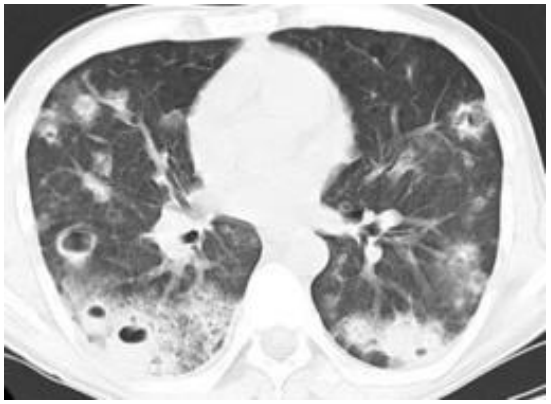

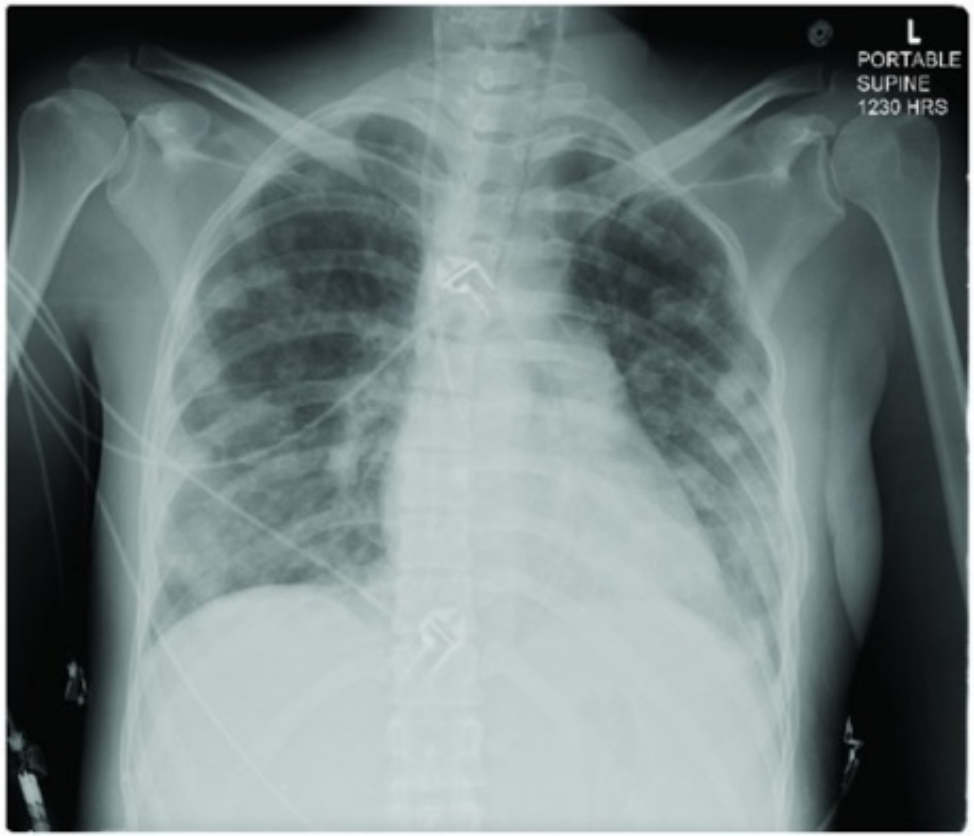

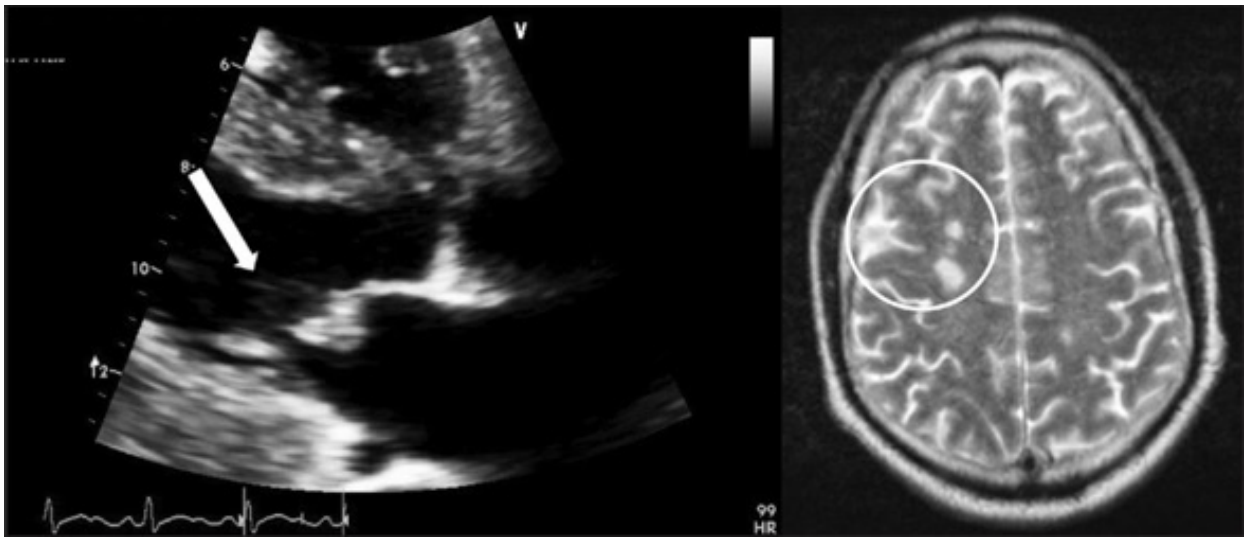

Elephantiasis in etwa „die Elefantenartigkeit“, von ὁ ἐλέφας, „der Elefant“; auch Elefantenmann-Syndrom) ist eine abnorme Vergrößerung eines Körperteils durch einen Lymphstau (Lymphödem). Meist sind die Beine oder die äußeren Geschlechtsteile betroffen.[1] Diese Krankheit ist vor allem in Entwicklungsländern verbreitet. Man unterscheidet erworbene von angeborenen Formen. Die Krankheit tritt als Elephantiasis tropica vorwiegend in tropischen Regionen auf und wird hier als Spätfolge verschiedener Infektionen, unter anderem durch Fadenwürmer wie Brugia malayi (auch Wuchereria malayi oder Filaria malayi genannt) oder Wuchereria bancrofti, aber auch durch Lepra, ausgelöst. Die Würmer gelangen durch den Stich einer Stechmücke in das lymphatische System und verursachen dort eine chronische Entzündungsreaktion mit Lymphstau, wodurch es mit der Zeit zu einer extremen Vergrößerung und Verhärtung der Haut kommt. Als Prophylaxe wird Schutz vor Moskitos durch Repellentien oder Moskitonetze empfohlen.

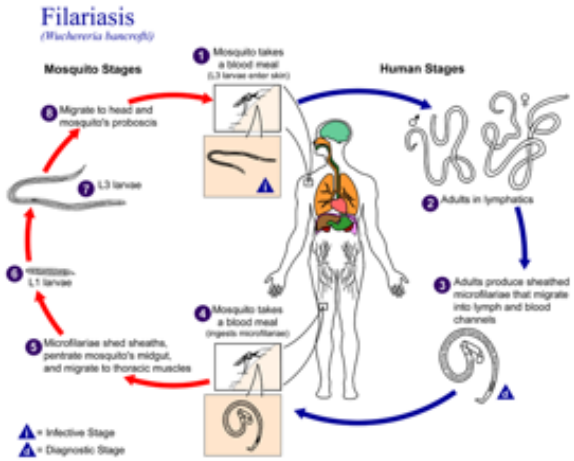

A Trial of a Triple-Drug Treatment for Lymphatic Filariasis

Lymphatic filariasis caused by mosquito-borne nematode parasites is usually characterized by lymphedema of the arms and legs ("elephantiasis"), hydrocele, and long-term disability. The life cycle of the parasite requires the uptake of microfilariae by mosquitoes during a blood meal and further development of the microfilariae into infective larvae, which are transmitted by the mosquitoes to initiate new infections in humans.

The World Health Organization has targeted lymphatic filariasis for global elimination by 2020 with a strategy of mass drug administration. This trial tested whether a single dose of a three-drug regimen of ivermectin plus diethylcarbamazine plus albendazole results in a greater sustained clearance of microfilariae than a single dose of a two-drug regimen of diethylcarbamazine plus albendazole and is noninferior to the two-drug regimen administered once a year for 3 years. In a randomized, controlled trial involving adults from Papua New Guinea with *Wuchereria bancrofti* microfilaremia, we assigned 182 participants to receive a single dose of the three-drug regimen (60 participants), a single dose of the two-drug regimen (61 participants), or the two-drug regimen once a year for 3 years (61 participants). Clearance of microfilariae from the blood was measured at 12, 24, and 36 months after trial initiation.

Characteristic	Three-Drug Regimen Administered Once (N=60)	Two-Drug Regimen Administered Once (N=61)	Two-Drug Regimen Administered Once a Year for 3 Yr (N=61)
Age — yr			
Median	40	34	37
Range	19–60	18–62	18–61
Sex — no.			
Male	28	34	30
Female	32	27	31
Hemoglobin — g/dl	11.4±1.8	11.2±1.8	11.2±1.7
Weight — kg	50±6	51±5	52±7
Geometric mean microfilarial count — microfilariae/ml	699	744	596
Range	55–15,621	52–8290	61–9656
Filarial antigen test-strip score†	2.8±0.4	2.8±0.5	2.7±0.5

Table 2. Clearance of Microfilaremia after Treatment for Lymphatic Filariasis.*

Treatment Group and Outcome	Months after Initial Treatment		
	12	24	36
Three-Drug Regimen Administered Once			
Participants — no.	57	54	57
Participants with complete clearance of microfilariae			
No.	55	52	55
% (95% CI)	96 (87–100)	96 (87–100)	96 (88–100)
Two-Drug Regimen Administered Once			
Participants — no.	56	55	52
Participants with complete clearance of microfilariae			
No.	18	31	43
% (95% CI)	32 (20–46)	56 (42–70)	83 (70–92)
P value†	<0.001	<0.001	0.02
Relative risk of incomplete clearance (95% CI)‡	0.05 (0.01–0.20)	0.08 (0.02–0.34)	0.20 (0.05–0.90)
P value	<0.001	<0.001	0.04
Two-Drug Regimen Administered Once a Year for 3 Yr			
Participants — no.	59	56	52
Participants with complete clearance of microfilariae			
No.	20	42	51
% (95% CI)	34 (22–47)	75 (62–86)	98 (90–100)
P value§	<0.001	0.002	>0.99
Relative risk of incomplete clearance (95% CI)¶	0.05 (0.01–0.20)	0.15 (0.04–0.62)	1.80 (0.17–18.90)
P value	<0.001	0.009	0.87

* The 95% confidence intervals (CIs) were calculated with the use of the binomial exact method.
† P values are for comparisons between the group that received the three-drug regimen and the group that received a single dose of the two-drug regimen, as assessed by chi-square analysis.
‡ Relative risks are shown for the group that received the three-drug regimen, as compared with the group that received a single dose of the two-drug regimen.
§ P values are for comparisons between the group that received the three-drug regimen and the group that received the two-drug regimen once a year for 3 years, as assessed by chi-square analysis.
¶ Relative risks are shown for the group that received the three-drug regimen, as compared with the group that received the two-drug regimen once a year for 3 years.

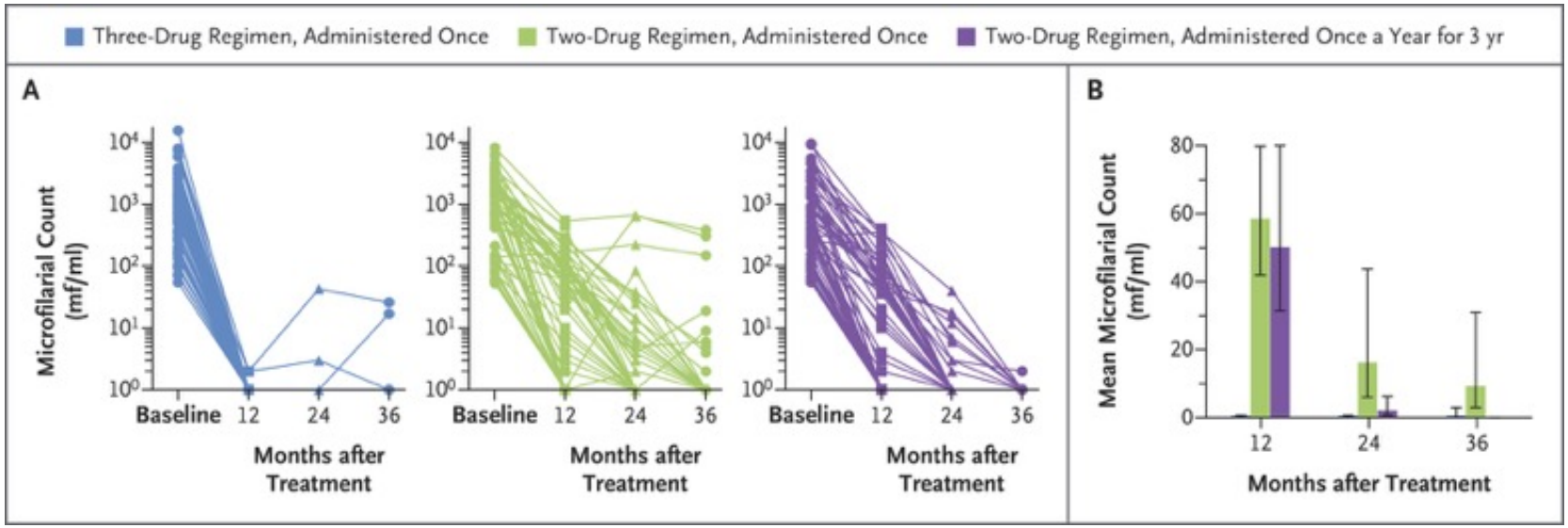

Changes in Microfilarial Counts in the Three Treatment Groups. Panel A shows the reductions in microfilarial counts (plotted on a logarithmic scale) at 12, 24, and 36 months after trial initiation. Panel B shows the model-adjusted mean microfilarial counts in each treatment group at 12, 24, and 36 months after trial initiation. The three-drug regimen was more effective in reducing microfilarial counts at 12, 24, and 36 months after trial initiation than the two-drug regimen administered once ($P<0.001$, $P<0.001$, and $P=0.007$, respectively). A negative binomial generalized estimating equation model that was adjusted for baseline microfilarial counts was used.

All participants were observed for adverse events for 10 hours after the initial treatment. A total of 73% of participants were assessed for adverse events 24 to 36 hours after returning to their villages. Adverse events occurred in five participants during the initial 10-hour observation period; three events were mild (headache, nausea, and fatigue in one participant each), one was moderate (temperature of 38.1° C and fatigue in one participant), and one was severe (described below). Other adverse events occurred later. The severe adverse event (grade 3) occurred in a 42-year-old woman who had a baseline microfilarial count of 792 mf per milliliter. She had headache, nausea, and chills starting 6 hours after the administration of the three-drug regimen. Physical examination revealed an auricular temperature of 41.1° C, orthostatic hypotension, and tachycardia. Her condition improved after she received oral treatment with fluids and acetaminophen, and she returned to her pretreatment state of health the next day.

Table 3. Adverse Events after Initial Treatment for Lymphatic Filariasis.

Variable	Three-Drug Regimen (N=41)	Two-Drug Regimen* (N=91)
	no. of participants with event (%)	
At least 1 adverse event	24 (59)	37 (41)
At least 2 adverse events	19 (46)†	24 (26)
Severe or serious adverse event	1 (2)	0
Fever‡	14 (34)	19 (21)
Hemodynamic changes§	5 (12)	4 (4)
Patient-reported grade 1 adverse event	22 (54)	36 (40)
Grade 2 or 3 adverse events¶	11 (27)‖	5 (5)
Fatigue	8 (20)	5 (5)
Headache	7 (17)	3 (3)
Nausea or vomiting or both	4 (10)	2 (2)
Itch or rash or both	2 (5)	0
Myalgia	5 (12)	3 (3)
Eye swelling	1 (2)	0
Scrotal pain or swelling or both	4 (10)	2 (2)
Dyspnea	2 (5)	0

* Data from the two groups that received the two-drug regimen (administered either once or once a year for 3 years) were combined.
† $P<0.05$ for the comparison between groups, as calculated with the use of the chi-square test.
‡ Fever was defined as an auricular body temperature of at least 37.5°C. The highest temperature recorded after the initial treatment was 41.1°C.
§ Hemodynamic change was defined as a change in systolic blood pressure of 30 mm Hg or a change in diastolic blood pressure of 20 mm Hg from the baseline measurement. Reduced blood pressure occurred in three of the five participants with hemodynamic change in the group that received the three-drug regimen and in all four participants with hemodynamic change in the combined two-drug–regimen groups.
¶ With the exception of one participant, all the participants who had a grade 2 or 3 adverse event had more than one adverse event.
‖ $P<0.001$ for the comparison between groups, as calculated with the use of the chi-square test.

Discussion

These results show that a single dose of a three-drug regimen of ivermectin plus diethylcarbamazine plus albendazole was more effective in clearing *W. bancrofti* microfilariae from the blood than a single dose of a two-drug regimen of diethylcarbamazine plus albendazole, which is the standard regimen used for mass drug administration for the elimination of lymphatic filariasis outside sub-Saharan Africa. The participants in this trial had not received previous treatment for lymphatic filariasis, and all had moderate to high microfilarial counts and filarial antigen levels at baseline. Clearance of microfilaremia was observed in almost all participants who received the three-drug regimen, and this effect persisted for at least 36 months. With respect to microfilarial clearance at 36 months, the three-drug regimen was superior to a single dose of the two-drug regimen and was noninferior to the two-drug regimen administered once a year for 3 years. The results observed after treatment with the two-drug regimen at 12 and 24 months were consistent with those reported in previous trials. Although microfilarial clearance did not occur in every participant who received the three-drug regimen, the residual microfilarial counts in the few outliers were reduced to levels that were unlikely to support mosquito-borne transmission. Thus, the triple-drug treatment has the potential to contribute to the elimination of lymphatic filariasis.

Elotuzumab ist ein immunstimulierender und indirekt zelltoxischer Wirkstoff aus der Gruppe der monoklonalen Antikörper, der in Kombination mit Lenalidomid und Dexamethason zur Behandlung des multiplen Myeloms eingesetzt wird. Der Antikörper aktiviert die natürlichen Killerzellen und bringt Killer- und Myelomzellen zusammen. Die Effekte beruhen auf der Bindung an das Protein SLAMF7 auf den Myelom- und den Killerzellen sowie an den Fc-Rezeptor auf den Killerzellen (dualer Wirkmechanismus). Es handelt sich um eine Krebsimmuntherapie. Das Arzneimittel wird als intravenöse Infusion verabreicht. Die häufigste mögliche unerwünschte Wirkung ist die Lymphopenie.

The surface antigen CD319 (SLAMF7) is a robust marker of normal plasma cells and malignant plasma cells in multiple myeloma. In contrast to CD138 (the traditional plasma cell marker), CD319/SLAMF7 is much more stable and allows robust isolation of malignant plasma cells from delayed or even cryopreserved samples. Elotuzumab is an antibody that targets this protein.

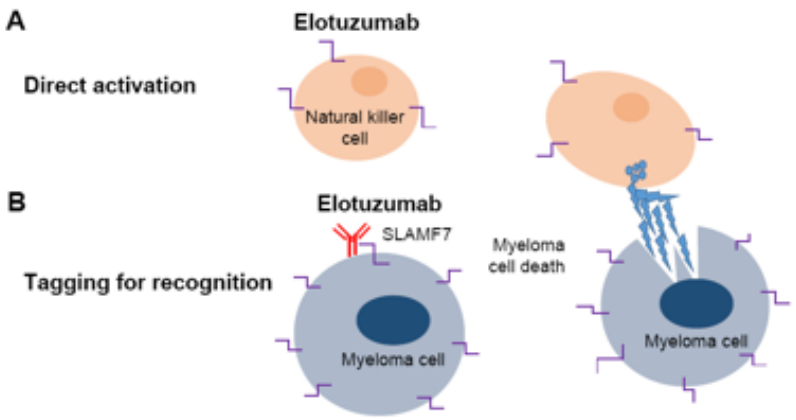

Figure 1 Elotuzumab: proposed mechanism of action in myeloma.
Notes: (**A**) Direct natural killer (NK) cell activation by elotuzumab. (**B**) Antibody-dependent NK cell-mediated cytotoxicity.
Abbreviation: SLAMF7, signaling lymphocytic activation molecule family member 7.

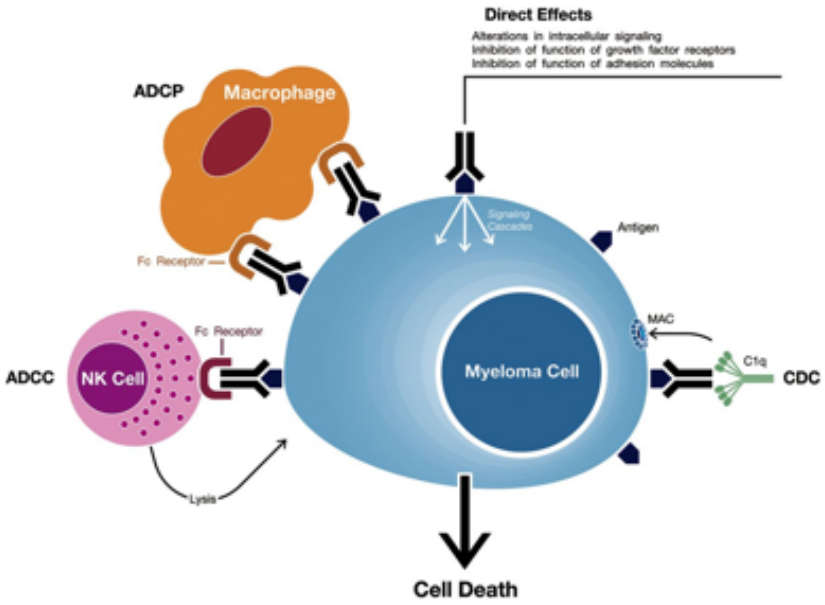

Elotuzumab plus Pomalidomide and Dexamethasone for Multiple Myeloma

Despite the widespread use of immunomodulatory agents and proteasome inhibitors, relapsed or refractory multiple myeloma is common, in part because of clonal heterogeneity and genomic complexity. The prognosis is poor once the disease becomes refractory to proteasome inhibitors and immunomodulatory drugs; indeed, a median overall survival of 9 months was reported after treatment failure with bortezomib and lenalidomide or thalidomide.

The immunostimulatory monoclonal antibody elotuzumab plus lenalidomide and dexamethasone has been shown to be effective in patients with relapsed or refractory multiple myeloma. The immunomodulatory agent pomalidomide plus dexamethasone has been shown to be effective in patients with multiple myeloma that is refractory to lenalidomide and a proteasome inhibitor. Patients with multiple myeloma that was refractory or relapsed and refractory to lenalidomide and a proteasome inhibitor were randomly assigned to receive elotuzumab plus pomalidomide and dexamethasone (elotuzumab group) or pomalidomide and dexamethasone alone (control group). The primary end point was investigator-assessed progression-free survival.

Characteristic	Elotuzumab Group (N=60)	Control Group (N=57)
Median age (range) — yr	69 (43–81)	66 (36–81)
Age category — no. (%)		
<65 yr	22 (37)	22 (39)
≥65 yr	38 (63)	35 (61)
<75 yr	47 (78)	45 (79)
≥75 yr	13 (22)	12 (21)
Male sex — no. (%)	32 (53)	35 (61)
International Staging System stage — no. (%)†		
I or II	53 (88)	50 (88)
III	7 (12)	7 (12)
Serum lactate dehydrogenase level — no. (%)		
<300 U/liter	43 (72)	41 (72)
≥300 U/ liter	14 (23)	15 (26)
Data not available	3 (5)	1 (2)
Cytogenetic abnormalities — no. (%)‡		
Del17p, t(4;14), or t(14;16)		
Yes	13 (22)	14 (25)
No	31 (52)	27 (47)
Data not available	16 (27)	16 (28)
1q21		
Yes	25 (42)	27 (47)
No	20 (33)	13 (23)
Data not available	15 (25)	17 (30)
Median no. of previous lines of therapy (range)	3 (2–8)	3 (2–8)
Number of previous lines of therapy — no. (%)		
2 or 3	36 (60)	36 (63)
≥4	24 (40)	21 (37)
Previous stem-cell transplantation — no. (%)	31 (52)	33 (58)
Previous therapies — no. (%)§		
Bortezomib	60 (100)	57 (100)
Lenalidomide	59 (98)	57 (100)
Melphalan	38 (63)	36 (63)
Thalidomide	25 (42)	19 (33)
Doxorubicin	18 (30)	15 (26)
Carfilzomib	9 (15)	16 (28)
Ixazomib	5 (8)	2 (4)
Daratumumab	1 (2)	2 (4)

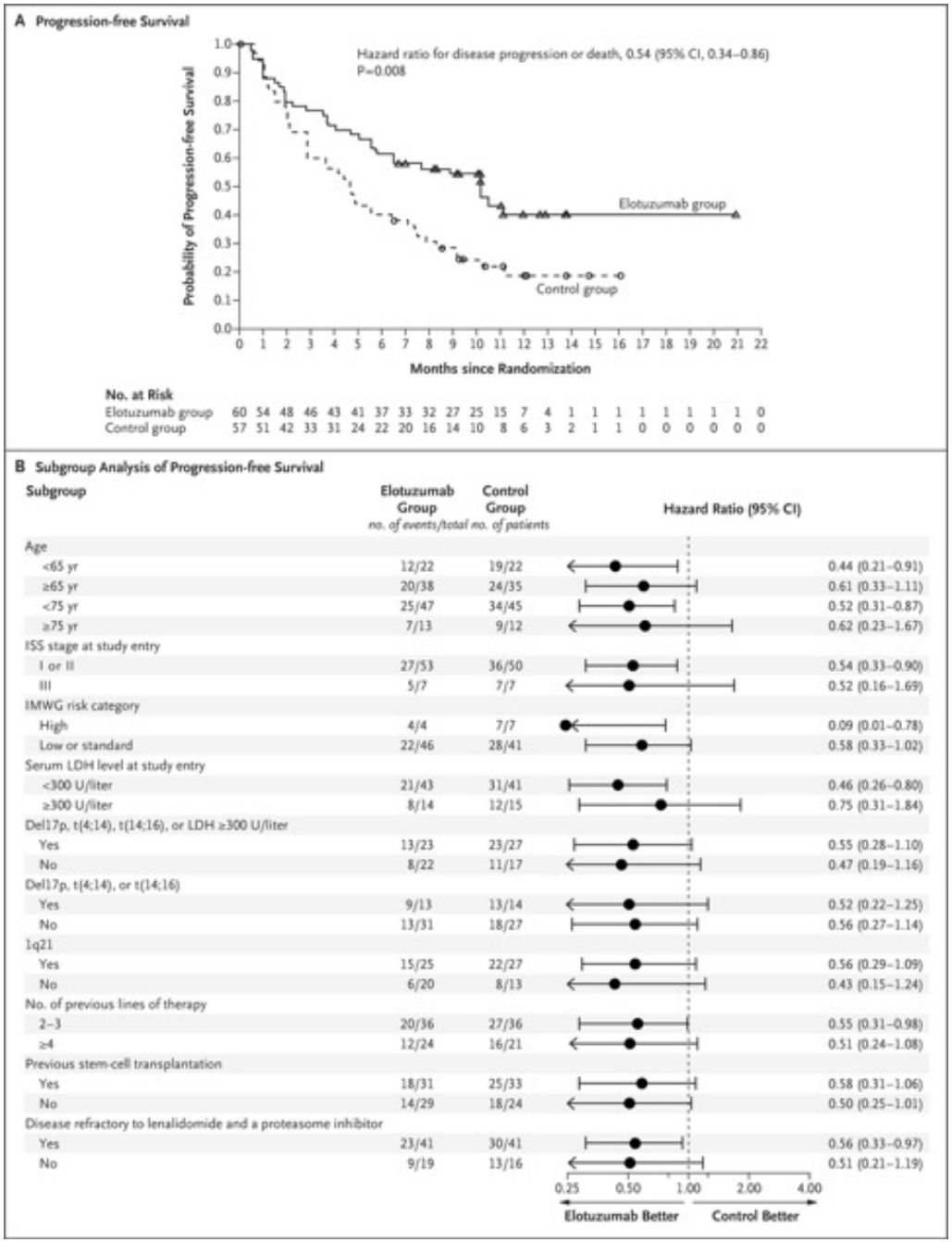

Progression-free Survival. Shown are the results of the Kaplan–Meier analysis of the primary end point, progression-free survival, in all patients who underwent randomization (Panel A) and the results of an analysis of progression-free survival in subgroups defined according to baseline characteristics (Panel B). The triangles and circles in Panel A represent censored data. The International Staging System (ISS) consists of three stages, with higher stages indicating more severe disease: stage I, serum β_2-microglobulin level lower than 3.5 mg per liter (300 nmol per liter) and albumin level 3.5 g per deciliter or higher; stage II, neither stage I nor III; and stage III, serum β_2-microglobulin 5.5 mg per liter or higher (470 nmol per liter). Risk categories were based on International Myeloma Working Group (IMWG) risk stratification. High risk was defined as ISS stage II or III and t(4;14) translocation or chromosome 17p deletion (del17p) abnormality. Low risk was defined as ISS stage I or II and absence of t(4;14) translocation, del17p, and 1q21 abnormalities, and an age younger than 55 years. Standard risk was defined as not meeting the criteria for high risk or low risk. LDH denotes lactate dehydrogenase.

Table 2. Investigator-Assessed Treatment Response.*

Response Category	Elotuzumab Group (N=60)	Control Group (N=57)
Overall response — no. (% [95% CI])	32 (53 [40–66])	15 (26 [16–40])
Best overall response — no. (%)		
Stringent complete response	2 (3)	0
Complete response	3 (5)	1 (2)
Very good partial response	7 (12)	4 (7)
Combined response†	12 (20)	5 (9)
Partial response	20 (33)	10 (18)
Minor response	4 (7)	8 (14)
Stable disease	13 (22)	16 (28)
Progressive disease	7 (12)	9 (16)
Response could not be evaluated or was not reported	4 (7)	9 (16)

* Included are all patients who underwent randomization. Definitions of response and disease progression were modified from International Myeloma Working Group criteria,[25,26] except for the definition of minor (minimal) response, which was derived from European Society for Blood and Marrow Transplantation criteria[28] (see the Supplementary Appendix).
† Combined response was defined as very good partial response or better.

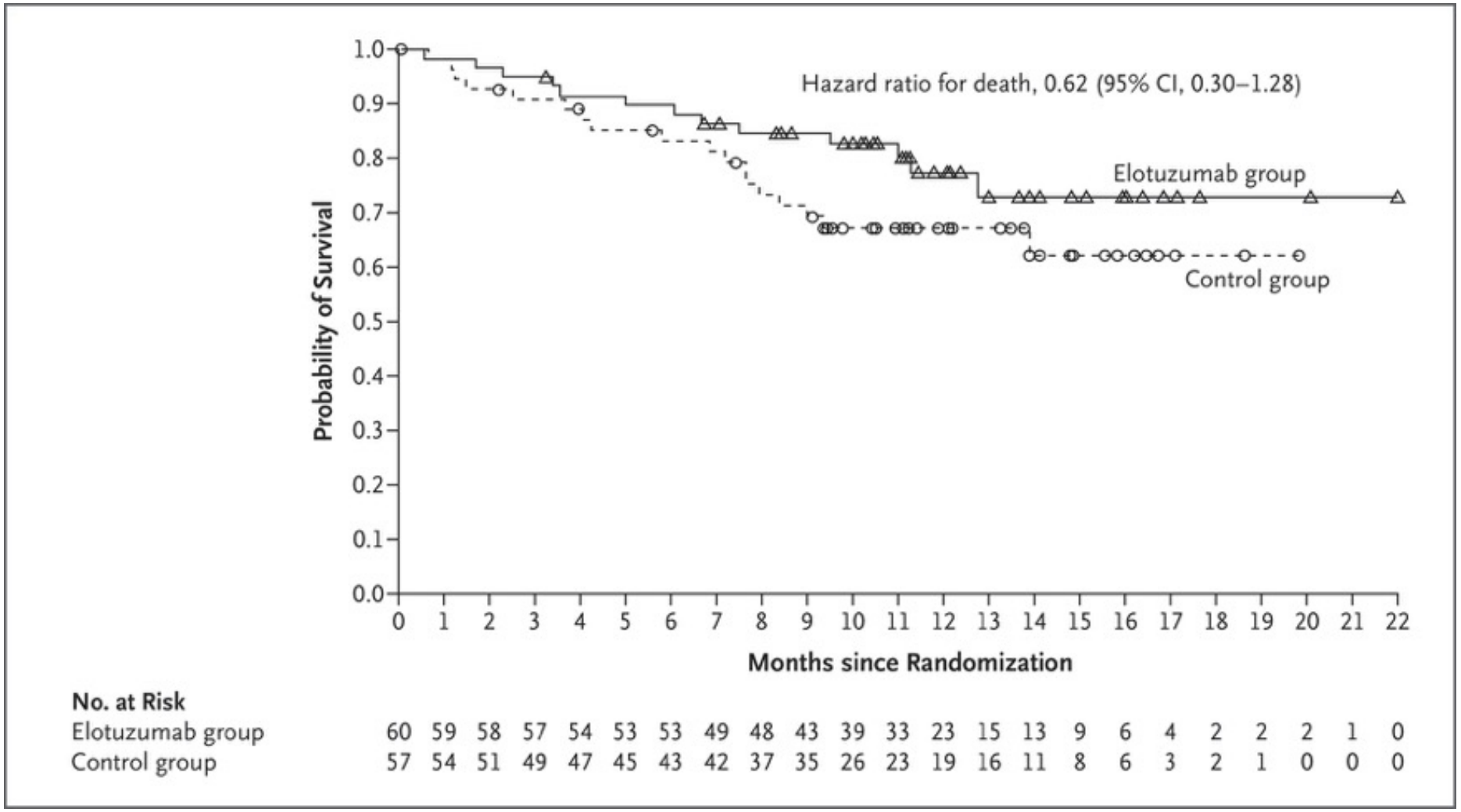

Preliminary Overall Survival. Shown are the results of the Kaplan–Meier analysis of overall survival in all patients who underwent randomization. The triangles and circles represent censored data.

Grade 3 or 4 adverse events were reported in 57% of the patients in the elotuzumab group and in 60% in the control group; the most common events were neutropenia (13% in the elotuzumab group vs. 27% in the control group), anemia (10% vs. 20%), and hyperglycemia (8% vs. 7%). Infections of any grade were reported in 65% of the patients in each of the two groups, with grade 3 or 4 infections occurring in 13% of the patients in the elotuzumab group and in 22% in the control group. When we adjusted for exposure to the trial medication, the rate of infection was 182 events per 100 patient-years in the elotuzumab group and 230 events per 100 patient-years in the control group.

Event	Elotuzumab Group (N=60)		Control Group (N=55)	
	Any Grade	Grade 3 or 4	Any Grade	Grade 3 or 4
	number of patients (percent)			
Any adverse event	58 (97)	34 (57)	52 (95)	33 (60)
Nonhematologic adverse events				
Constipation	13 (22)	1 (2)	6 (11)	0
Hyperglycemia	12 (20)	5 (8)	8 (15)	4 (7)
Diarrhea	11 (18)	0	5 (9)	0
Fatigue	9 (15)	0	9 (16)	2 (4)
Bone pain	9 (15)	2 (3)	5 (9)	0
Dyspnea	9 (15)	2 (3)	4 (7)	1 (2)
Pyrexia	8 (13)	0	14 (25)	0
Insomnia	8 (13)	1 (2)	6 (11)	0
Peripheral edema	8 (13)	0	4 (7)	0
Muscle spasms	8 (13)	0	3 (5)	0
Asthenia	7 (12)	1 (2)	5 (9)	2 (4)
Rash	6 (10)	0	6 (11)	1 (2)
Hypokalemia	4 (7)	0	7 (13)	3 (5)
Increased blood creatinine	3 (5)	0	6 (11)	2 (4)
Malignant neoplasm progression	1 (2)	1 (2)	6 (11)	2 (4)
Hematologic adverse events	31 (52)	23 (38)	30 (55)	23 (42)
Anemia	15 (25)	6 (10)	20 (36)	11 (20)
Neutropenia	14 (23)	8 (13)	17 (31)	15 (27)
Thrombocytopenia	9 (15)	5 (8)	10 (18)	3 (5)
Lymphopenia	6 (10)	5 (8)	1 (2)	1 (2)
Adverse events of special interest				
Infections	39 (65)	8 (13)	36 (65)	12 (22)
Nasopharyngitis	10 (17)	0	8 (15)	0
Respiratory tract infection	10 (17)	0	5 (9)	1 (2)
Upper respiratory tract infection	7 (12)	0	8 (15)	1 (2)
Bronchitis	6 (10)	1 (2)	5 (9)	1 (2)
Pneumonia	4 (7)	3 (5)	6 (11)	5 (9)
Herpes zoster infection	3 (5)	0	1 (2)	0
Other adverse events				
Vascular disorders	8 (13)	2 (3)	5 (9)	0
Cardiac disorders	7 (12)	4 (7)	6 (11)	2 (4)
Neoplasms†	1 (2)	1 (2)	12 (22)	6 (11)

The findings from this randomized trial showed that the addition of the monoclonal antibody elotuzumab to pomalidomide and dexamethasone resulted in a significant improvement over pomalidomide and dexamethasone alone in treatment outcomes of relapsed or refractory multiple myeloma. Specifically, the Kaplan–Meier curves for progression-free survival showed early separation that was sustained over time, with a risk of progression or death that was 46% lower in the elotuzumab group than in the control group. In addition, the odds ratio for the overall response rate showed that patients in the elotuzumab group were 3.25 times as likely to have a response to treatment as patients in the control group. These clinical data confirm the findings of preclinical studies in mice, which showed that elotuzumab, pomalidomide, and dexamethasone synergize to kill myeloma cells.

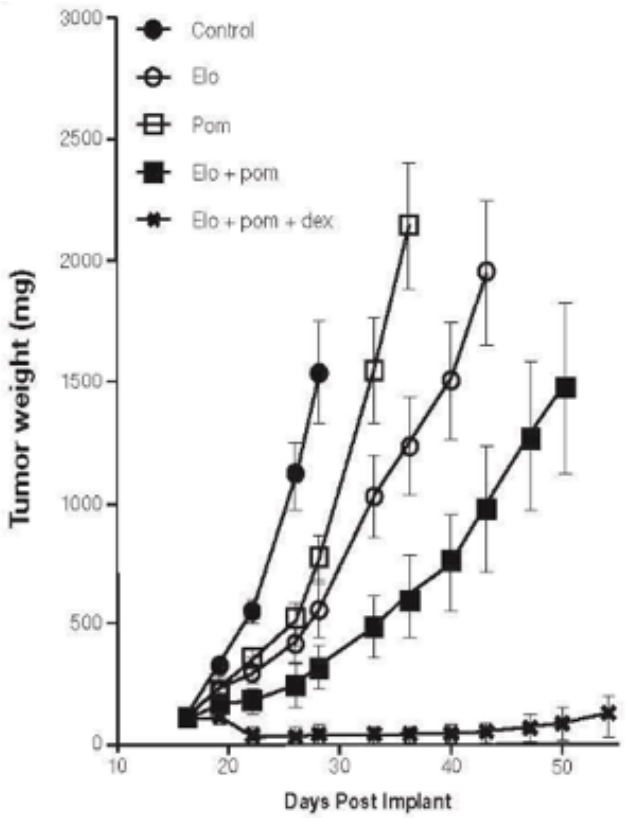

Results in mice look better than those in humans

Energy-Dense versus Routine Enteral Nutrition in the Critically Ill

For critically ill patients, guidelines recommend that energy intake match energy expenditure in order to prevent cumulative energy deficits, which have been associated with adverse outcomes. Accordingly, enteral nutrition is commonly commenced early after admission to the intensive care unit (ICU) with the use of a formulation that has an energy content of approximately 1 kcal per milliliter, prescribed at a rate of approximately 1 ml per kilogram of body weight per hour. Because of factors such as gastrointestinal intolerance (defined as large gastric residual volumes, regurgitation, and vomiting)[8] and fasting for procedures,[9] less than 60% of recommended energy intake is usually delivered to patients.

The effect of delivering nutrition at different calorie levels during critical illness is uncertain, and patients typically receive less than the recommended amount. We conducted a multicenter, double-blind, randomized trial, involving adults undergoing mechanical ventilation in 46 Australian and New Zealand intensive care units (ICUs), to evaluate energy-dense (1.5 kcal per milliliter) as compared with routine (1.0 kcal per milliliter) enteral nutrition at a dose of 1 ml per kilogram of ideal body weight per hour, commencing at or within 12 hours of the initiation of nutrition support and continuing for up to 28 days while the patient was in the ICU. The primary outcome was all-cause mortality within 90 days.

Characteristic	1.5-kcal Group (N=1971)	1.0-kcal Group (N=1986)
Age — yr	57.2±16.6	57.5±16.5
Male sex — no. (%)	1221 (61.9)	1272 (64.0)
Actual body weight — kg	84.6±23.3	84.9±23.6
Ideal body weight — kg	64.4±11.1	64.7±10.9
Body-mass index†	29.2±7.7	29.3±7.9
ICU admission category — no. (%)		
Nonoperative	1443 (73.2)	1435 (72.3)
Emergency operative	331 (16.8)	352 (17.7)
Elective operative	197 (10.0)	199 (10.0)
Insulin-treated diabetes mellitus — no. (%)	146 (7.4)	133 (6.7)
APACHE II score at ICU admission‡	22.0±8.3	22.1±8.5
Median time from ICU admission to randomization (IQR) — hr	14.1 (6.0–24.4)	14.3 (6.3–25.4)
Organ support at randomization — no. (%)		
Invasive ventilation§	1970 (100)	1980 (99.8)
Vasopressor infusion	1235 (62.7)	1253 (63.1)
New renal replacement therapy	172 (8.7)	177 (8.9)

Measure	1.5-kcal Group (N=1971)	1.0-kcal Group (N=1985)†	Difference or Relative Risk (95% CI)‡
Median time from ICU admission to commencing trial nutrition (IQR) — hr	15.8 (7.7 to 26.3)	15.9 (7.9 to 28.3)	−0.4 (−1.1 to 0.4)
Median duration of trial nutrition (IQR) — days§	6.0 (3.0 to 11.0)	6.0 (3.0 to 11.0)	0
Volume of trial nutrition delivered — ml/day¶	1242±318	1262±313	−20 (−40 to 0)
Percentage of trial target rate delivered	81±17	82±16	−1 (−2 to 0)
Calories delivered — kcal/day¶			
Trial nutrition	1863±478	1262±313	601 (576 to 626)
Trial nutrition plus other sources‖	1930±547	1407±397	523 (493 to 553)
Calories delivered — kcal/kg of ideal body weight per day¶			
Trial nutrition	29.1±6.2	19.6±4.0	9.5 (9.2 to 9.9)
Trial nutrition plus other sources‖	30.2±7.5	21.9±5.6	8.3 (7.9 to 8.7)
Calories delivered — kcal/kg of actual body weight per day¶**			
Trial nutrition	23.1±7.1	15.6±4.8	7.5 (7.1 to 7.9)
Trial nutrition plus other sources‖	23.9±7.8	17.4±5.5	6.6 (6.2 to 7.0)
Protein delivered¶			
Trial nutrition — g/day	69.6±17.8	69.4±17.2	0.1 (−1.0 to 1.2)
Trial nutrition — g/kg of ideal body weight per day	1.09±0.22	1.08±0.23	0.01 (−0.01 to 0.02)
Gastrointestinal tolerance			
Median largest gastric residual volume (IQR) — ml††	250 (100 to 441)	180 (65 to 360)	40 (30 to 50)
Regurgitation or vomiting — no./total no. (%)‡‡	370/1959 (18.9)	309/1966 (15.7)	1.20 (1.05 to 1.38)
Receipt of promotility agents — no./total no. (%)‡‡	929/1959 (47.4)	779/1966 (39.6)	1.20 (1.11 to 1.29)
Median bowel movements per day (IQR)‡‡§§	0.5 (0 to 1.3)	0.6 (0 to 1.3)	0
Median insulin administration (IQR) — IU/day¶¶	3.0 (0 to 41.8)	0 (0 to 30.6)	0
Median highest daily blood glucose concentration (IQR) — mg/dl¶¶	225.2 (185.6 to 277.4)	212.6 (174.7 to 261.2)	12.6 (9.0 to 18.0)

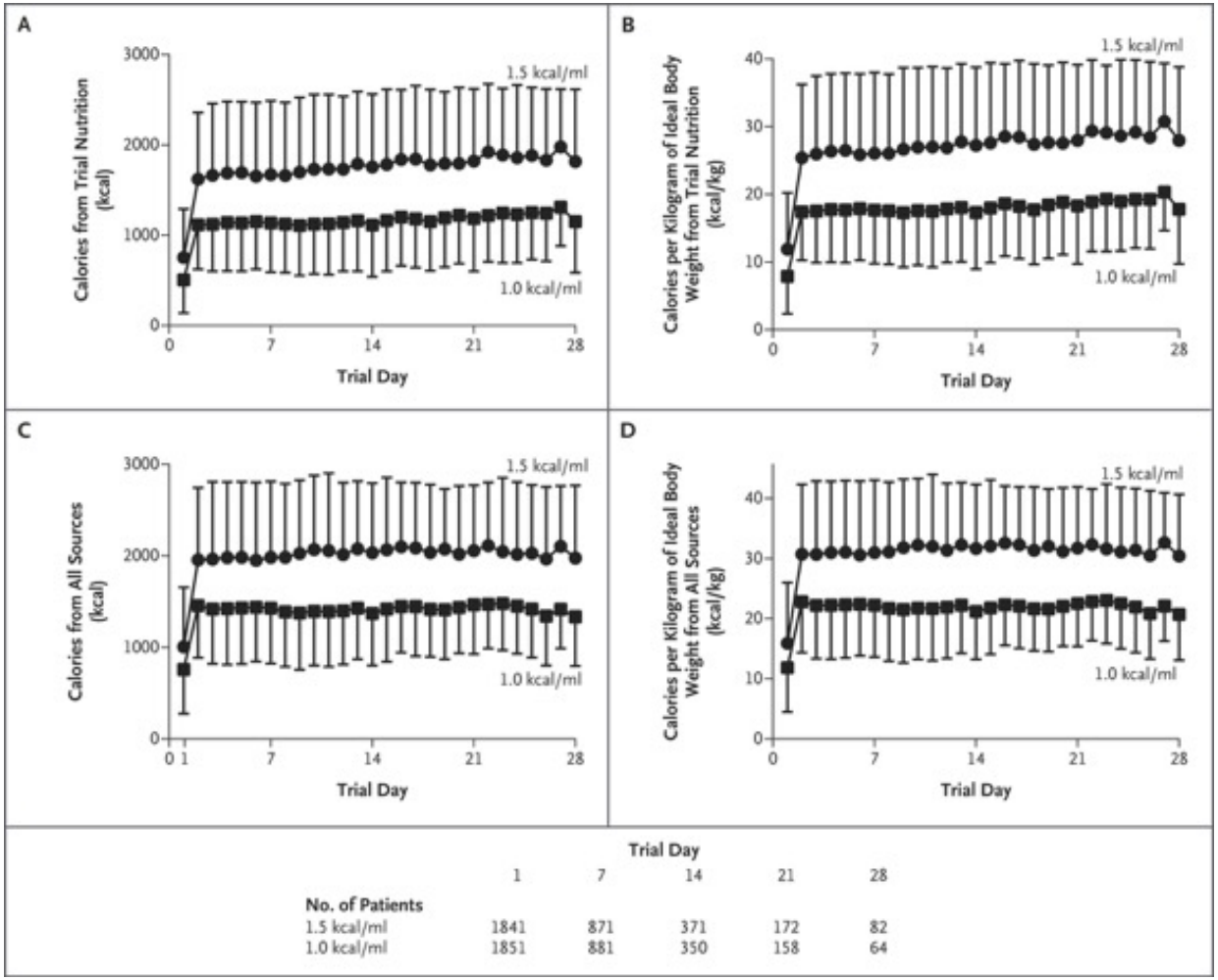

Daily Calorie Delivery over the 28-Day Trial Period. Panel A shows the mean (±SD) calories delivered from the trial enteral nutrition, and Panel B shows the calories delivered per kilogram of ideal body weight.[21] Panel C shows the total calories delivered from all calorie sources and Panel D the calories delivered per kilogram of ideal body weight from all calorie sources. Calorie sources include trial and nontrial enteral nutrition, parenteral nutrition, other dextrose solutions, propofol, and citrate infusion for renal replacement therapy. Daily data were calculated from the time of commencement of the trial enteral nutrition until cessation of the last episode of trial enteral nutrition, excluding 29 patients who never received trial enteral nutrition, 1 patient who withdrew from the trial on day 1 without daily data, and 1 patient with missing trial nutrition volume on all days.

Outcome	1.5-kcal Group	1.0-kcal Group	Difference or Relative Risk (95% CI)*
Primary outcome: death by day 90 — no./total no. (%)	523/1948 (26.8)	505/1966 (25.7)	1.05 (0.94 to 1.16)†
Secondary outcomes			
Death by the time of hospital discharge — no./total no. (%)	468/1967 (23.8)	470/1981 (23.7)	1.00 (0.97 to 1.04)
Death by day 28 — no./total no. (%)	450/1961 (22.9)	455/1976 (23.0)	1.00 (0.89 to 1.12)
Median days alive and not in ICU (IQR)‡	17.0 (0 to 23.0)	17.4 (0 to 23.1)	0
Median days alive and not in hospital (IQR)‡	2.9 (0 to 15.7)	2.9 (0 to 15.3)	0
Use and duration of organ support§			
Received invasive mechanical ventilation — no./total no. (%)	1971/1971 (100)	1982/1984 (99.9)	
Median days alive and free of invasive ventilation (IQR)	20.0 (0 to 25.0)	20.0 (0 to 25.0)	0
Received vasopressor support — no./total no. (%)	1599/1971 (81.1)	1615/1984 (81.4)	1.00 (0.97 to 1.03)
Median days alive and free of vasopressor support (IQR)	23.0 (2.0 to 26.0)	23.0 (4.0 to 26.0)	0
Received renal replacement therapy — no./total no. (%)	367/1946 (18.9)	361/1955 (18.5)	1.02 (0.90 to 1.16)
Median days alive and free of renal replacement therapy (IQR)	28.0 (8.0 to 28.0)	28.0 (10.0 to 28.0)	0
Microbiology — no./total no. (%)¶			
Positive blood cultures	228/1971 (11.6)	221/1984 (11.1)	1.04 (0.87 to 1.24)
Administration of intravenous antimicrobial agent	1662/1971 (84.3)	1658/1985 (83.5)	1.01 (0.98 to 1.04)
Adverse events — no./total no. of adverse events‖			
Electrolyte abnormality	45/69	42/63	
Gastrointestinal event	22/69	20/63	
Other	2/69	1/63	
Serious adverse events — no./total no.‖	1/1971	1/1986	

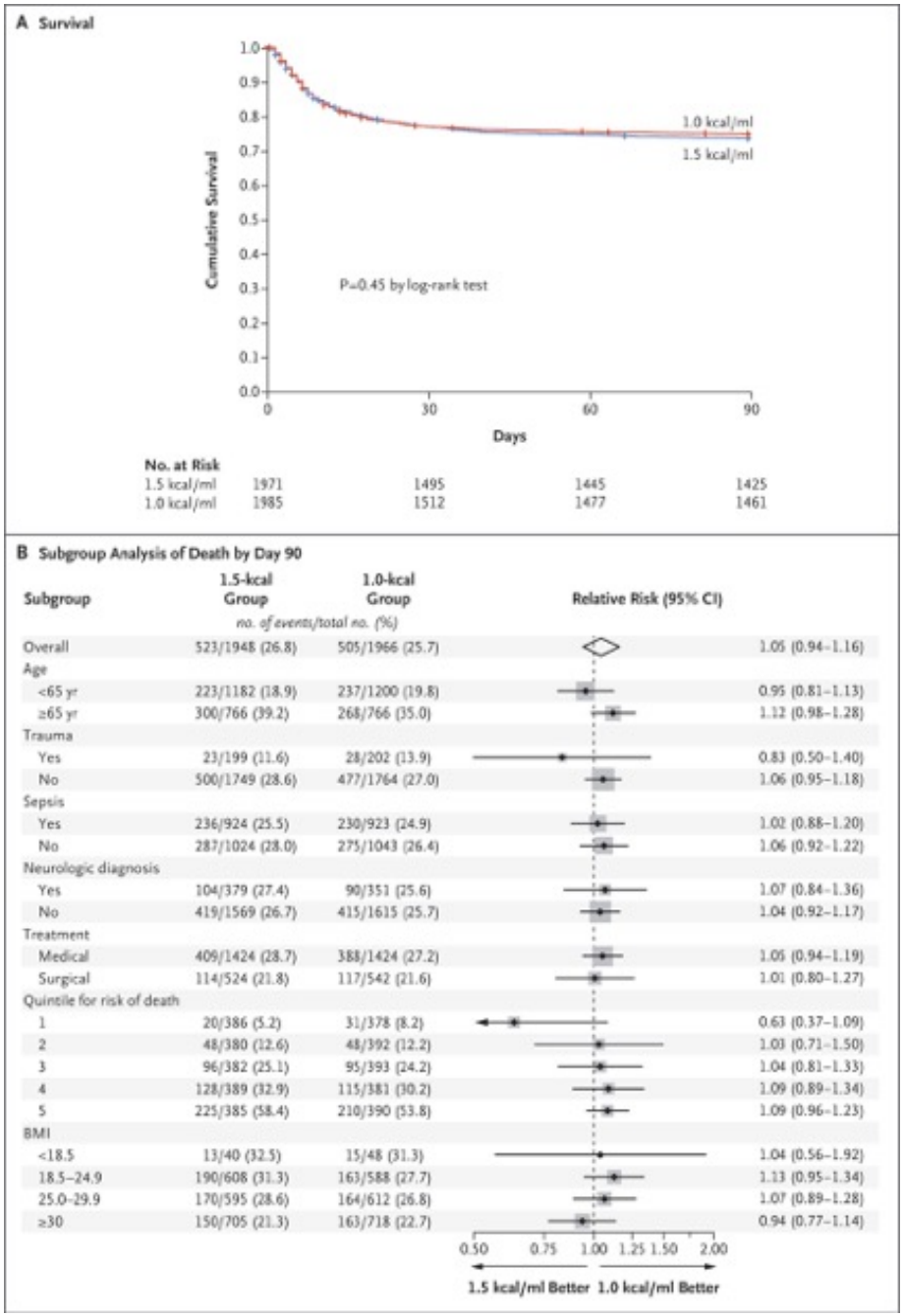

Time-to-Death and Subgroup Analyses of the Risk of Death by Day 90. Panel A shows the Kaplan–Meier estimates for the probability of death from randomization to day 90, excluding 1 patient for whom the date of death was unknown. Panel B shows the relative risk of death up to day 90 after randomization in the two treatment groups, among all patients and in the seven prespecified subgroups. A relative risk of less than 1.0 indicates better results for the 1.5-kcal group. The size of the square represents the relative number within each subgroup, and the horizontal bars represent the 95% confidence interval. Sepsis was categorized according to the Sepsis-3 criteria[22] with the use of the physiological and biochemical data that were recorded closest to, but before, randomization. The quintiles for the risk of death were based on the Australian and New Zealand Intensive Care Risk of Death model; quintile 1 indicates the lowest and quintile 5 the highest risk of death,[23] and the quartiles for body-mass index (BMI, the weight in kilograms divided by the square of the height in meters) were based on the World Health Organization classification system.[25] Risk of death and BMI as continuous variables did not differ significantly between the groups: P=0.64 (base 1) and P=0.23 (base 2) for the risk of death and P=0.09 (linear interaction) and P=0.10 (quadratic interaction) for BMI.

In this multicenter, double-blind, randomized trial, we compared energy-dense enteral nutrition with standard enteral nutrition in critically ill adults. The use of energy-dense nutrition increased energy intake to approximate full recommended goals but did not affect mortality or key secondary outcomes, including organ support and duration of hospital stay. Several open-label, randomized trials have evaluated energy delivery during critical illness. These and subsequent meta-analyses have not reported improved outcomes in association with increased intake. Nonetheless, guidelines recommend an energy intake of 25 to 30 kcal per kilogram per day to match expenditure. Our findings do not support that recommendation.

The effect on outcome did not differ across clinically important subgroups. Of particular interest are patients who are poorly nourished at baseline. Because there is no agreed-on approach for the accurate quantification of baseline nutritional status in large nutrition trials, we used BMI as a surrogate marker. Only 89 patients (2%) had a BMI of less than 18.5, which precluded inferences about the effect of energy delivery in such patients. In contrast, one third of the patients were obese (BMI >30). Guidance documents based on expert opinion recommend hypocaloric (11 to 14 kcal per kilogram per day), high-protein feeding for obese patients.[1] Our results suggest that hypocaloric and eucaloric feeding have similar effects on survival when the protein dose is kept constant.

Figure S2A. Enteral nutrition study formulae supplied in identical, red, non-transparent study bags

Bei der Gonorrhoe handelt es sich um eine weltweit vorkommende, ausschließlich beim Menschen auftretende sexuell übertragbare Erkrankung. Die korrekte Benutzung eines Kondoms oder von Lecktüchern schützt vor einer Infektion. Die Krankheit kann von der erkrankten Mutter während der Geburt auf das Kind übertragen werden. Bis zum Jahr 2000 war die Erkrankung in Deutschland meldepflichtig. Die Meldepflicht wurde aufgehoben mit Einführung des Infektionsschutzgesetzes, welches das Bundes-Seuchengesetz und das Gesetz zur Bekämpfung der Geschlechtskrankheiten ablöste. Die Erkrankungszahlen sind seit Ende der 1970er Jahre rückläufig, in den 1990er Jahren gingen die Trends in Europa jedoch auseinander. In der zweiten Hälfte der neunziger Jahre vermeldeten Belgien, Großbritannien und Frankreich eine Zunahme der Erkrankungen, in anderen Ländern blieb die Inzidenz dagegen gleich oder war rückläufig.
Weltweit stellt die Gonorrhoe ein großes gesundheitliches Problem dar. Nach Schätzungen der Weltgesundheitsorganisation liegt die Zahl der Neuerkrankungen jedes Jahr bei 60 Millionen,[4] das ist ungefähr ein Prozent der Weltbevölkerung.

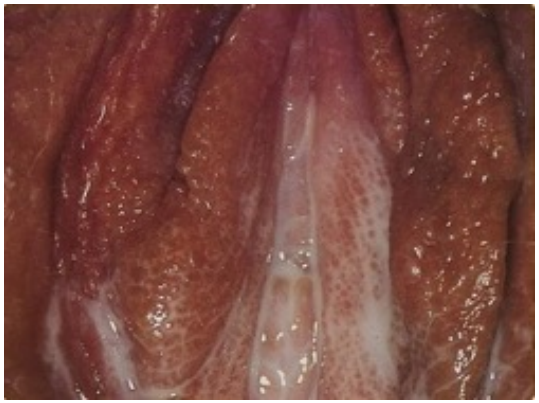

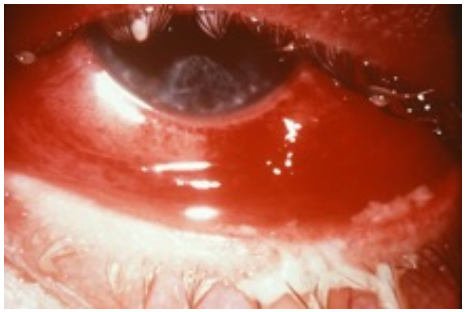

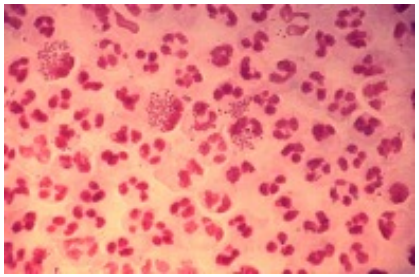

Single-Dose Zoliflodacin (ETX0914) for Treatment of Urogenital Gonorrhea

The incidence of gonorrhea in the United States increased by 67% from 2013 through 2017. Concomitantly, the antimicrobial susceptibility of *Neisseria gonorrhoeae* has diminished. Decreased susceptibility and increased resistance to macrolides and cephalosporins have been reported in the United States and around the world, and treatment failures have been noted. *N. gonorrhoeae* isolates that are resistant to the currently recommended regimen of ceftriaxone and azithromycin have also been reported.

Antibiotic-resistant *Neisseria gonorrhoeae* has prompted the development of new therapies. Zoliflodacin is a new antibiotic that inhibits DNA biosynthesis. In this multicenter, phase 2 trial, zoliflodacin was evaluated for the treatment of uncomplicated gonorrhea. We randomly assigned eligible men and women who had signs or symptoms of uncomplicated urogenital gonorrhea or untreated urogenital gonorrhea or who had had sexual contact in the preceding 14 days with a person who had gonorrhea to receive a single oral dose of zoliflodacin (2 g or 3 g) or a single 500-mg intramuscular dose of ceftriaxone in a ratio of approximately 70:70:40. A test of cure occurred within 6±2 days after treatment, followed by a safety visit 31±2 days after treatment. The primary efficacy outcome measure was the proportion of urogenital microbiologic cure in the microbiologic intention-to-treat (micro-ITT) population.

Characteristic	University of Washington (N=66)	Louisiana State University (N=46)	Indiana University (N=34)	University of Alabama (N=22)	University of North Carolina (N=12)	All Sites (N=180)
Age						
Mean	29.7±8.3	28.4±8.1	30.2±10.1	25.8±5.1	27.5±6.3	28.8±8.2
Median (IQR)	27 (19–53)	27 (18–53)	27 (18–53)	26 (19–40)	27 (18–42)	27 (18–53)
Sex — no. (%)						
Male	64 (97)	46 (100)	34 (100)	13 (59)	10 (83)	167 (93)
Female†	2 (3)	0	0	9 (41)	2 (17)	13 (7)
Race — no. (%)						
Black	15 (23)	34 (74)	26 (76)	22 (100)	10 (83)	107 (59)
White	42 (64)	10 (22)	5 (15)	0	1 (8)	58 (32)
Other, multiracial, or unknown‡	9 (14)	2 (4)	3 (9)	0	1 (8)	15 (8)
Ethnicity — no. (%)						
Non-Hispanic	59 (89)	44 (96)	33 (97)	22 (100)	9 (75)	167 (93)
Hispanic	7 (11)	2 (4)	1 (3)	0	3 (25)	13 (7)
Sexual partner of male participants — no. (%)						
Women only	13 (20)	30 (65)	26 (76)	13 (100)	8 (80)	90 (54)
Men only	45 (70)	13 (28)	6 (18)	0	2 (20)	66 (40)
Men and women	6 (9)	3 (7)	2 (6)	0	0	11 (7)

Table 2. Microbiologic Cure Rates at Test-of-Cure Visit — Micro-ITT and Per-Protocol Populations.

Population, Site, and Treatment	Confirmed Infections	Cures	Microbiologic Cure
	number		*% (95% CI)*
Micro-ITT			
Urethra or cervix			
Zoliflodacin, 2 g	57	55	96 (88–100)
Zoliflodacin, 3 g	56	54	96 (88–100)
Ceftriaxone, 500 mg	28	28	100 (88–100)
Rectum			
Zoliflodacin, 2 g	5	5	100 (48–100)
Zoliflodacin, 3 g	7	7	100 (59–100)
Ceftriaxone 500 mg	3	3	100 (29–100)
Pharynx			
Zoliflodacin, 2 g	8	4	50 (16–84)
Zoliflodacin, 3 g	11	9	82 (48–98)
Ceftriaxone, 500 mg	4	4	100 (40–100)
Per protocol			
Urethra or cervix			
Zoliflodacin, 2 g	49	48	98 (89–100)
Zoliflodacin, 3 g	47	47	100 (92–100)
Ceftriaxone, 500 mg	21	21	100 (84–100)
Rectum			
Zoliflodacin, 2 g	4	4	100 (40–100)
Zoliflodacin, 3 g	6	6	100 (54–100)
Ceftriaxone, 500 mg	3	3	100 (29–100)
Pharynx			
Zoliflodacin, 2 g	6	4	67 (22–96)
Zoliflodacin, 3 g	9	7	78 (40–97)
Ceftriaxone, 500 mg	4	4	100 (40–100)

In the micro-ITT population, among participants with signs and symptoms of *N. gonorrhoeae* infection at baseline, cure occurred in 52 of 57 participants (91%; 95% confidence interval [CI], 80 to 97) in the group that received 2 g of zoliflodacin, 46 of 49 participants (94%; 95% CI, 83 to 99%) in the group that received 3 g of zoliflodacin, and 26 of 27 participants (96%; 95% CI, 81 to 100) in the group that received ceftriaxone. Clinical cure rates were similar in the per-protocol population. As assessed on NAAT, nucleic acid clearance occurred in the micro-ITT population in 48 of 57 participants (84%; 95% CI, 72 to 93) in the group that received 2 g of zoliflodacin, 42 of 52 participants (81%; 95% CI, 67 to 90) in the group that received 3 g of zoliflodacin, and 25 of 28 participants (89%; 95% CI, 71 to 98) in the group that received ceftriaxone. All participants with rectal gonorrhea detected on NAAT at enrollment had nucleic acid clearance at the test-of-cure visit. Nucleic acid clearance at test of cure was lowest in the pharynx, in 2 of 8 participants (25%) in the group that received 2 g of zoliflodacin, 6 of 11 (55%) in the group that received 3 g of zoliflodacin, and 2 of 4 (50%) in the group that received ceftriaxone. Findings were similar in the per-protocol population.

Table 3. Participants with Adverse Events According to MedDRA System Organ Class, Severity, Relationship to Trial Drug, and Treatment.*

MedDRA System Organ Class	Zoliflodacin, 2 g (N=72)					Zoliflodacin, 3 mg (N=67)					Ceftriaxone, 500 mg (N=40)				
	Severity†			Relationship to Trial Drug†		Severity†			Relationship to Trial Drug†		Severity†			Relationship to Trial Drug†	
	Mild	*Moderate*	*Severe*	*Not Related*	*Related*	*Mild*	*Moderate*	*Severe*	*Not Related*	*Related*	*Mild*	*Moderate*	*Severe*	*Not Related*	*Related*
	number (percent)														
Any system organ class	14 (19)	4 (6)	0	9 (13)	9 (13)	20 (30)	3 (4)	1 (1)	12 (18)	12 (18)	14 (35)	4 (10)	0	12 (30)	6 (15)
Gastrointestinal disorders	5 (7)	0	0	1 (1)	4 (6)	8 (12)	0	0	1 (1)	7 (10)	3 (8)	0	0	1 (3)	2 (5)
General disorders	1 (1)	0	0	0	1 (1)	0	0	0	0	0	2 (5)	0	0	1 (3)	1 (3)
Investigations	1 (1)	3 (4)	0	2 (3)	2 (3)	1 (1)	1 (1)	0	2 (3)	0	0	1 (3)	0	1 (3)	0
Nervous-system disorders	0	0	0	0	0	6 (9)	0	0	1 (1)	5 (7)	2 (5)	0	0	1 (3)	1 (3)

* A complete list of adverse events is available in Table S2 in the Supplementary Appendix. MedDRA denotes *Medical Dictionary for Regulatory Activities.*
† With regard to severity and relationship to trial drug, a participant is counted only once per preferred term.

A total of 84 adverse events (24 in the group that received 2 g of zoliflodacin, 37 in the group that received 3 g of zoliflodacin, and 23 in the ceftriaxone group) were reported by 59 participants (33%). The events included 11 moderate and 1 serious adverse event, a nonfatal gunshot wound considered by the investigators to be unrelated to zoliflodacin. A total of 21 participants reported adverse events that investigators assessed as being related to zoliflodacin; most such events were gastrointestinal and self-limiting (5 events occurred in the group that received 2 g of zoliflodacin and 8 events occurred in the group that received 3 g of zoliflodacin).

Table 4. Comparison of Zoliflodacin with Currently Recommended Antimicrobials for the Treatment of Gonorrhea According to Site of Infection (Micro-ITT Population).*

Specimen and Antimicrobial Drug	MIC Breakpoint	MIC50 (μg/ml)	MIC90 (μg/ml)	Range (μg/ml)	Proportion at or above MIC Breakpoint
					no./total no. (%)
Urethra or cervix — 140 isolates					
Zoliflodacin	≥0.5	0.093	0.250	0.008–0.250	0/140
Azithromycin	≥2	0.250	1.000	0.060–4.000	3/140 (2)
Ceftriaxone	≥0.125	0.008	0.015	0.001–0.060	0/140
Rectum — 14 isolates					
Zoliflodacin	≥0.5	0.060	0.250	0.008–0.250	0/14
Azithromycin	≥2	0.250	1.000	0.125–1.000	0/14
Ceftriaxone	≥0.125	0.006	0.008	0.001–0.015	0/14
Pharynx — 23 isolates					
Zoliflodacin	≥0.5	0.125	0.250	0.008–0.250	0/23
Azithromycin	≥2	0.500	1.000	0.060–2.000	1/23
Ceftriaxone	≥0.125	0.008	0.030	0.001–0.060	0/23

* Values for minimum inhibitory concentration (MIC) were defined as the lowest concentration of the antibiotic at which 90% (MIC90) and 50% (MIC50) of the isolates were inhibited.

Zoliflodacin was effective in treating gonococcal urogenital and rectal infections. In the micro-ITT population, 96% of infected participants in the group that received a single oral dose of 2 g of zoliflodacin and in the group that received 3 g of zoliflodacin had microbiologic cure at urogenital sites. Although there were few participants with rectal infections, all had microbiologic cure. The efficacy of zoliflodacin was lower among participants with pharyngeal infections than among those with urogenital and rectal infections.

Zoliflodacin was not as effective as ceftriaxone in treating pharyngeal gonorrhea, which is generally more difficult to treat than urethral, cervical, or rectal gonorrhea. Currently, this limitation has not curtailed recommendations for the use of drugs such as spectinomycin or fluoroquinolones for the treatment of gonorrhea. In previous studies, pharyngeal isolates obtained from participants in whom treatment was not successful did not show antibiotic resistance or meaningful change in antimicrobial susceptibility after treatment, as we observed in this trial. Thus, it has been speculated that poor drug penetration into pharyngeal tissue may be responsible for most pharyngeal treatment failures rather than reinfection or resistant organisms. The traditional criterion for a recommendation of antibiotics for uncomplicated urogenital gonorrhea is a cure rate of more than 95%, with the lower boundary of the confidence interval greater than 95%. To be recommended as an alternative, the cure rate must be higher than 95%, with the lower boundary of the confidence interval higher than 90%. Although the cure rates for 2 g of zoliflodacin, 3 g of zoliflodacin, and 500 mg of ceftriaxone met the point-estimate criteria for efficacy at the urogenital and rectal sites, only ceftriaxone met that criterion for the pharyngeal site. In our trial, the criteria for the lower boundaries of the confidence intervals were not met by either zoliflodacin or ceftriaxone for any anatomical site.

Daratumumab for Delayed Red-Cell Engraftment after Allogeneic Transplantation

Allogeneic stem-cell transplantation is a curative treatment option for patients with malignant hematologic diseases, including myelodysplastic syndromes. In 25 to 50% of transplantations, HLA-matched allogeneic stem-cell donors have some degree of ABO blood-group incompatibility with the recipient, since HLA and ABO genes are inherited independently. Daratumumab is a human IgG1κ monoclonal antibody directed against CD38, which is expressed at high levels on plasma cells. The mechanisms of action of daratumumab include complement-dependent cytotoxicity, antibody-dependent cellular cytotoxicity, antibody-dependent cellular phagocytosis, and apoptotic signaling.

Daratumumab, a human IgG1κ monoclonal antibody targeting CD38, is used to treat multiple myeloma. We describe successful treatment with daratumumab in a case of treatment-refractory pure red-cell aplasia after ABO-mismatched allogeneic stem-cell transplantation. The patient was a 72-year-old man with the myelodysplastic syndrome who received a transplant from an HLA-matched, unrelated donor with a major ABO incompatibility (blood group A in the donor and blood group O in the recipient). The patient had persistent circulating anti-A antibodies and no red-cell recovery 200 days after transplantation. Standard treatments had no effect. Within 1 week after the initiation of treatment with daratumumab, he no longer required transfusions.

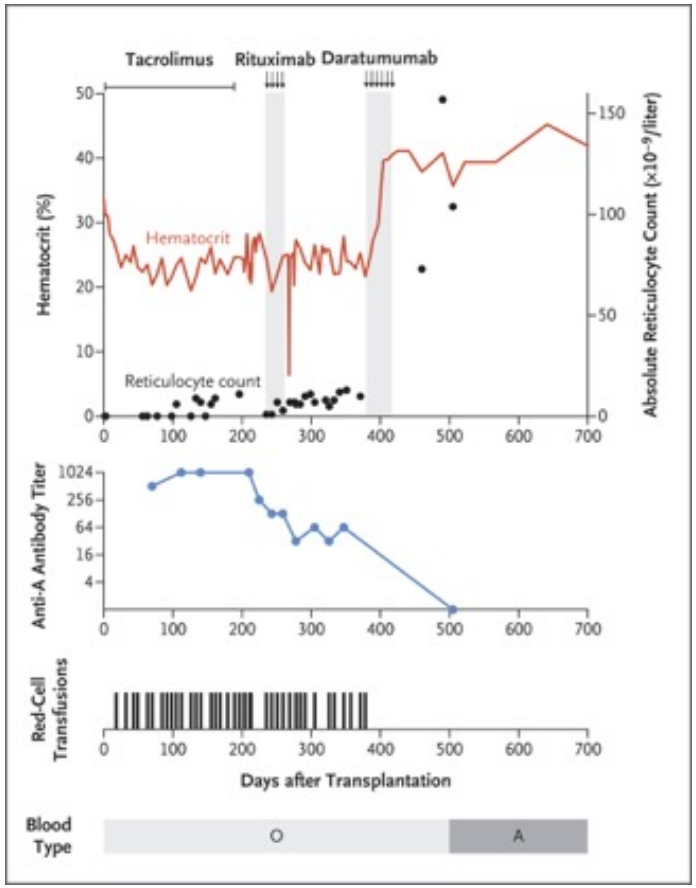

Shown are the hematocrit, reticulocyte count, anti-A antibody titer, red-cell transfusion requirement, and blood type before and after treatment first with rituximab and then with daratumumab (shading). The variation in the hematocrit after rituximab therapy reflects continued management with red-cell transfusions; the patient received a transfusion immediately before the initiation of daratumumab therapy. The patient received four doses of rituximab and six doses of daratumumab, as indicated by the arrows.

The patient received a diagnosis of post-transplantation pure red-cell aplasia, defined by persistent reticulocytopenia and an absence of erythroid precursors in the bone marrow, as well as an absence of infection, drug toxicity, and relapse. Persistently elevated anti–donor isohemagglutinins with high anti-A antibody titers (peak titer, 1:1024) for more than 200 days after transplantation were the cause of the pure red-cell aplasia. Delayed red-cell recovery and transient pure red-cell aplasia after nonmyeloablative allogeneic hematopoietic stem-cell transplantation with major ABO incompatibility, as seen in this patient, has been documented in multiple studies. In our case, the reduction of immunosuppressive therapy had some effect on anti-A isohemagglutinin titers, which decreased by a factor of 2 and probably represented graft-versus-plasma-cell activity. GVHD did not develop in this patient, and despite the decrease in isohemagglutinins, no improvement in erythropoiesis or reticulocyte levels was seen.
Given the pathophysiology of post-transplantation pure red-cell aplasia due to residual isohemagglutinin-producing plasma cells, we hypothesized that a selective treatment targeting these plasma cells should eliminate the pathogenic plasma-cell population and overcome the refractory pure red-cell aplasia.

Post-transplantation pure red-cell aplasia is a well-recognized complication after ABO-incompatible allogeneic stem-cell transplantation. Most cases resolve spontaneously or with immunomodulatory or immunosuppressive treatments. The results in this patient with refractory post-transplantation pure red-cell aplasia suggest that direct targeting of residual host plasma cells with an anti-CD38 agent such as daratumumab might be a valid treatment option to consider in patients with no response to standard treatments.

The Charlie Gard case was a best interests case in 2017 involving Charles Matthew William Gard (4 August 2016 – 28 July 2017), an infant boy from London, born with mitochondrial DNA depletion syndrome (MDDS), a rare genetic disorder that causes progressive brain damage and muscle failure. MDDS has no treatment and usually causes death in infancy. The case became controversial because the medical team and parents disagreed about whether experimental treatment was in the best interests of the child. In October 2016, Charlie was transferred to London's Great Ormond Street Hospital (GOSH), a National Health Service (NHS) children's hospital, because he was failing to thrive and his breathing was shallow. He was placed on mechanical ventilation and MDDS was diagnosed. A neurologist in New York, Michio Hirano, who was working on an experimental treatment based on nucleoside supplementation with human MDDS patients was contacted. He and GOSH agreed to proceed with the treatment, to be conducted at GOSH and paid for by the NHS. Hirano was invited to come to the hospital to examine Charlie but did not visit at that time. In January, after Charlie had seizures that caused brain damage, GOSH formed the view that further treatment was futile and might prolong suffering. They began discussions with the parents about ending life support and providing palliative care. Charlie's parents still wanted to try the experimental treatment and raised funds for a transfer to a hospital in New York. In February 2017, GOSH asked the High Court to override the parents' decision, questioning the potential of nucleoside therapy to treat Charlie's condition. The British courts supported GOSH's position. The parents appealed the case to the Court of Appeal, the Supreme Court and the European Court of Human Rights. The decision of the court at first instance was upheld at each appeal. In July 2017, after receiving a letter signed by several international practitioners defending the potential of the treatment and claiming to provide new evidence, GOSH applied to the High Court for a new hearing. The second hearing at the High Court, which had been arranged to hear and examine the new evidence then became concerned with the arrangements for the withdrawal of life support. On 27 July, by consent, Charlie was transferred to a hospice, mechanical ventilation was withdrawn, and he died the next day at the age of 11 months and 24 days.

Ethical Problems in Decision Making in the Neonatal ICU

In the neonatal intensive care unit (NICU), disagreements about whether life-sustaining treatment can ethically be withheld or withdrawn are not uncommon. Usually, the dilemma comes down to questions about the value of life with severe physical or cognitive impairments. Disagreements can go in both directions. Sometimes, doctors recommend treatments and parents refuse. Sometimes, parents request continued treatment that doctors think inappropriate. Such conflicts have occurred in cases of hypoxic encephalopathy,[1] degenerative neurologic diseases,[2] and even brain death. These disagreements can cause moral distress among doctors and nurses and debates about the ethical justifiability of unilateral decisions that treatment is futile and should be withdrawn. Usually, disagreements are resolved by ongoing discussion between doctors and parents, by bringing in other family members, or by consulting an ethics committee. Most intensivists learn how to negotiate with families in these situations. Occasionally, disagreements become intractable, and cases end up in court. Some states have statutes in place that guide judicial decisions. Laws in Texas, California, and Virginia empower doctors to withdraw life-sustaining treatment unilaterally. By contrast, laws in Kansas, Oklahoma, and New York empower patients and families to prevail in disagreements.

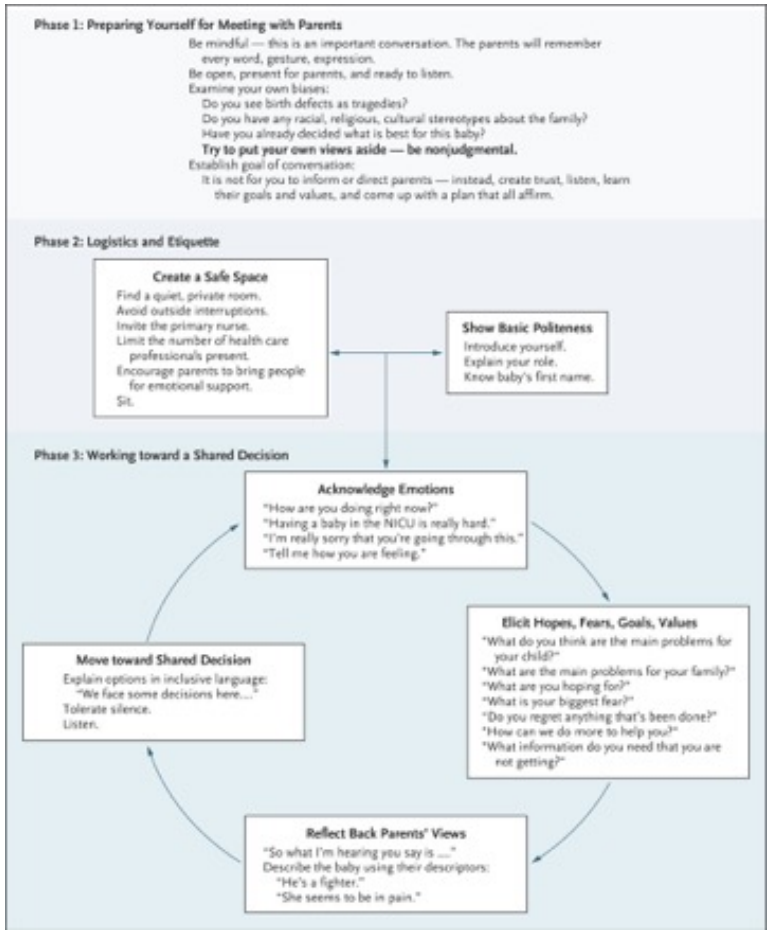

Shared Decision Making in the Neonatal Intensive Care Unit (NICU). Shown is a three-phase process of shared decision making for gray-zone cases in the NICU. Phase 3 is a circular, reiterative process.

The first line of research undermining the old approach comes from studies showing that, contrary to some widely held beliefs, most disagreements between doctors and parents about treatment choices do not arise because doctors hide bleak information that would lead parents to request withdrawal of treatment. Instead, disagreements occur because, even when parents are given information about the possibility of bleak outcomes, most parents want treatment that doctors think is inappropriate or futile. Parents are more accepting of severe disability among surviving babies than are most health professionals. The recent case of Charlie Gard in the United Kingdom epitomizes this type of disagreement.

Table 1. Comparison between Data-Guided Parental Choice and Shared Decision Making in the NICU.*

An approach focused on the process of shared decision making
Start with open-ended invitations:
Is now a good time to talk?
Tell me how you're feeling today.
How does your child look to you?
Tell me more.
Let parents tell you what they know and how they feel:
What have other doctors and nurses told you about your child?
What do you fear?
What do you hope for?
Stop talking.
Let parents speak.
Listen actively.
Make eye contact, nod head, and focus on person speaking.
Circle back: "What I'm hearing you say is.... Did I get that right?"
Find common ground; use "we":
"We are both hoping for that goal!"
"Here are some of the options and the decisions that we have to make."
An approach focused on giving parents information and asking for a decision
For each gestational age, provide parents with data in an "outcome-by-gestational-age" format for babies born at 22, 23, and 24 weeks.
Short-term outcomes
Percent of babies who survive
Percent of babies who leave the NICU with respiratory problems
Percent of babies with abnormal findings on ultrasonography of the head
Percent of babies with jaundice requiring phototherapy
Average number of days in hospital
Long-term outcomes
Percent of babies who need tracheostomy
Percent of babies who need gastrostomy tube
Percent of babies with cerebral palsy
Percent of babies with cognitive impairment
Percent of babies with visual impairment
Ask the parents whether, given the information provided, they want to choose life-sustaining treatment or comfort care only.

* The description of shared decision making is adapted from Madrigal and Kelly.[18] The description of data-guided parental choice is adapted from Koh et al.[19] NICU denotes neonatal intensive care unit.

Table 2. Three Important Domains of Research about Ethical Decisions in the NICU.

Most disagreements that arise are unrelated to doctors' withholding bleak information.
Parents want honesty but tempered with hope.
Parents generally are more accepting of disability than are health professionals.
Most disagreements arise when parents demand treatment that doctors think is inappropriate, not when parents refuse treatment.
Neonatologists endorse shared decision making but do not practice it.
Few neonatologists allow parents' preferences to prevail.
Parents want to participate but also want doctors' help.
People do not usually base decisions on objective data alone.
Many known biases lead people to make decisions that contradict their own values.
Facts are inevitably framed in a way that shapes choices.
Doctors' biases might lead them to frame the facts in a way that inadvertently sways parents.

CASE 1

A neonatologist went to speak to the teenage parents of a premature baby, Gabriel, who had been born at a gestational age of 27 weeks.[59] The parents were married and had two other children. Neither parent had finished high school.

By day 3 of life, Gabriel had pulmonary and intraventricular hemorrhages. After reviewing these findings, the doctor spoke with the parents about their baby's condition and poor prognosis. She was going to recommend discontinuation of life support. Instead, she asked if they had any questions. The father asked, "Will I be able to love him, even if he is handicapped?" The doctor reassured the father that Gabriel would be very lovable. The mother asked, "Will he be able to love us?" The doctor replied, "He will love you as much as any other child, probably more."

The father told the doctor that they had a nephew with Down's syndrome whom they adored. He asked if Gabriel would be like that nephew. The doctor told them that it was too early to predict the long-term effects of Gabriel's brain hemorrhage. She promised to meet with the parents every morning and update them on his condition and prognosis. The discussion never explicitly addressed questions about whether to discontinue life support. But the doctor got a good sense of the parents' values, and the discussion built a basis for trust.

CASE 2

A neonatologist was called for a prenatal consultation concerning a woman with premature rupture of membranes who was in labor at 25 weeks of gestation. The obstetricians said that she would deliver within the next few hours. The pregnancy was complicated by a prenatal diagnosis of a large omphalocele on an ultrasound examination performed at 18 weeks of gestation. The parents said they wanted everything done to save the baby. The neonatologist was tempted to simply tell the parents that treatment would be futile and that the only option was comfort care. Instead, he asked them what it was like when they first heard the diagnosis of omphalocele. He asked what they were hoping for and what they feared most. The mother expressed her shock, confusion, and grief. She wondered whether she had done something wrong to cause the baby's problems. The doctor assured her that she had not. The father wondered whether treatment in the NICU would cause pain. The doctor said that they do their best to control pain but that it would depend on how sick the baby was and what interventions were needed. Together, the parents and doctor agreed not to make any decision until the baby was born.

At birth, the baby had a heart rate of 50 beats per minute, a large omphalocele, and physical findings consistent with a gestational age of 25 weeks. The doctor told the parents that their baby could not be saved. The mother asked to hold her baby. The neonatologist wrapped the motionless and apneic baby in a warm blanket. A few minutes later, the infant was pronounced dead. The neonatologist's focus on the parents' emotional state, rather than on the futility of treatment, helped build the trust that enabled a shared decision to be made in the delivery room.[60]

Toward the Future

The central argument of this review is that an important and necessary shift is occurring in the focus of neonatal bioethics. The focus used to be on empowering parents by giving them information and on rule making to define the zone of parental discretion. Today, the focus is shifting toward an ethics of relational autonomy. Doctors need to develop new communication skills to help parents clarify their values. Doctors must also be aware of their own values as they design the choice architecture within which parents will be empowered to make choices. This self-awareness and these communication skills will be especially important as pediatrics changes and decisions become even more complex and value-laden.

Three emerging technologies are likely to loom large in the future of neonatal bioethics, testing doctors' skills in helping parents make good decisions. First, we will see continued advances in prenatal diagnosis and fetal therapy. Genomic testing with the use of cell-free fetal DNA in maternal serum will allow more and more fetal anomalies to be diagnosed early in pregnancy. Parents will then face more complex choices than they do today about terminating pregnancy, trying innovative fetal therapy, or waiting for postnatal treatment options. Many parents choose to terminate pregnancies after severe fetal anomalies have been diagnosed, but others choose to continue their pregnancies. The likely effect of better prenatal diagnosis will be that parents who learn that the fetus has congenital anomalies and who choose not to terminate the pregnancy will want treatment in the NICU for their babies. This effect could increase the number of situations in which doctors recommend withholding treatment but parents request it.

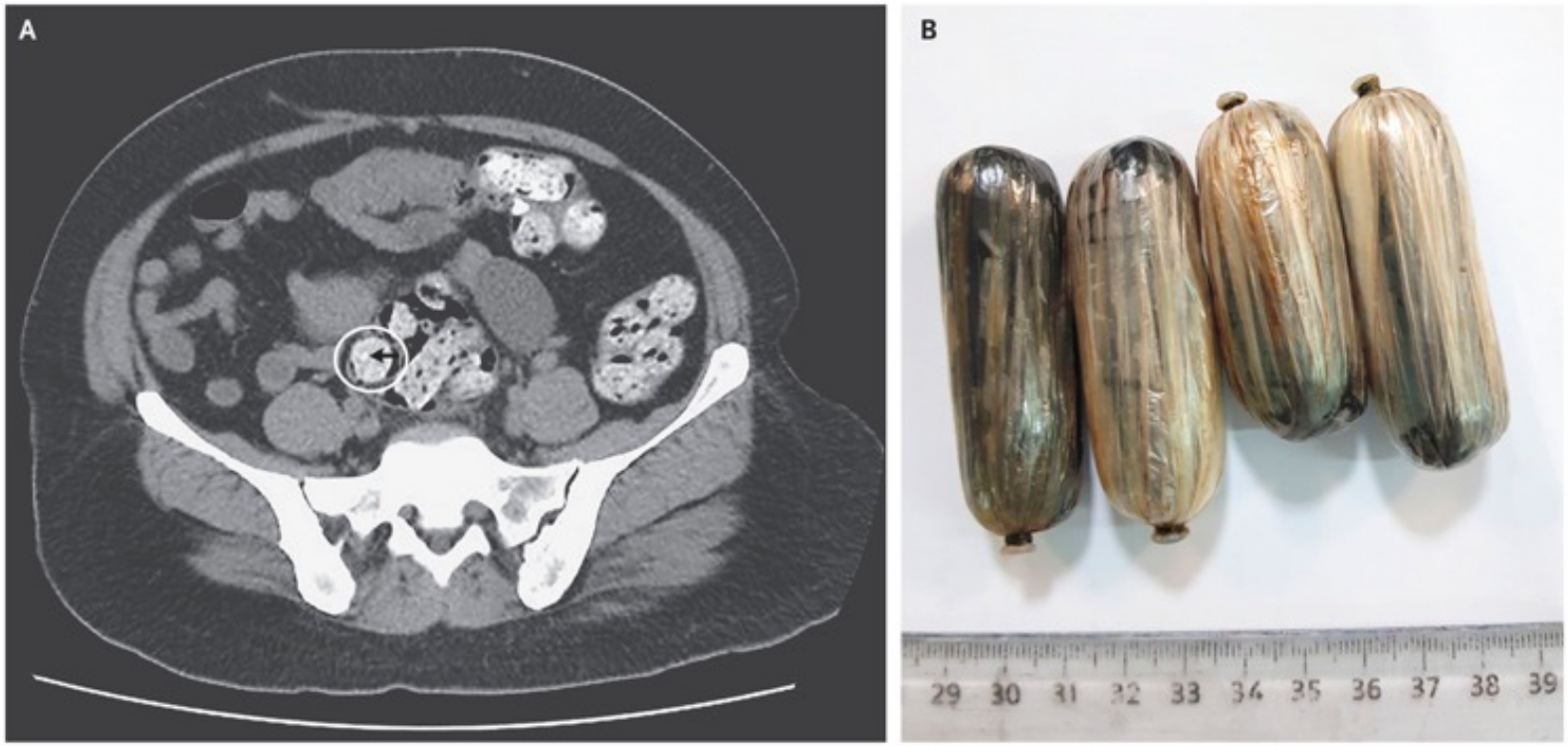

A 51-year-old woman was brought to the emergency department from a local international airport after reporting the ingestion of 30 packs of opium weighing 50 g each. The patient had no symptoms, and the results of physical examination were normal. Computed tomography of the abdomen and pelvis revealed several oval structures (Panel A, circle) with visible opacities (arrow); there was no evidence of bowel obstruction. Ingestion of lead-contaminated drug packs was suspected. Oral polyethylene glycol was administered, and the patient passed all packs (Panel B) without complication. Laboratory analysis of the contents of one pack confirmed the presence of opium; no other drugs were detected. The lead concentration in an opium sample was 3200 ppm. Because opium is often sold according to weight, heavy metals such as lead may be added to the opium during manufacturing or at the time of packing to increase its weight. Exposure to lead at such high concentrations can cause severe toxic effects that can manifest as neurologic and gastrointestinal signs and symptoms, including encephalopathy, altered mental status, seizures, abdominal pain, vomiting, constipation, and anorexia. The patient remained asymptomatic at the time of discharge, but the use and smuggling of lead-contaminated drugs is a public health concern.

A 39-year-old man presented to the emergency department with a 4-week history of increasing abdominal pain and constipation. Physical examination of the abdomen and the results on abdominal imaging, including ultrasonography and computed tomography, were normal. Laboratory investigations revealed a hemoglobin level of 12.5 g per deciliter (normal range, 14.0 to 17.5). Findings on upper endoscopy and colonoscopy were normal. Since the cause of the gastrointestinal symptoms was unclear, laboratory investigations for porphyria were performed. A 24-hour urine test showed an excretion level of delta aminolevulinic acid of 545 μmol per day (normal range, <49), and the lead level in blood was markedly elevated at 136 μg per deciliter (6.55 μmol per liter). Physical examination was repeated, and a gray line along the margins of the lower gums, known as Burton's line, was noted (arrow). Burton's line is a sign of chronic lead intoxication that develops when lead reacts with oral bacteria metabolites. The patient then confirmed a 10-year history of chewing opium. Analysis of a sample of the patient's opium revealed a lead concentration of 17 mg per 1 g of opium. Lead may sometimes be added to opium to increase its weight when it is sold. The patient was treated with chelating agents and was counseled about the importance of oral hygiene; he also stopped chewing opium. At follow-up 7 months after the initiation of treatment, the patient's abdominal pain and constipation had resolved, and Burton's line was markedly diminished.

A 58-Year-Old Woman with Paresthesia and Weakness of the Left Foot and Abdominal Wall

The patient had been well until 10 weeks before this presentation, when back pain developed between the shoulder blades. The pain resolved during the next 2 weeks, without an intervention. Six weeks before this presentation, numbness developed in a bandlike distribution around her trunk, with involvement of the area between the shoulder blades and the area under the breasts. Five weeks before this presentation, the numbness extended to the upper abdomen. The patient was unable to sit up from the supine position without using her arms, and she had abdominal distention. Four weeks before this presentation, paresthesia developed in the third, fourth, and fifth fingers of the left hand and the fourth and fifth fingers of the right hand. The patient was seen at a clinic at another hospital, and magnetic resonance imaging (MRI) of the spine was scheduled. However, 2 weeks before this presentation, the numbness extended to the genital area and urinary incontinence developed, prompting the patient to present to the emergency department of this hospital for evaluation. She had a history of hypertension, hypothyroidism, and symptomatic spinal stenosis, for which she had undergone L4–L5 decompression and bilateral medial facetectomy 6 years before this presentation. The blood glucose level was 291 mg per deciliter (16.2 mmol per liter; reference range, 70 to 110 mg per deciliter [3.9 to 6.1 mmol per liter]). The blood electrolyte levels were normal, as were the results of tests of renal and liver function, the complete blood count, and the differential count. Imaging studies were obtained.Three months before this presentation, the patient had noted an area of nonpruritic, nonpainful erythema (measuring 8 cm in diameter) on the left gluteal fold, surrounding what she had thought to be an insect bite.

MRI of the thoracic spine was performed 1 week after the patient was evaluated in the emergency department. Sagittal images of the thoracic spine were obtained along the midline. A T_2-weighted image (Panel A), a T_1-weighted image without contrast enhancement (Panel B), and a fat-saturated, T_1-weighted image with contrast enhancement (Panel C) show no specific evidence of cord signal abnormality, high-grade spinal stenosis, or abnormal enhancement, with allowance for expected vascularity along the cord surface.

We are not told whether she had Beevor's sign (deflection of the umbilicus away from a weak segment of the rectus abdominis muscle on activation of the abdominal-wall muscles). However, we know that she was unable to sit up from the supine position and had abdominal distention that was related to diminished abdominal-wall muscle tone. The presence of concurrent numbness rules out a myopathy, so I suspect the weakness of the abdominal-wall muscles localizes to the lower thoracic or upper lumbar nerve roots.

Let us now consider the patient's sensory symptoms. Reduced truncal sensation implies dysfunction of the sensory tracts in the spinal cord, sensory nerve roots, dorsal-root ganglia, or segmental nerves at the affected levels. This patient's sensory loss had a bandlike or suspended distribution, meaning that it had superior and inferior boundaries. The presence of a suspended sensory level could be consistent with a small central cord lesion or syrinx with interruption of decussating spinothalamic-tract fibers in the ventral commissure. Central cord lesions can cause pain, and if they are large enough, they can affect the anterior horns, resulting in areflexic segmental weakness. However, several features of this patient's presentation argue against a central cord lesion. Central cord lesions typically result in contiguous deficits, whereas this patient had noncontiguous numbness involving the lower cervical, lower thoracic, and sacral segments, without involvement of upper cervical and lower lumbar segments.

Diabetic Polyradiculopathy

There are several disorders that cause or mimic subacute polyradiculopathy or polyradiculoneuropathy with potentially normal findings on imaging of the spine, as described in this patient. Among the most common of these disorders is diabetic thoracic polyradiculopathy, which is the pathophysiological equivalent of diabetic cervical or lumbosacral radiculoplexus neuropathy. One quarter of cases of acute-to-subacute thoracic polyradiculopathy coincide with a new diagnosis of diabetes mellitus, which fits with this patient's newly discovered elevated blood glucose and glycated hemoglobin levels.

Multiple Mononeuropathies

Although the syndrome of multiple mononeuropathies (mononeuritis multiplex) is not a polyradiculopathy, it must be considered in this patient with painful, multifocal sensory loss, given the importance of early recognition of an underlying systemic or peripheral nervous system vasculitis.[3] However, in patients with multiple mononeuropathies, symptoms develop in a haphazard peripheral-nerve distribution, and this patient's symptoms were more radicular.

Inflammatory Polyneuropathy

Another important consideration in this patient is multifocal acquired demyelinating sensory and motor neuropathy (MADSAM), a variant of chronic inflammatory demyelinating polyradiculoneuropath

Cancer

Leptomeningeal carcinomatosis or lymphomatosis is a diagnostic consideration in this patient. Spinal and cranial nerve roots may be damaged as they pass through diseased meninges. However, this syndrome is rarely part of the initial presentation of cancer, and this patient did not have other signs or symptoms suggestive of advanced cancer. In addition, she did not have findings suggestive of leptomeningeal disease on MRI. Although cerebrospinal fluid (CSF) analysis or meningeal biopsy would be necessary to rule out this diagnosis, I suspect that other possible causes of her illness are more likely.

Neurosarcoidosis

Neurosarcoidosis has protean manifestations, which can include thoracic polyradiculopathy. Sarcoidosis has a predilection for involvement of sensory nerve roots and ganglia but most commonly affects cranial nerve roots and the optic nerves.

Infection

Could this patient have herpes zoster? Reactivation of latent varicella–zoster virus arises in the dorsal-root ganglia and spreads centrifugally to the skin along sensory nerves or vasa nervorum. Patients with herpes zoster often have severe dermatomal pain and sensory deficits; a segmental rash is common but not always present. In some cases, patients with herpes zoster have segmental weakness of the arms, legs, or thoracic-wall muscles. Patients who have Lyme meningoradiculitis typically present 2 to 18 weeks after infection, during the early disseminated phase, with pain, sensory loss, and areflexic weakness. Over half of patients with Lyme meningoradiculitis present with seventh cranial nerve palsy — a manifestation of Lyme disease that many recognize — but any cranial or spinal nerve root may be involved. Several clues in this patient's history point us toward this diagnosis. First, she was living in a wooded area in a region of the country where Lyme disease is endemic. Second, she presented in early autumn, and approximately 3 months earlier, she had had a small, uniformly erythematous, painless, nonpruritic rash that was consistent with the hallmark skin lesion of early Lyme disease, erythema migrans. Although the classic rash of Lyme disease is described as having an area of central clearing (bull's eye), in many cases, it does not. Third, the location of the patient's rash on the left gluteal fold is a common site of tick bites; other locations include the axillae, hairline, groin, and beltline.[6] Given the seasonal timing of this patient's presentation, the history of a rash consistent with erythema migrans, and her clinical syndrome of polyradiculopathy, I suspect that this patient had Lyme meningoradiculitis in the context of early disseminated Lyme disease. The next step in the diagnosis would be serum and CSF analysis for antibodies against *Borrelia burgdorferi*.

We thought this patient's presentation was most consistent with an infectious polyradiculopathy; her recent rash and associated risk factors for Lyme disease made Lyme radiculopathy our leading diagnosis. A lumbar puncture was performed, and CSF analysis revealed a glucose level of 115 mg per deciliter (6.4 mmol per liter; reference range, 50 to 75 mg per deciliter [2.8 to 4.2 mmol per liter]), a total protein level of 128 mg per deciliter (reference range, 5 to 55), and a nucleated-cell count of 46 per cubic millimeter (reference range, 0 to 5). We requested CSF and serum serologic testing for Lyme disease to establish the diagnosis.

The laboratory tests that were performed to support the diagnosis were serum antibody tests for Lyme borreliosis. A first-tier enzyme-linked immunosorbent assay (ELISA) was reactive, prompting the performance of second-tier IgM and IgG immunoblot assays. The serum IgM immunoblot assay showed 1 of 3 specific bands (the 39-kDa band), which is a negative outcome according to Centers for Disease Control and Prevention (CDC) criteria. The serum IgG immunoblot assay showed 9 of 10 specific bands, which is a positive outcome according to CDC criteria. The tests indicated an expanded *B. burgdorferi* antibody response with a switch of immunoglobulin class from IgM to IgG; these results are associated with *B. burgdorferi* infection of at least 1 or 2 months' duration, and they correlate well with the patient's clinical history. In addition to serum antibody testing, CSF IgM and IgG immunoblot assays for *B. burgdorferi* and CSF polymerase-chain-reaction (PCR) assays for *B. burgdorferi*, *B. mayonii*, *B. garinii*, and *B. afzelii* were performed.

The absence of distal symmetric sensory peripheral neuropathy and the rapid development of asymmetric polyradiculopathy accompanied by CSF pleocytosis made the diagnosis of diabetic polyradiculopathy improbable. The patient's pain diminished over a 4-week period. When we saw her in the clinic 4 months after the initiation of treatment with ceftriaxone, her sensation and strength of the abdominal wall had increased such that she could contract the rectus abdominis muscles while standing, but she continued to have difficulty sitting up from the supine position. The weakness of the left foot had diminished, but she still had difficulty walking on the heel.

THE LANCET

Volume 392 · Number 10159 · Pages 1683-2138 · November 10-16, 2018 www.thelancet.com

The Global Burden of Disease Study 2017

Das Projekt Global Burden of Disease (GBD) hat sich die Quantifizierung von Todesfällen, Krankheit, Behinderung und Risikofaktoren zur Aufgabe gemacht; aufgeteilt nach Regionen und Bevölkerungsgruppen. Anhand dieser Informationen ist es möglich, wichtige Informationen abzuwägen, die von politischen Entscheidungsträgern zur Prioritätensetzung genutzt werden können. Die GBD-Studie wurde 1992 von der Harvard School of Public Health (an der Harvard University), der Weltgesundheitsorganisation und der Weltbank ins Leben gerufen. Sie quantifiziert und untersucht 135 Krankheiten und Behinderungen, und versucht anhand dieser Daten weltweit die Ursachen für Sterblichkeit und Krankheiten zu ergründen. Ziel ist es, anhand dieser Daten, Prognosen zu erstellen, die eine weltweite Verbesserung der Gesundheitszustände erlauben.
Als Maßeinheit für 'Lebensqualität' wurde das Disability-Adjusted Life Year (DALY) eingeführt – ein negativer Behinderungsindex, der bei hohen Werten eine niedrige Lebensqualität beschreibt. Das DALY misst Gesundheitslücken. Es beschreibt den Unterschied zwischen einer tatsächlichen Situation und einer idealen Situation, in der jede Person bei voller Gesundheit bis zu dem Alter lebt, das den Standardwerten der Lebenserwartung entspricht. Diese Standard-Lebenserwartung ist basierend auf Sterbetafeln bei der Geburt mit 80 Jahren für Männer und 82,5 Jahren für Frauen festgelegt. Die mit einer Behinderung gelebte und die durch vorzeitigen Tod verlorene Lebenszeit wird im DALY kombiniert: die durch vorzeitigen Tod verlorenen Lebensjahre (Years of life lost = YLL) entsprechen im Wesentlichen der Anzahl von Todesfällen multipliziert mit der verbliebenen Lebenserwartung in dem Alter, in dem der Tod vorzeitig eintritt.
Die Quantifizierung der Krankheitslast hilft mittels einer nachvollziehbaren und standardisierten Herangehensweise, Prioritäten für eine Verbesserung der Gesundheit der Bevölkerung zu definieren. Allerdings sollten die Informationen zu Mortalität, Risikofaktoren und Krankheitslast durch Untersuchungen zur Kosteneffektivität und Interventionen und zu sozioökonomischen und kulturellen Faktoren und Präferenzen ergänzt werden.
Developed by GBD researchers and used to help produce these estimates, the Socio-demographic Index (SDI) is a summary measure of a geography's socio-demographic development. It is based on average income per person, educational attainment, and total fertility rate (TFR). SDI contains an interpretable scale: zero represents the lowest income per capita, lowest educational attainment, and highest TFR observed across all GBD geographies from 1980 to 2015, and one represents the highest income per capita, highest educational attainment, and lowest TFR. This dataset provides tables with SDI values for all estimated GBD 2015 geographies for 1980–2015 and groupings by geography based on 2015 values.

Global, regional, and national age-sex-specific mortality and life expectancy, 1950–2017: a systematic analysis for the Global Burden of Disease Study 2017

Assessments of age-specific mortality and life expectancy have been done by the UN Population Division, Department of Economics and Social Affairs (UNPOP), the United States Census Bureau, WHO, and as part of previous iterations of the Global Burden of Diseases, Injuries, and Risk Factors Study (GBD). Previous iterations of the GBD used population estimates from UNPOP, which were not derived in a way that was internally consistent with the estimates of the numbers of deaths in the GBD. The present iteration of the GBD, GBD 2017, improves on previous assessments and provides timely estimates of the mortality experience of populations globally. The GBD uses all available data to produce estimates of mortality rates between 1950 and 2017 for 23 age groups, both sexes, and 918 locations, including 195 countries and territories and subnational locations for 16 countries. Data used include vital registration systems, sample registration systems, household surveys (complete birth histories, summary birth histories, sibling histories), censuses (summary birth histories, household deaths), and Demographic Surveillance Sites. In total, this analysis used 8259 data sources. Estimates of the probability of death between birth and the age of 5 years and between ages 15 and 60 years are generated and then input into a model life table system to produce complete life tables for all locations and years. Fatal discontinuities and mortality due to HIV/AIDS are analysed separately and then incorporated into the estimation. We analyse the relationship between age-specific mortality and development status using the Socio-demographic Index, a composite measure based on fertility under the age of 25 years, education, and income. There are four main methodological improvements in GBD 2017 compared with GBD 2016: 622 additional data sources have been incorporated; new estimates of population, generated by the GBD study, are used; statistical methods used in different components of the analysis have been further standardised and improved; and the analysis has been extended backwards in time by two decades to start in 1950.

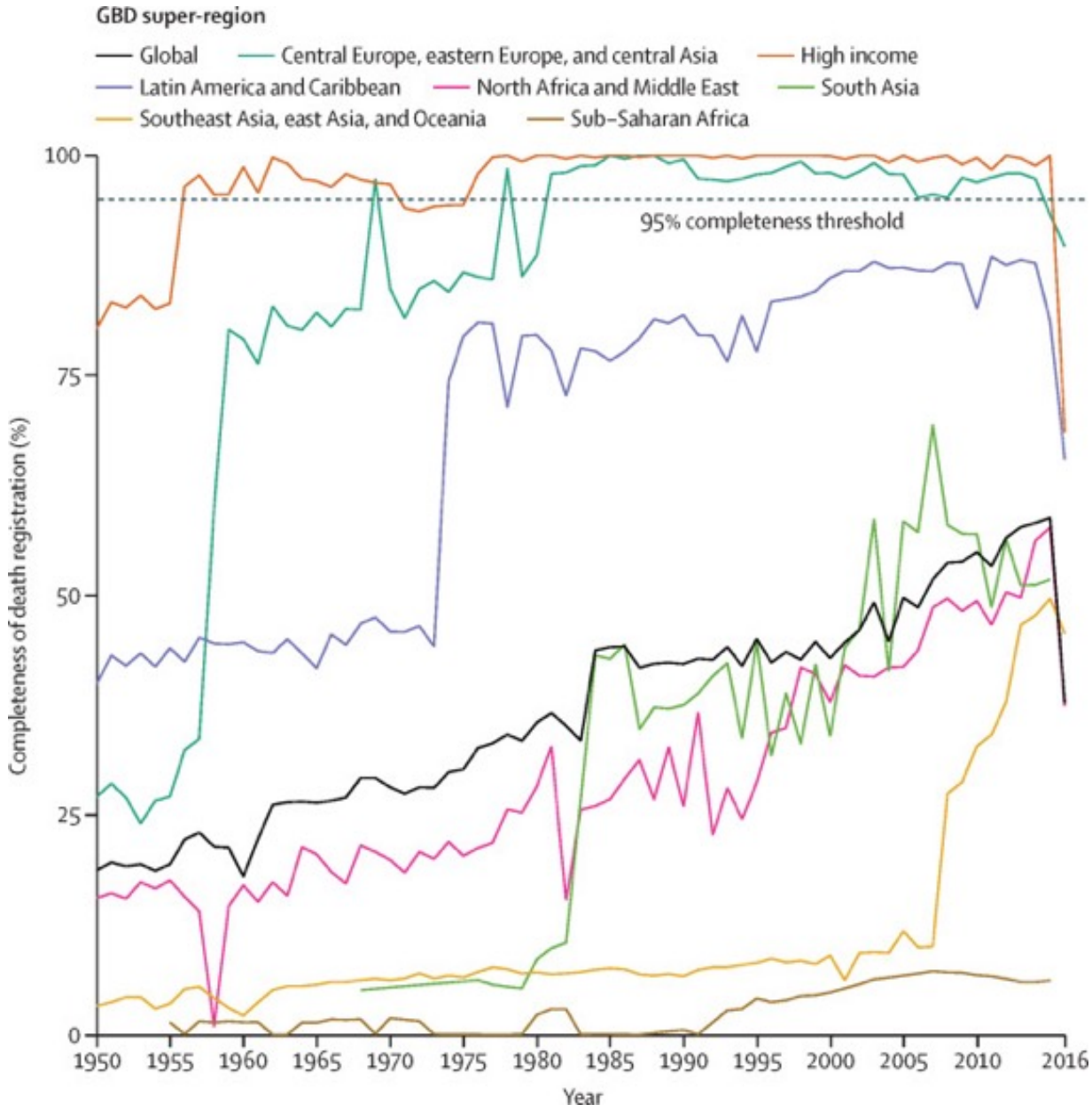

Estimated proportion of deaths that are registered and reported globally and by GBD super-region, for both sexes combined, 1950–2016

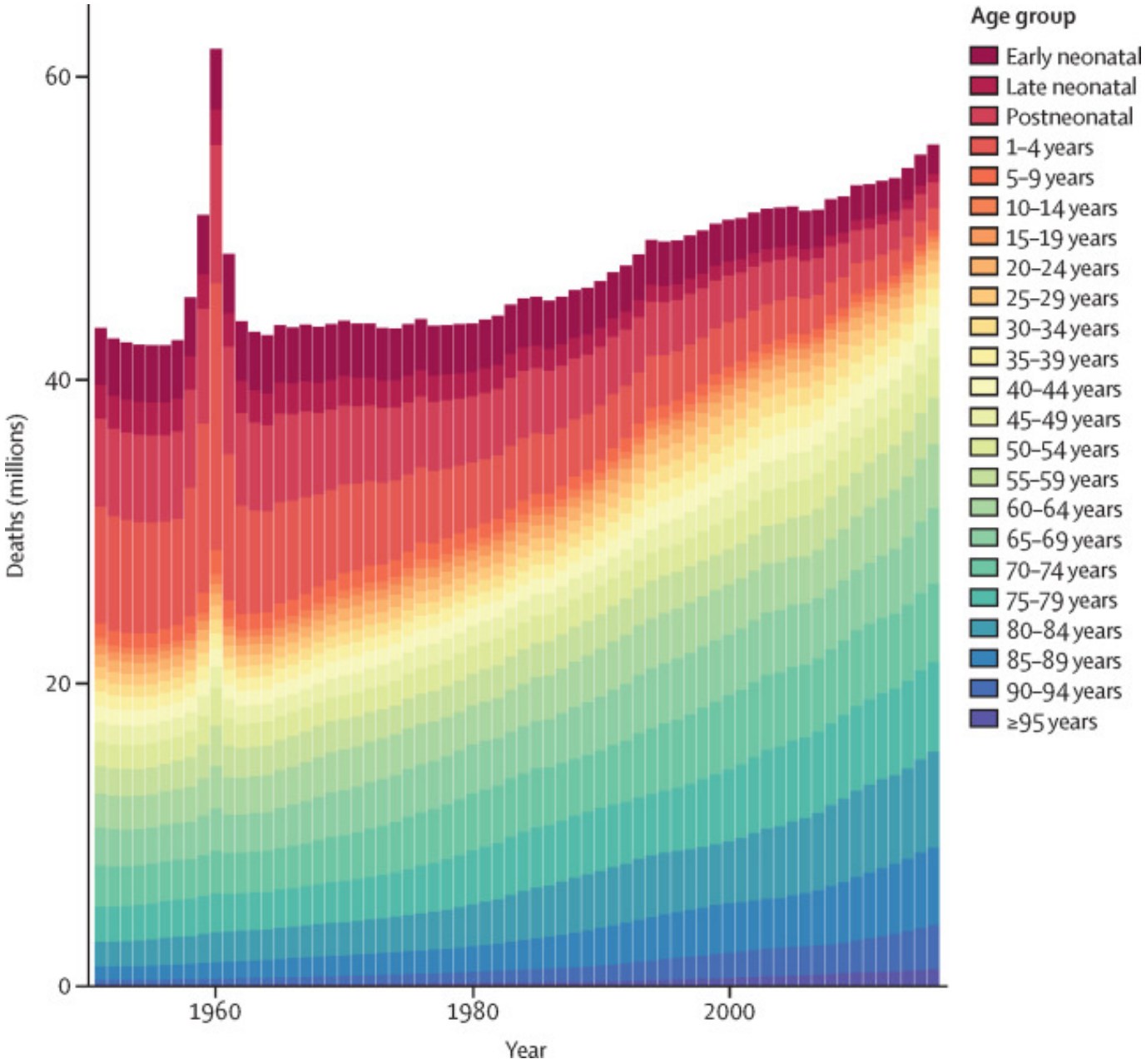

Total number of deaths by age, globally, for both sexes combined, 1950–2017

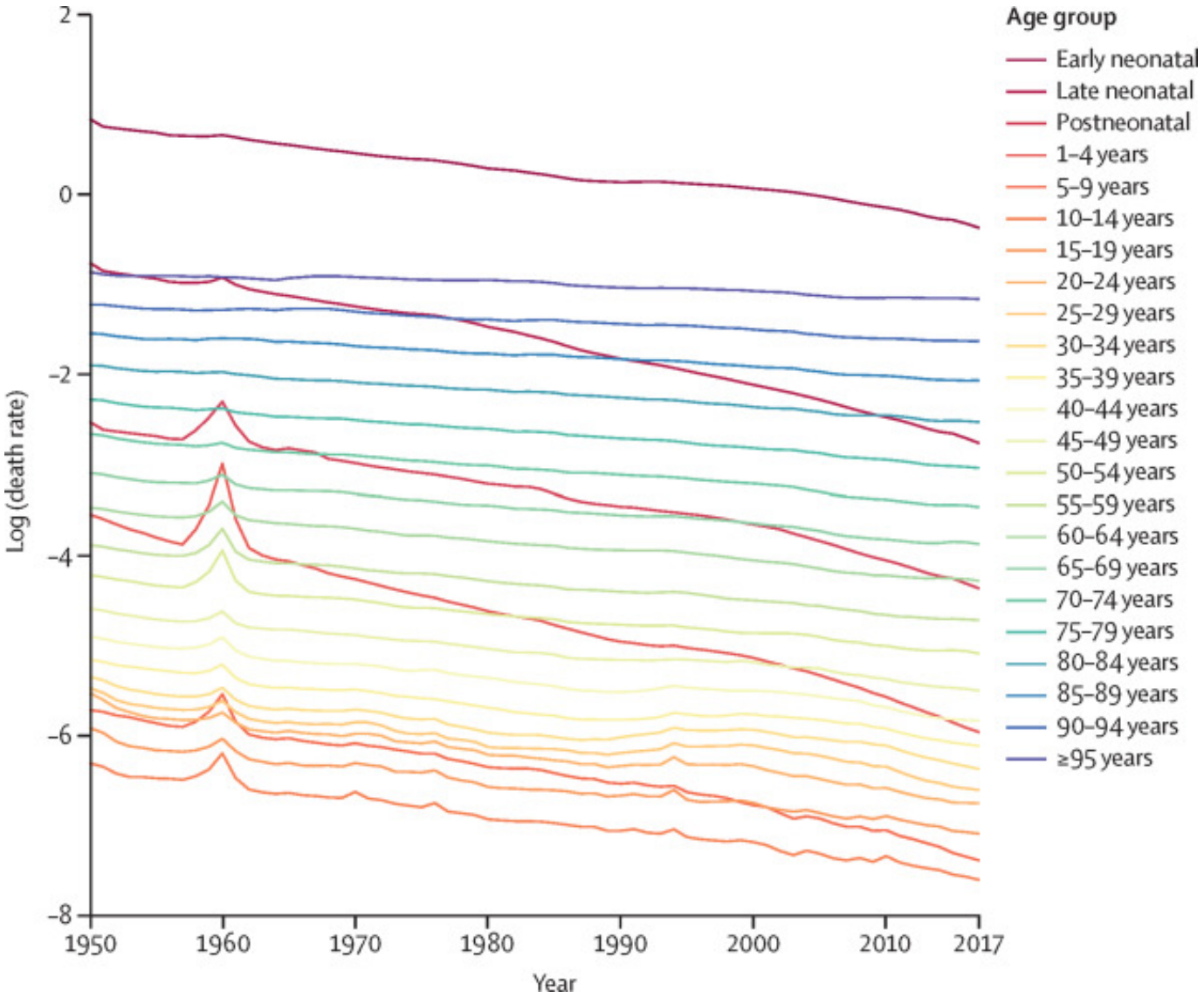

Natural logarithm of age-specific mortality rates, globally, for both sexes combined, 1950–2017

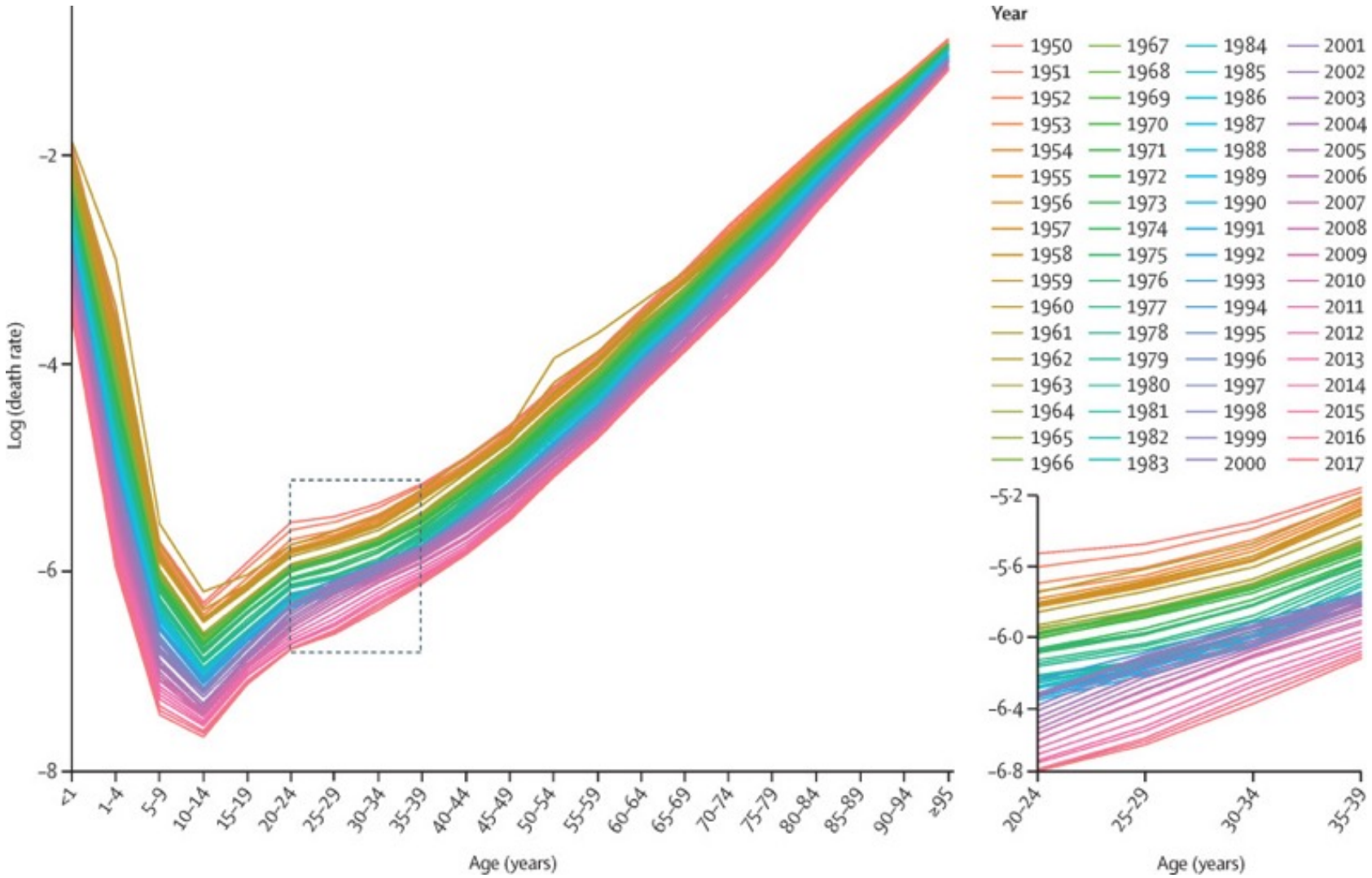

Global log (death rate) age-pattern for both sexes combined, by year, 1950–2017

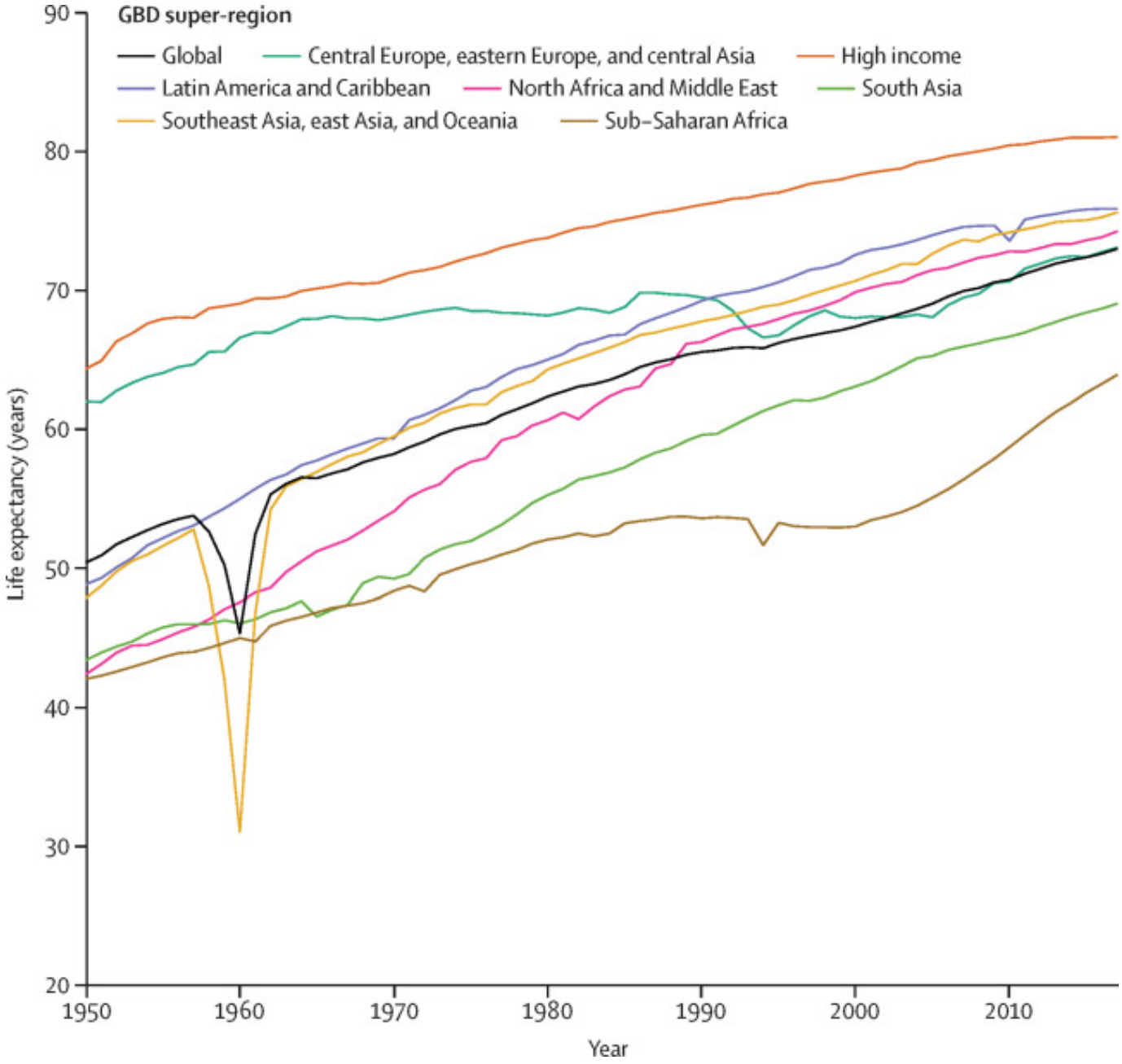

Life expectancy at birth and by GBD super-region for both sexes combined, 1950–2017

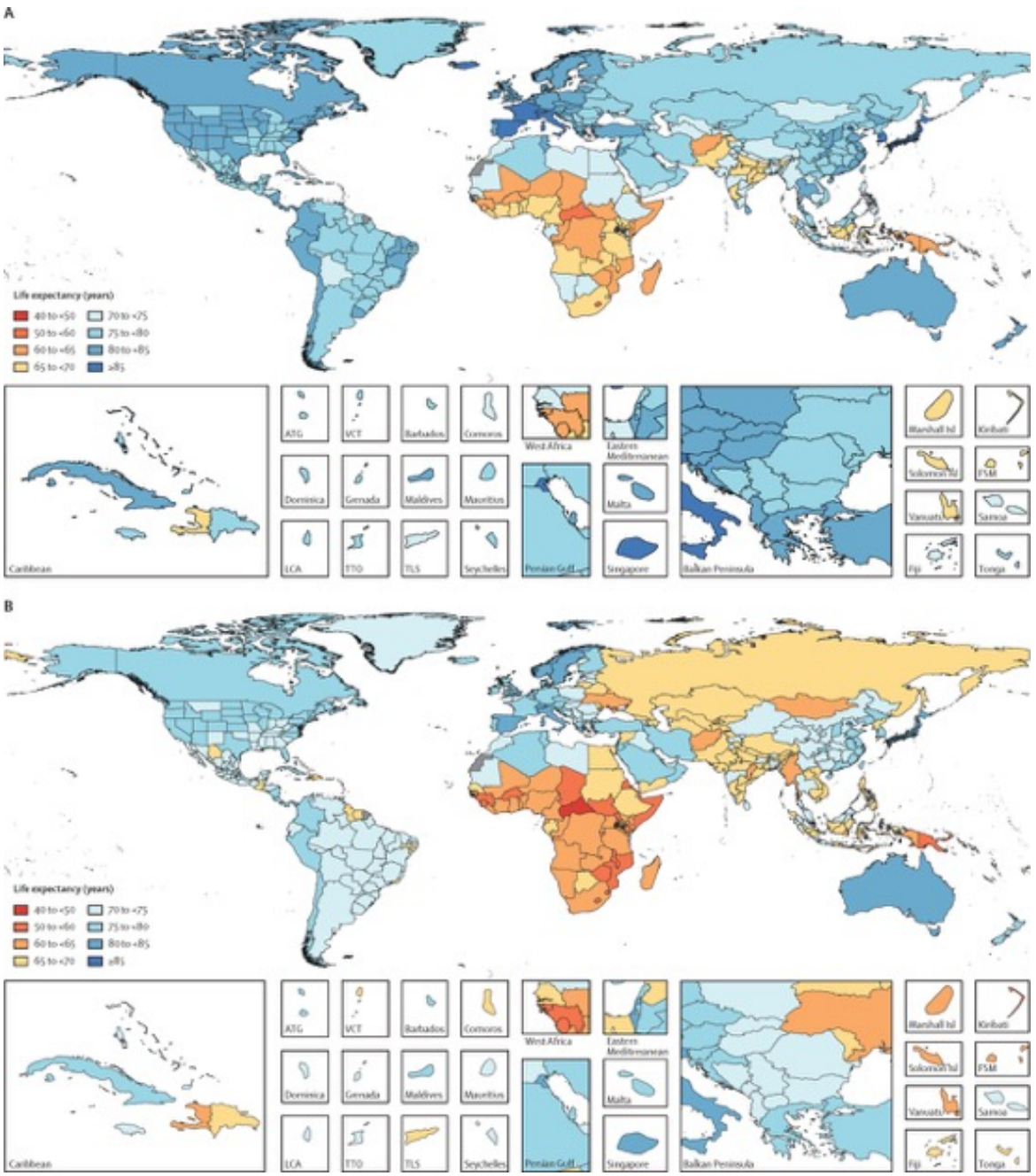

Life expectancy at birth, by location, for females (A) and males (B), 2017, and difference in life expectancy at birth, by location, for females (C) and males (D) between 2017 and 1950

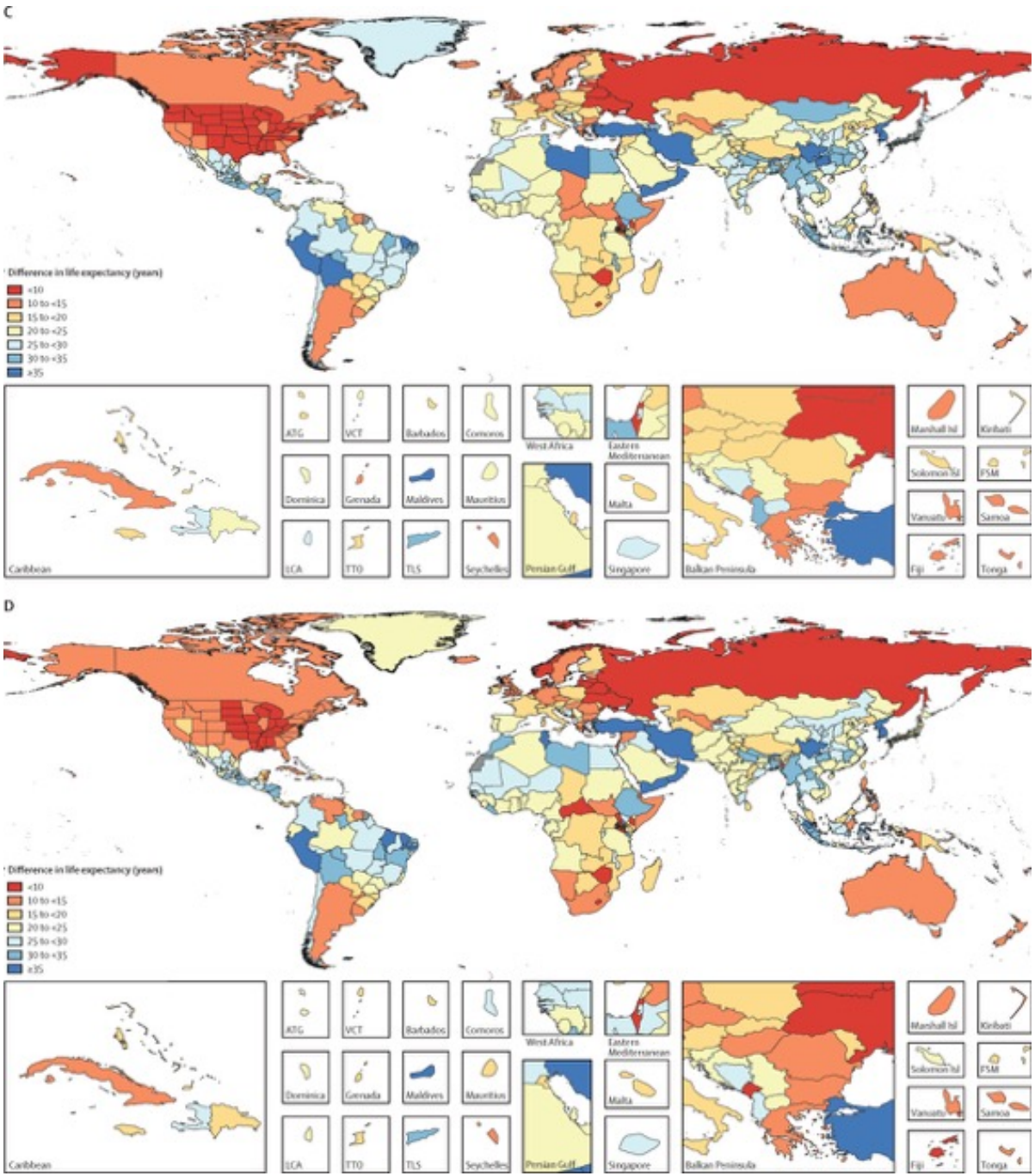

Life expectancy at birth, by location, for females (A) and males (B), 2017, and difference in life expectancy at birth, by location, for females (C) and males (D) between 2017 and 1950

Added value of this study

The most important changes in GBD 2017 are the independent estimation of population and a comprehensive update on fertility, which are described in a separate paper. There are several countries with significant differences in population size between the UNPOP estimates and the new GBD estimates. Since population is the denominator for mortality calculations, this leads to substantial changes in life expectancy and age-specific mortality rates in several countries. There were four major data additions and improvements that related to the estimation of mortality. First, for the estimation of population size, we systematically searched for census data and found data from 1257 censuses, which are now used in the analysis and which enabled an extended analysis of completeness using death distribution methods in more locations than previous iterations. Second, in the estimation of adult mortality, we included data from 31 Demographic Surveillance Sites (DSS) which were adjusted based on the relationship between DSS under-5 death rates and national under-5 death rates. Third, we used published sources to create a database of fatal discontinuities from conflicts and natural disasters that extends back to 1950; each fatal discontinuity has been given a unique ID that tags the reported deaths to a location, date, and type of discontinuity. Fourth, GBD 2017 included an additional 622 data sources that were not available for GBD 2016 and which do not fall into the three categories already described. The main methodological improvements fall into two categories: the first category is enhancements to the modelling framework, which improved the estimation of both child mortality, defined as the probability of death below the age of 5 years, and adult mortality, a term we use to refer to the probability of death between ages 15 and 60 years. For child mortality, we standardised hyperparameter selection for the spatiotemporal Gaussian process regression models, which enhances the comparability of results between locations and across time. For adult mortality, we also standardised hyperparameter selection and added child mortality as a covariate to the model. These changes had minimal effect on the mean estimate but changed the width of the uncertainty intervals in small populations and locations with sparse data. The second category encompasses three substantial improvements to the GBD model life table system: first, we revised the entire database to reflect the change in population counts. Second, each life table in the database was assigned a quality score using explicit criteria related to the variance in the slope of the death rate with respect to age, reductions in mortality at older ages compared with younger ages (age >60 years), and other unexpected crossovers. On the basis of these quality scores, life tables have been assigned to three categories: high quality for universal use, acceptable quality for use in the creation of location-specific standards, and unacceptable quality. Third, we estimated complete single-year life tables for each sex, location, and year instead of abridged life tables as in previous iterations of the GBD. In GBD 2017, for the first time, we are reporting a complete time series of trends in age-specific mortality and life expectancy since 1950. The extension of the analysis back in time provides the opportunity to analyse and report on longer-term trends in age-specific mortality.

Global, regional, and national comparative risk assessment of 84 behavioural, environmental and occupational, and metabolic risks or clusters of risks for 195 countries and territories, 1990–2017: a systematic analysis for the Global Burden of Disease Study 2017

Summary

Background

The Global Burden of Diseases, Injuries, and Risk Factors Study (GBD) 2017 comparative risk assessment (CRA) is a comprehensive approach to risk factor quantification that offers a useful tool for synthesising evidence on risks and risk–outcome associations. With each annual GBD study, we update the GBD CRA to incorporate improved methods, new risks and risk–outcome pairs, and new data on risk exposure levels and risk–outcome associations.

Methods

We used the CRA framework developed for previous iterations of GBD to estimate levels and trends in exposure, attributable deaths, and attributable disability-adjusted life-years (DALYs), by age group, sex, year, and location for 84 behavioural, environmental and occupational, and metabolic risks or groups of risks from 1990 to 2017. This study included 476 risk–outcome pairs that met the GBD study criteria for convincing or probable evidence of causation. We extracted relative risk and exposure estimates from 46 749 randomised controlled trials, cohort studies, household surveys, census data, satellite data, and other sources. We used statistical models to pool data, adjust for bias, and incorporate covariates. Using the counterfactual scenario of theoretical minimum risk exposure level (TMREL), we estimated the portion of deaths and DALYs that could be attributed to a given risk. We explored the relationship between development and risk exposure by modelling the relationship between the Socio-demographic Index (SDI) and risk-weighted exposure prevalence and estimated expected levels of exposure and risk-attributable burden by SDI. Finally, we explored temporal changes in risk-attributable DALYs by decomposing those changes into six main component drivers of change as follows: (1) population growth; (2) changes in population age structures; (3) changes in exposure to environmental and occupational risks; (4) changes in exposure to behavioural risks; (5) changes in exposure to metabolic risks; and (6) changes due to all other factors, approximated as the risk-deleted death and DALY rates, where the risk-deleted rate is the rate that would be observed had we reduced the exposure levels to the TMREL for all risk factors included in GBD 2017.

Key messages

- The Global Burden of Diseases, Injuries, and Risk Factors Study (GBD) 2017 expands on GBD 2016 with the estimation of one new risk factor—bullying victimisation—and 80 new risk–outcome pairs, making a total of 476 risk–outcome pairs. The study further investigates the drivers of changes in risk-attributable burden and explores the relationship between development and risk exposure.
- In 2017, 34·1 million (95% uncertainty interval [UI] 33·3–35·0) deaths and 1·21 billion (1·14–1·28) disability-adjusted life-years (DALYs) were attributable to risk factors included in GBD 2017. All included risks combined contributed to 61·0% (59·6–62·4) of deaths and 48·3% (46·3–50·2) of DALYs worldwide.
- The five leading risks in 2017 were high systolic blood pressure, smoking, high fasting plasma glucose, high body-mass index, and short gestation for birthweight.
- DALY-based ranks for all metabolic risks increased between 1990 and 2017 for both males and females. Consequently, four of the five leading risks were behavioural risks in 1990, whereas three of the five leading risks were metabolic risks in 2017.
- Between 2007 and 2017, the absolute number of risk-attributable DALYs declined by 3·44% (95% UI 2·47–4·40). During that period, exposures to behavioural, environmental, and occupational risks declined (improved), but these gains were somewhat offset by increases in exposure to metabolic risks, population growth, and population ageing.
- Socioeconomic development was strongly associated with exposure levels for many risks. Among the leading risks, unsafe water, household air pollution, and child wasting show pronounced decreasing trends with development. Conversely, smoking, alcohol use, drug use, and high low-density lipoprotein cholesterol all show a pronounced increasing trend with development.

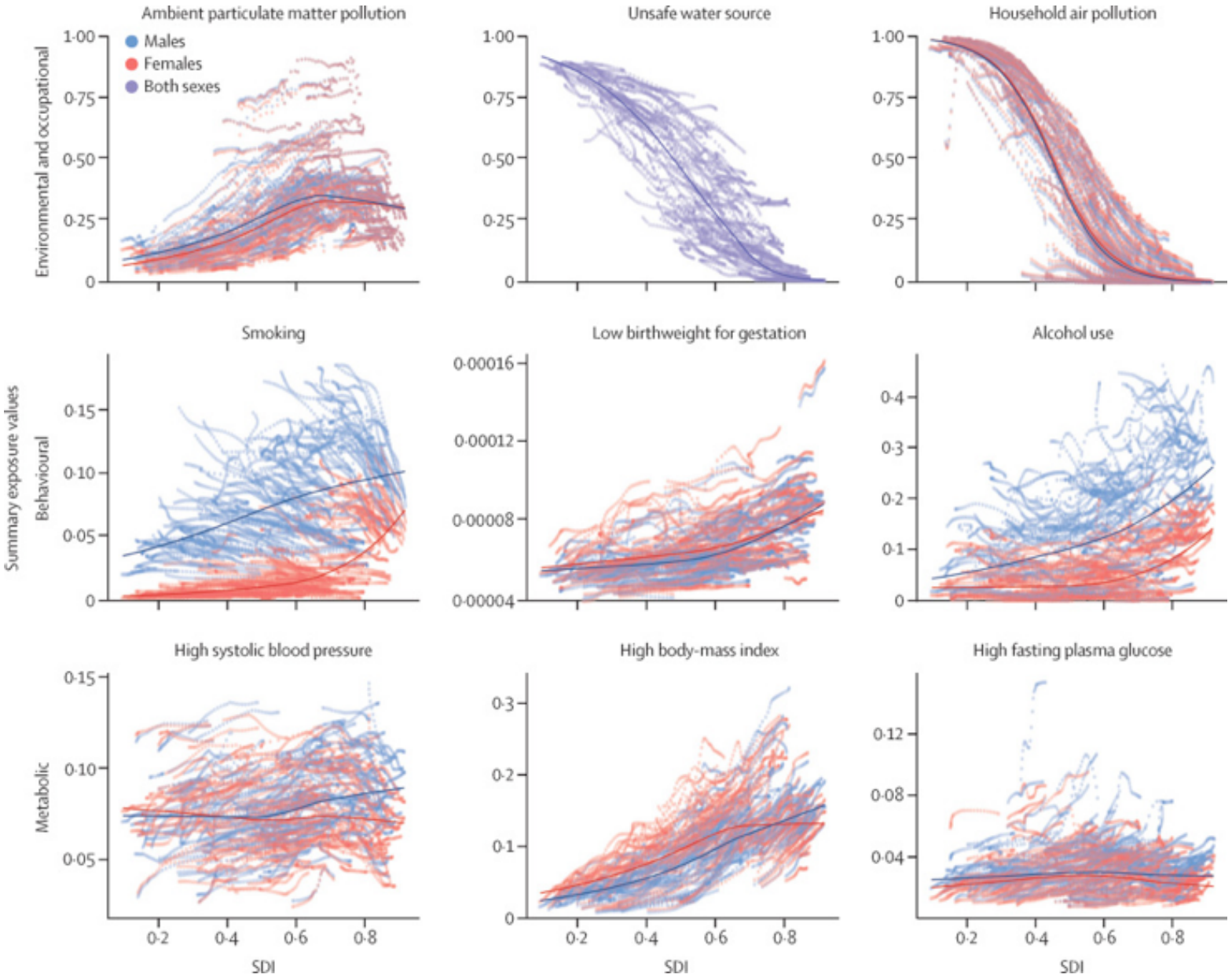

Relationship between age-standardised summary exposure values and SDI for three of the top environmental and occupational, behavioural, and metabolic risk factors by number of attributable DALYs globally

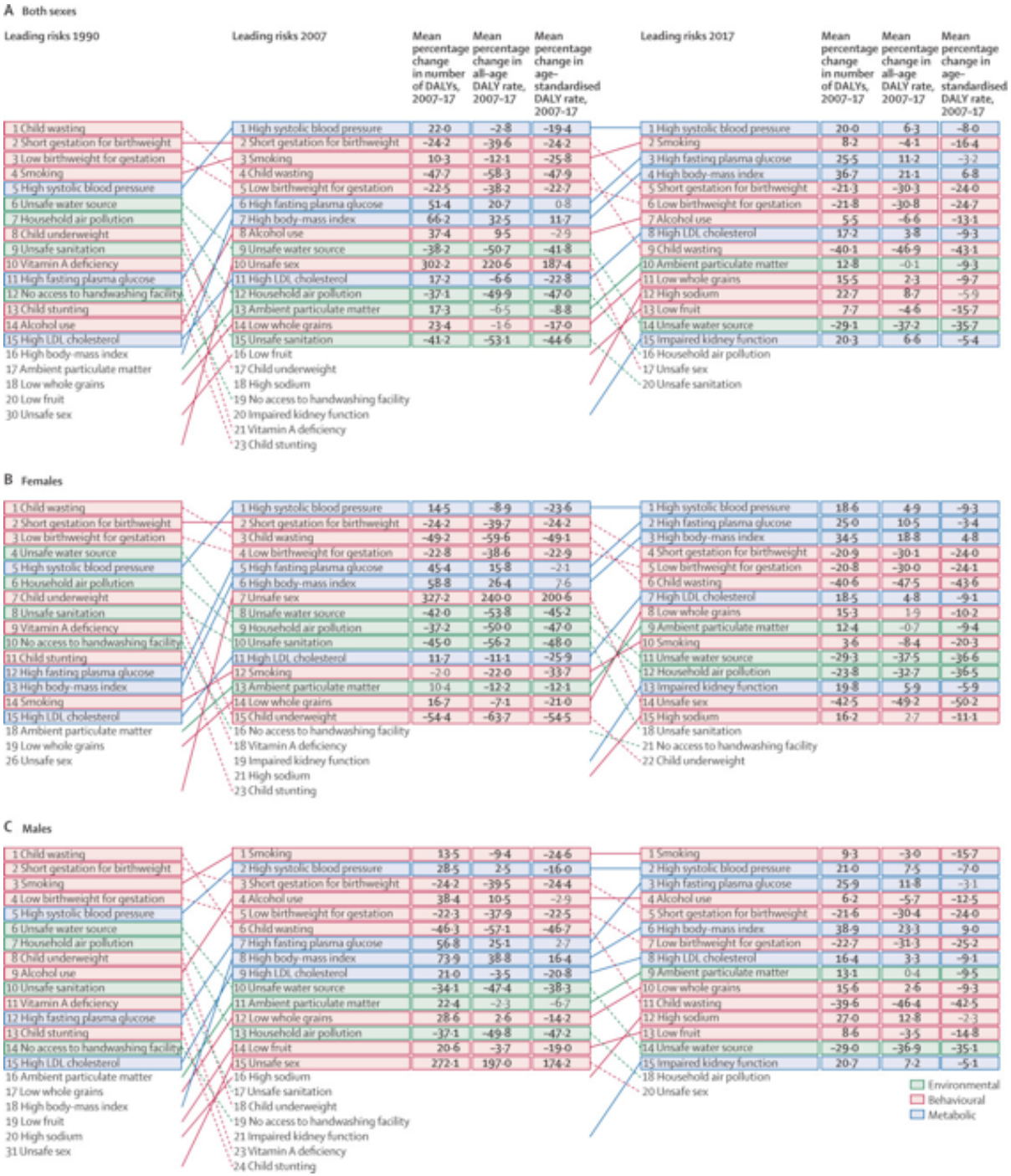

Leading 15 Level 4 risk factors by attributable DALYs at the global level, 1990, 2007, and 2017, for both sexes (A), females (B), and males (C)

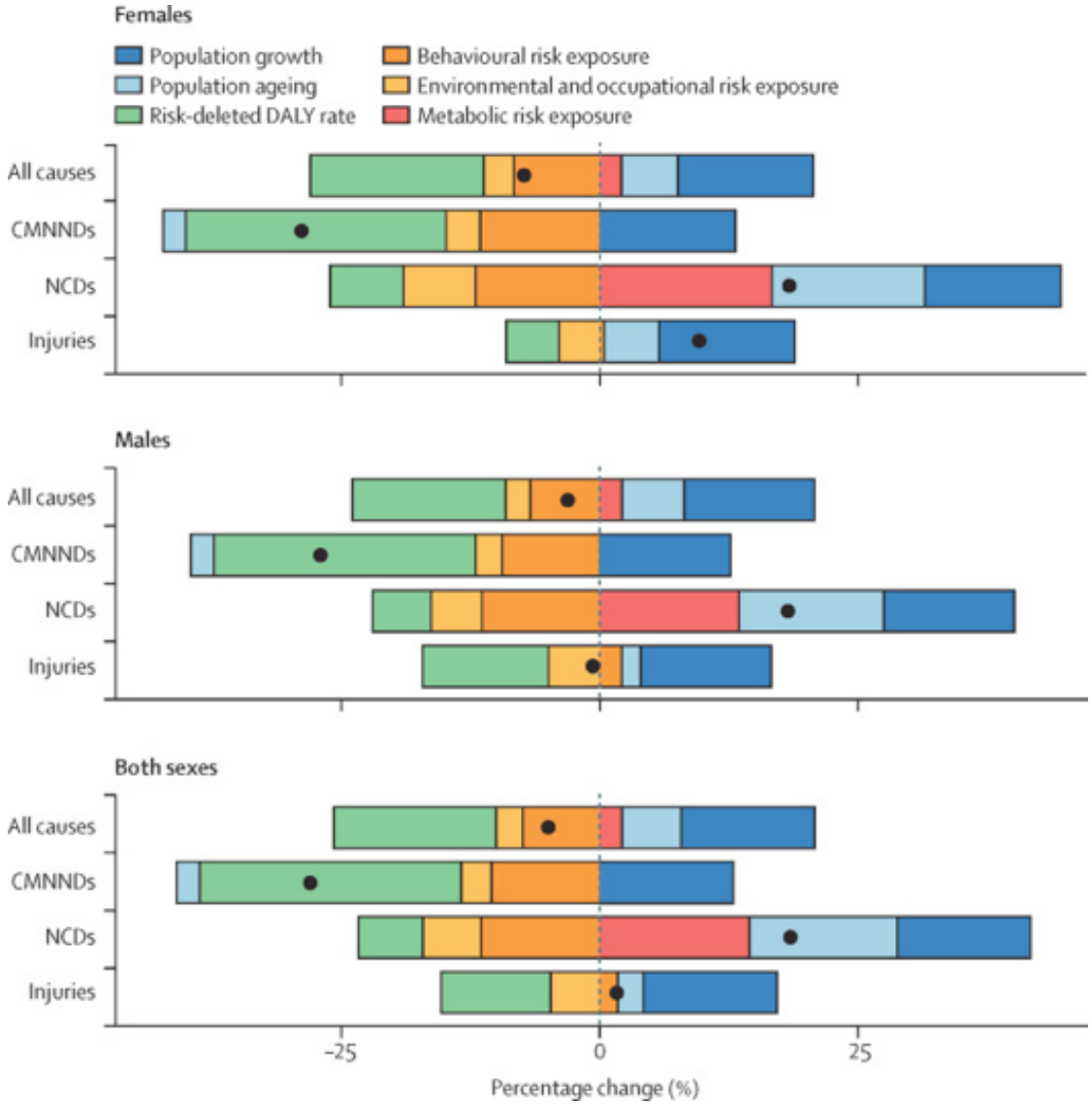

Percentage change in risk-attributable DALYs at the global level in 2007–17, due to population growth, population ageing, changes in exposure to Level 1 risk factors, and changes in risk-deleted DALY rates, for females, males, and both sexes
Results are shown for all causes combined, CMNNDs, NCDs, and injuries. The black dot on each bar shows total percentage change. The risk-deleted DALY rate is the expected DALY rate if the exposure level for all risk factors were reduced to the theoretical minimum risk exposure level. Changes in the risk-deleted rate might result from changes in risks and risk–outcome pairs that are not currently included in the Global Burden of Diseases, Injuries, and Risk Factors Study or changes in other factors such as treatment. The change in CMNNDs and injuries due to metabolic risk exposure for both males and females is not zero but is too small to visualise because of the small number of risk–outcome pairs. CMNNDs=communicable, maternal, neonatal, and nutritional diseases. DALYs=disability-adjusted life-years. NCDs=non-communicable diseases.

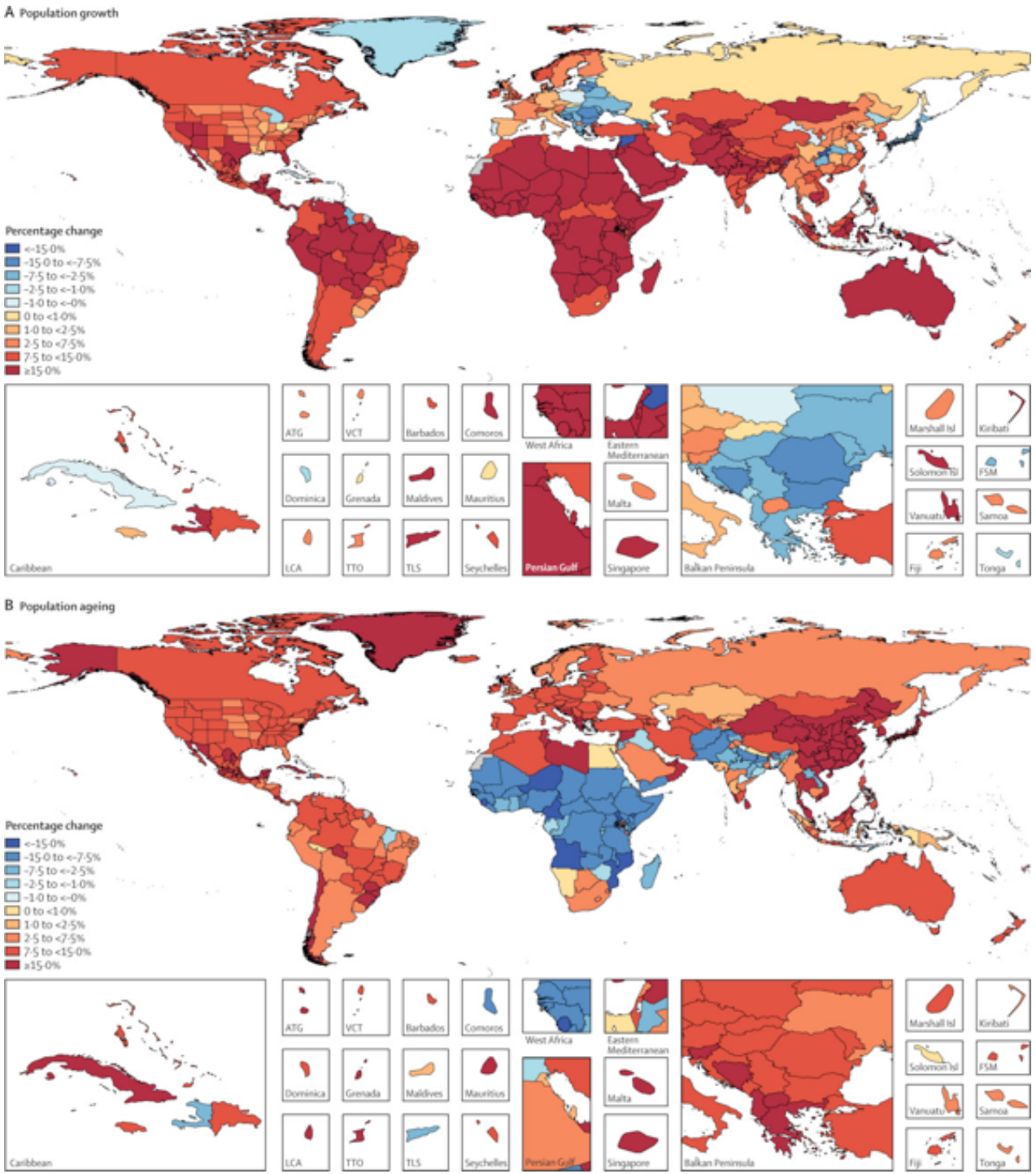

Percentage change in the absolute number of all-cause risk-attributable DALYs for both sexes, by location, 2007–17

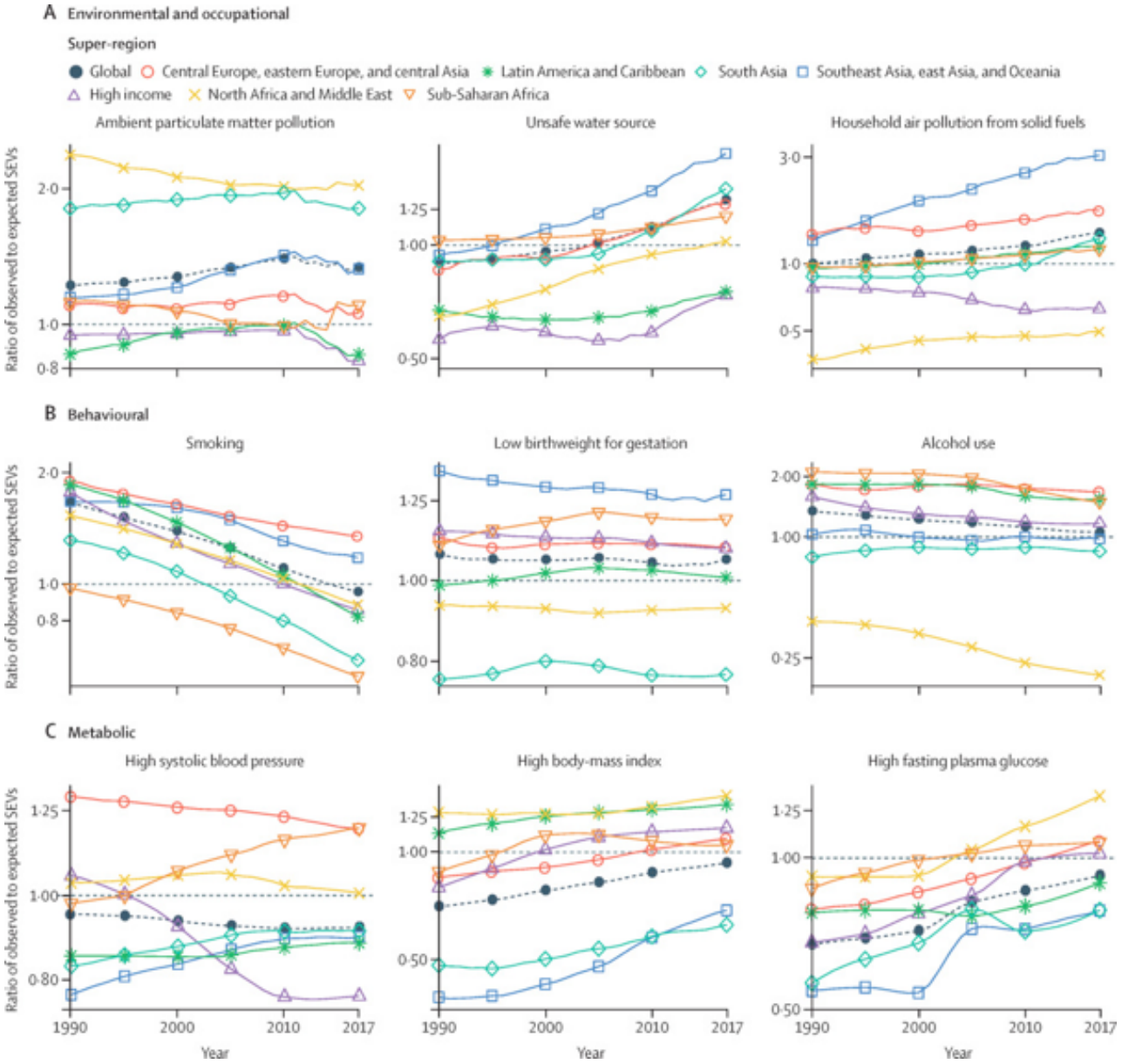

Trends in the ratios of observed SEVs to SEVs expected based on SDI, by super-region, for both sexes, 1990–2017

Trends are for three of the top environmental (A), behavioural (B), and metabolic (C) risk factors by number of attributable DALYs globally. Observed to expected ratios are based on age-standardised SEVs. y-axes are on a log scale with the range scaled appropriately for each risk factor. DALYs=disability-adjusted life-years. SDI=Socio-demographic Index. SEV=summary exposure value.

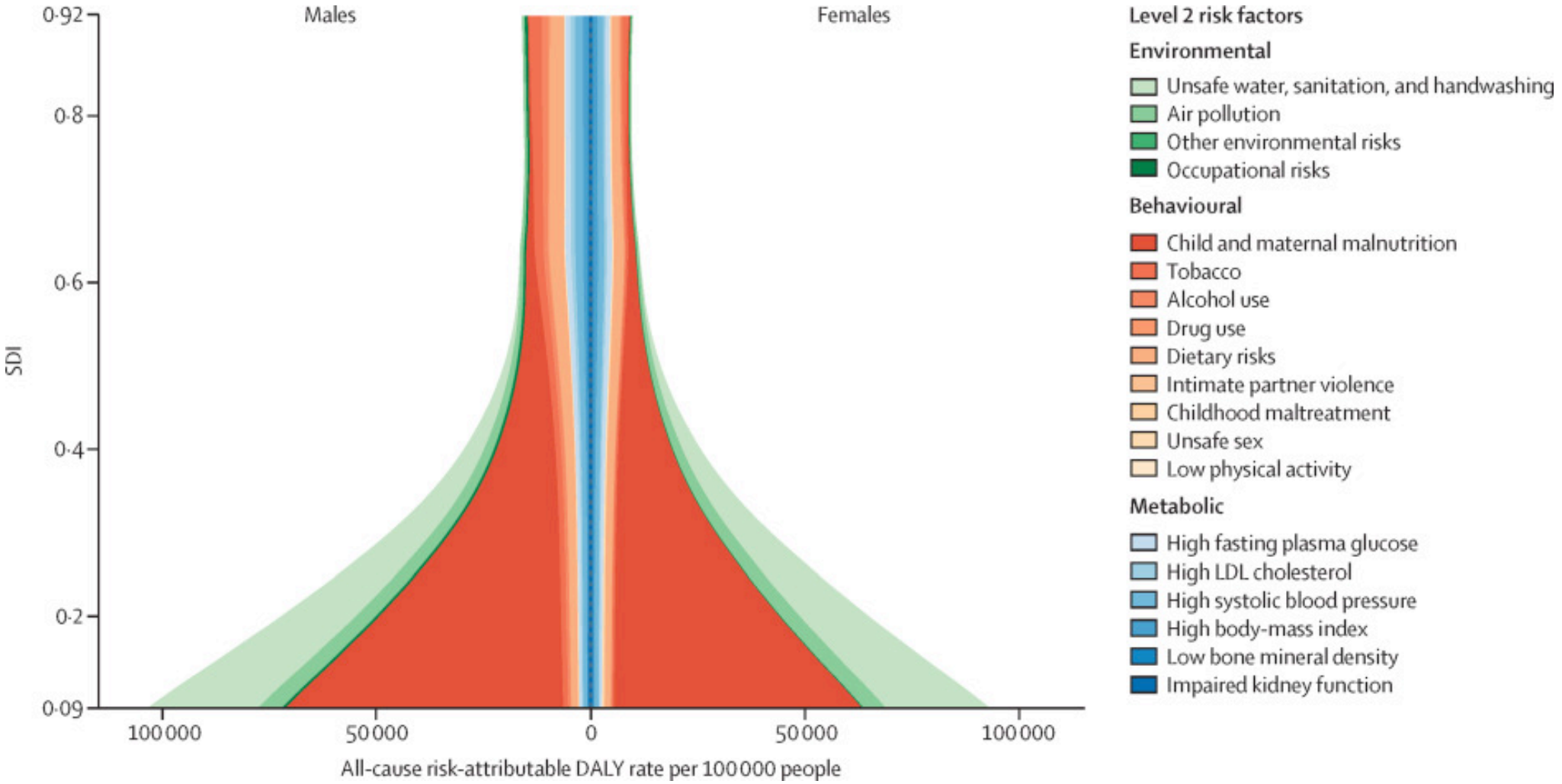

Expected relationship between all-age, all-cause risk-attributable DALY rates and SDI for each GBD Level 2 risk, 1990–2017

Stacked curves show males (left) and females (right) after adjusting for mediation, scaling to account for overlapping risks, and aggregating so that total expected DALY rates reflect the true all-cause total expected DALY rates attributable to all risk factors. The y-axis shows lowest SDI (0·09) to highest SDI (0·92) for all GBD countries and territories, 1990–2017. Coloured regions are the proportion of the total attributable DALY rate corresponding to that risk factor. DALYs=disability-adjusted life-years. GBD=Global Burden of Diseases, Injuries, and Risk Factors Study. LDL=low-density lipoprotein. SDI=Socio-demographic Index.

Added value of this study

GBD 2017 expands the scope of GBD 2016 with the estimation of one new risk factor—bullying victimisation—and 80 new risk–outcome pairs, with a total of 476 risk–outcome pairs. GBD 2017 incorporates 46 749 sources. We have expanded our estimation locations with the addition of subnational locations for Ethiopia, Iran, Norway, and Russia, and estimates for Māori and non-Māori populations in New Zealand. We implemented broad improvements to methods to better estimate risk factor exposures and relative risks. Notably, we have moved from total cholesterol to low-density lipoprotein cholesterol, implemented continuous measures of exposure for smoking, and updated the ambient particulate matter pollution model with new ground measurement data from almost 4000 sites. We expanded upon our decomposition analyses to investigate the drivers of risk-attributable burden and the changes in burden by country, and to decompose risk-attributable changes between broad categories of risks, thus providing deeper insight into changing patterns of risk-attributable burden and their underlying causes. We broadened our analyses of geographical and temporal trends in risk exposure and burden by estimating expected risk-weighted prevalence of exposures based on Socio-demographic Index. We explored the observed relationship between development status and risk exposure across all locations and years, and for the first time we described spatiotemporal patterns in the ratio of observed-to-expected levels of risk exposure.

Implications of all the available evidence

Decomposing trends by their underlying drivers reveals improvements in risk-deleted burden (ie, burden not attributed to risks in the GBD analysis), and broadly, improvements in exposure to environmental and behavioural risks. Conversely, increasing exposure to metabolic risks is driving increases in burden, indicating a crucial need for risk mitigation policies in this area. By quantifying the relationship between development and risk exposure, we highlight which risks appear sensitive to development and, of those, which are likely to improve or worsen with development. This analysis highlights areas where countries are either overperforming or underperforming relative to their economic peers and provides insight into areas where risk-modification strategies might be the best targets to improve health.

Population and fertility by age and sex for 195 countries and territories, 1950–2017: a systematic analysis for the Global Burden of Disease Study 2017

Population estimates underpin demographic and epidemiological research and are used to track progress on numerous international indicators of health and development. To date, internationally available estimates of population and fertility, although useful, have not been produced with transparent and replicable methods and do not use standardised estimates of mortality. We present single-calendar year and single-year of age estimates of fertility and population by sex with standardised and replicable methods. We estimated population in 195 locations by single year of age and single calendar year from 1950 to 2017 with standardised and replicable methods. We based the estimates on the demographic balancing equation, with inputs of fertility, mortality, population, and migration data. Fertility data came from 7817 location-years of vital registration data, 429 surveys reporting complete birth histories, and 977 surveys and censuses reporting summary birth histories. We estimated age-specific fertility rates (ASFRs; the annual number of livebirths to women of a specified age group per 1000 women in that age group) by use of spatiotemporal Gaussian process regression and used the ASFRs to estimate total fertility rates (TFRs; the average number of children a woman would bear if she survived through the end of the reproductive age span [age 10–54 years] and experienced at each age a particular set of ASFRs observed in the year of interest). Because of sparse data, fertility at ages 10–14 years and 50–54 years was estimated from data on fertility in women aged 15–19 years and 45–49 years, through use of linear regression. Age-specific mortality data came from the Global Burden of Diseases, Injuries, and Risk Factors Study (GBD) 2017 estimates. Data on population came from 1257 censuses and 761 population registry location-years and were adjusted for underenumeration and age misreporting with standard demographic methods. Migration was estimated with the GBD Bayesian demographic balancing model, after incorporating information about refugee migration into the model prior. Final population estimates used the cohort-component method of population projection, with inputs of fertility, mortality, and migration data. Population uncertainty was estimated by use of out-of-sample predictive validity testing. With these data, we estimated the trends in population by age and sex and in fertility by age between 1950 and 2017 in 195 countries and territories.

From 1950 to 2017, TFRs decreased by 49·4% (95% uncertainty interval [UI] 46·4–52·0). The TFR decreased from 4·7 livebirths (4·5–4·9) to 2·4 livebirths (2·2–2·5), and the ASFR of mothers aged 10–19 years decreased from 37 livebirths (34–40) to 22 livebirths (19–24) per 1000 women. Despite reductions in the TFR, the global population has been increasing by an average of 83·8 million people per year since 1985. The global population increased by 197·2% (193·3–200·8) since 1950, from 2·6 billion (2·5–2·6) to 7·6 billion (7·4–7·9) people in 2017; much of this increase was in the proportion of the global population in south Asia and sub-Saharan Africa. The global annual rate of population growth increased between 1950 and 1964, when it peaked at 2·0%; this rate then remained nearly constant until 1970 and then decreased to 1·1% in 2017. Population growth rates in the southeast Asia, east Asia, and Oceania GBD super-region decreased from 2·5% in 1963 to 0·7% in 2017, whereas in sub-Saharan Africa, population growth rates were almost at the highest reported levels ever in 2017, when they were at 2·7%. The global average age increased from 26·6 years in 1950 to 32·1 years in 2017, and the proportion of the population that is of working age (age 15–64 years) increased from 59·9% to 65·3%. At the national level, the TFR decreased in all countries and territories between 1950 and 2017; in 2017, TFRs ranged from a low of 1·0 livebirths (95% UI 0·9–1·2) in Cyprus to a high of 7·1 livebirths (6·8–7·4) in Niger. The TFR under age 25 years (TFU25; number of livebirths expected by age 25 years for a hypothetical woman who survived the age group and was exposed to current ASFRs) in 2017 ranged from 0·08 livebirths (0·07–0·09) in South Korea to 2·4 livebirths (2·2–2·6) in Niger, and the TFR over age 30 years (TFO30; number of livebirths expected for a hypothetical woman ageing from 30 to 54 years who survived the age group and was exposed to current ASFRs) ranged from a low of 0·3 livebirths (0·3–0·4) in Puerto Rico to a high of 3·1 livebirths (3·0–3·2) in Niger. TFO30 was higher than TFU25 in 145 countries and territories in 2017. 33 countries had a negative population growth rate from 2010 to 2017, most of which were located in central, eastern, and western Europe, whereas population growth rates of more than 2·0% were seen in 33 of 46 countries in sub-Saharan Africa. In 2017, less than 65% of the national population was of working age in 12 of 34 high-income countries, and less than 50% of the national population was of working age in Mali, Chad, and Niger.

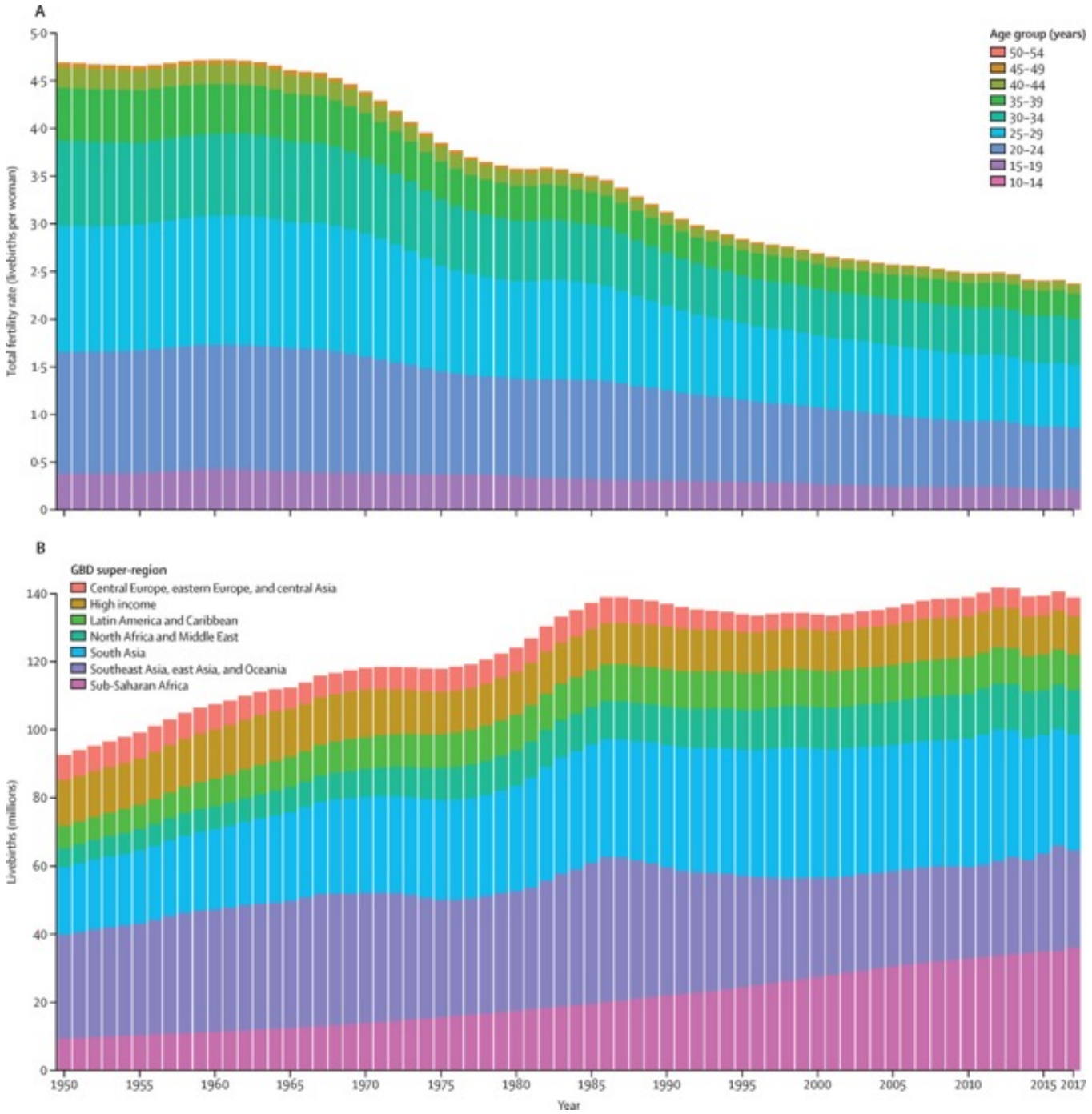

Global total fertility rate distributed by maternal age group (A) and number of livebirths by GBD super-region, for both sexes combined (B), 1950–2017

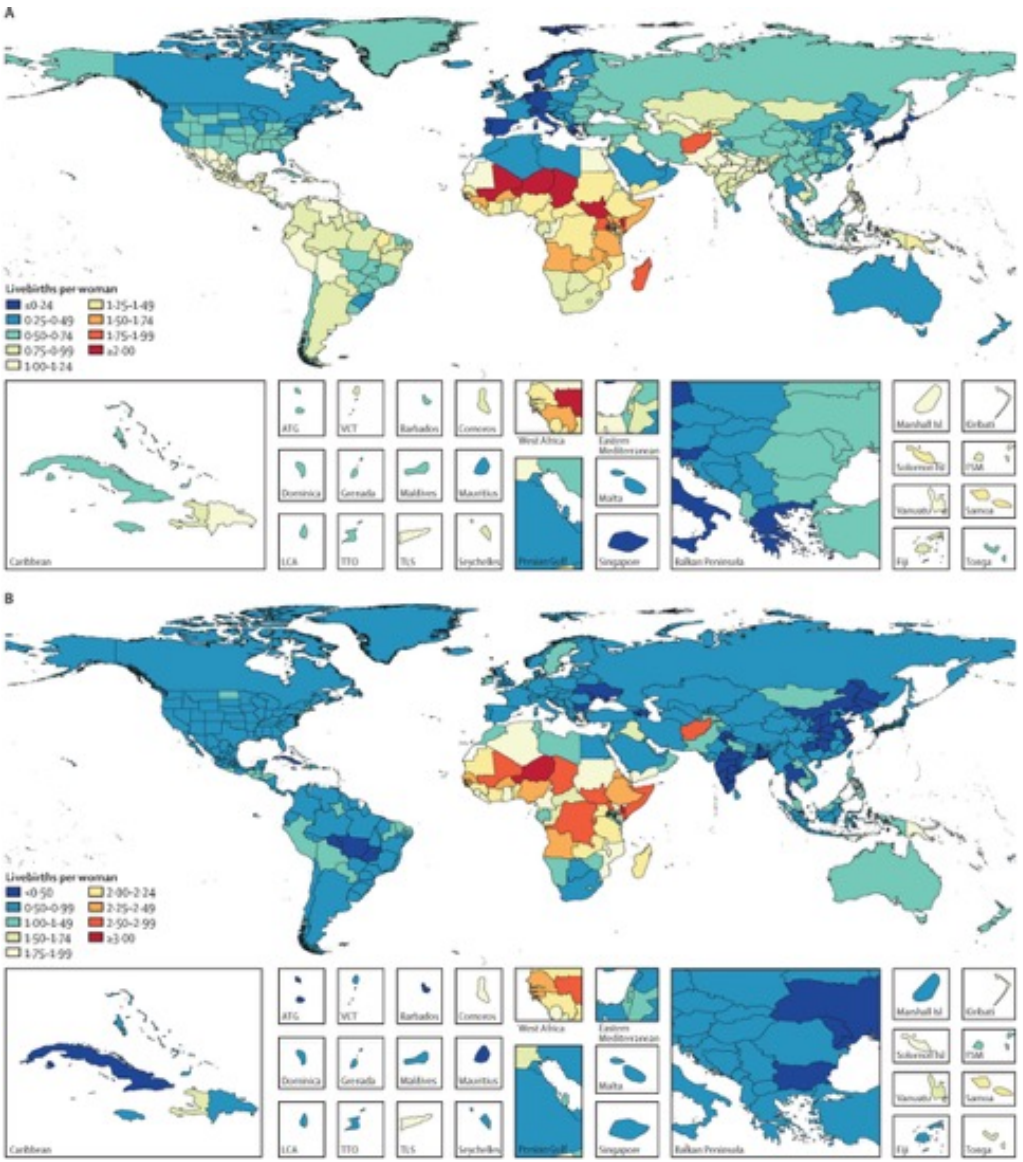

Total fertility rates under age 25 years (A) and total fertility rate over age 30 years (B), in 2017, by location. Data are the number of livebirths expected for a hypothetical woman by age 25 years (A) or ageing from 30 to 54 years (B) who survived the age group and was exposed to current ASFRs. ATG=Antigua and Barbuda. FSM=Federated States of Micronesia. Isl=Islands. LCA=Saint Lucia. TLS=Timor-Leste. TTO=Trinidad and Tobago. VCT=Saint Vincent and the Grenadines.

Percentage change in total fertility rates from 1975 to 2017 for women aged 30–54 years (A) and sex ratio at birth in 2017 (B), by location.

Data are the number of livebirths expected for a hypothetical woman ageing from 30 to 54 years who survived the age group and was exposed to current age-specific fertility rates (A) and the ratio of males to females at birth (B). ATG=Antigua and Barbuda. FSM=Federated States of Micronesia. Isl=Islands. LCA=Saint Lucia. TLS=Timor-Leste. TTO=Trinidad and Tobago. VCT=Saint Vincent and the Grenadines.

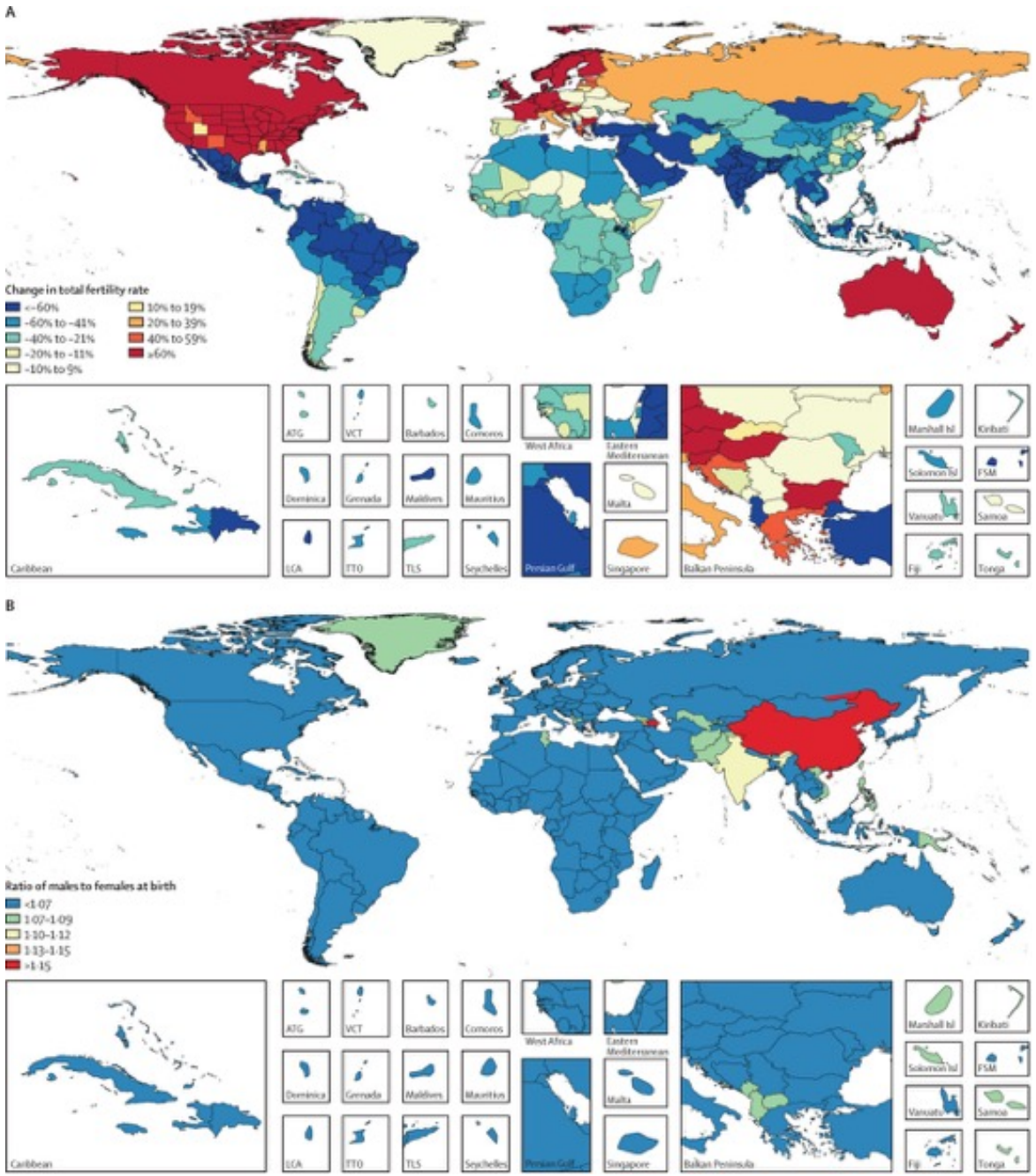

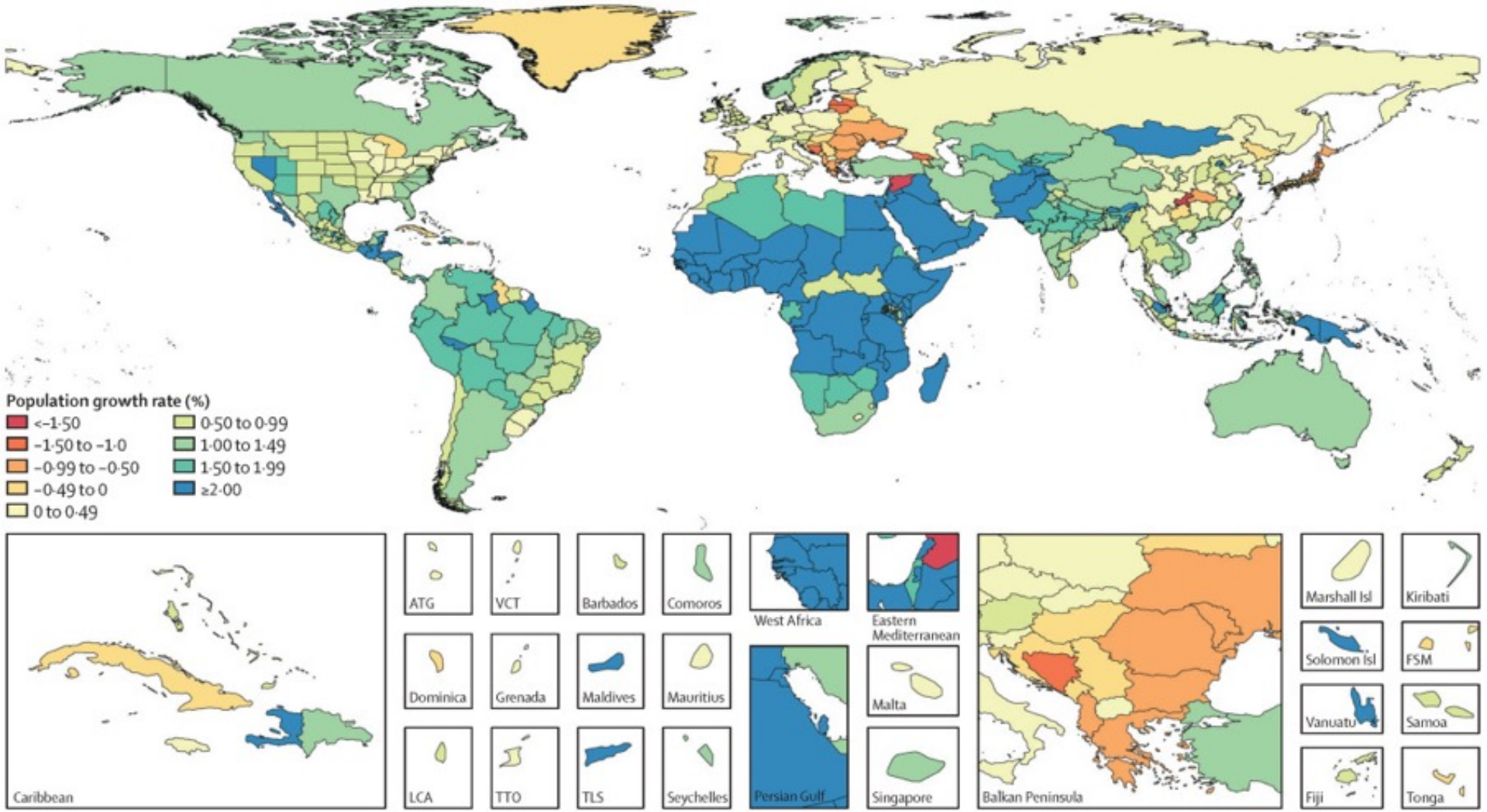

Population growth rate from 2010 to 2017, by location

ATG=Antigua and Barbuda. FSM=Federated States of Micronesia. Isl=Islands. LCA=Saint Lucia. TLS=Timor-Leste. TTO=Trinidad and Tobago. VCT=Saint Vincent and the Grenadines.

Conclusion

Population size and age structure have substantial consequences on every aspect of social and economic life in every location. Over the past 70 years, there have been huge changes in ASFR, mortality, and migration that have reshaped population structures. Trends have not been homogeneous across and within countries and, although global population growth rates have decreased, the absolute increase in global population every year has remained notably constant for many decades. Linear growth in the global population is occurring despite population decreases in some parts of the world, particularly eastern Europe, and large population increases in sub-Saharan Africa. Demographic changes will continue to have substantial social and economic effects, highlighting the importance of close monitoring and analysis of fertility and population at the local level. The statistical methods for estimation that we present will hopefully facilitate this need, providing the essential demographic intelligence for countries to reliably inform their health and social development strategies.

Added value of this study

To our knowledge, this study presents the first estimates of population by location from 1950 to 2017 that are based on transparent data and replicable analytical code, applying a standardised approach to the estimation of population for each single year of age for each calendar year from 1950 to 2017 for 195 countries and territories and for the globe. This study provides improved population estimates that are internally consistent with the Global Burden of Diseases, Injuries, and Risk Factors Study's assessment of fertility and mortality, which are important inputs to other epidemiological research and government planning.

Implications of all the available evidence

Population counts by age and sex that are produced with a transparent and empirical approach will be useful for epidemiological and demographic analyses. The production of annual estimates will also facilitate timely tracking of progress on global indicators, including the Sustainable Development Goals. In the future, the methods applied here can be used to enhance population estimation at the subnational level.

Linagliptin (BI-1356, Markenname: Trajenta®) ist ein Arzneistoff zur peroralen Behandlung von Typ 2-Diabetes. Im August 2011 erteilte die Europäische Kommission die Zulassung für das von dem pharmazeutischen Unternehmen Boehringer Ingelheim entwickelte Medikament. Linagliptin ist ein Wirkstoff aus der Gruppe der Dipeptidylpeptidase-4-Inhibitoren. Diese hemmen das EnzymDipeptidylpeptidase 4 (DPP-4). Linagliptin ist ein Inhibitor des Dipeptylpeptidase-Isoenzyms DPP-4, welches er kompetitiv und selektiv gegenüber anderen Isoenzymen, wie die Dipeptylpeptidasen DPP-8 und DPP-9, hemmt. Als Dipeptylpeptidase-4-Inhibitor hemmt es den Abbau des Inkretin-HormonsGlucagon-like-peptide 1 (GLP-1). Im Vergleich zu den 2008 bereits kommerziell genutzten Gliptinen Sitagliptin, Saxagliptin und Vildagliptin zeichn ete sich Linagliptin in Zellkulturen sowie in Tierversuchen an Ratten durch eine höhere Wirkpotenz und eine längere Wirkdauer aus.

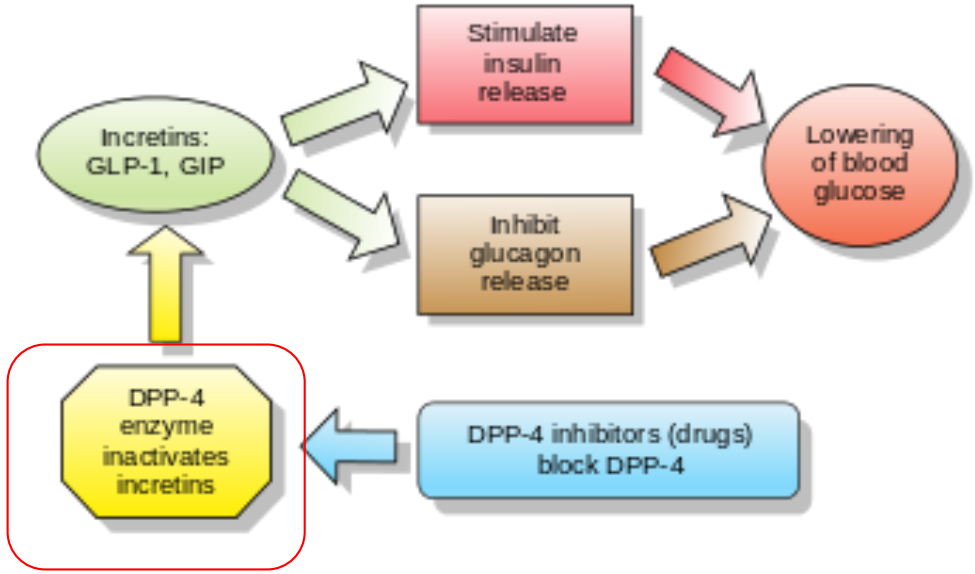

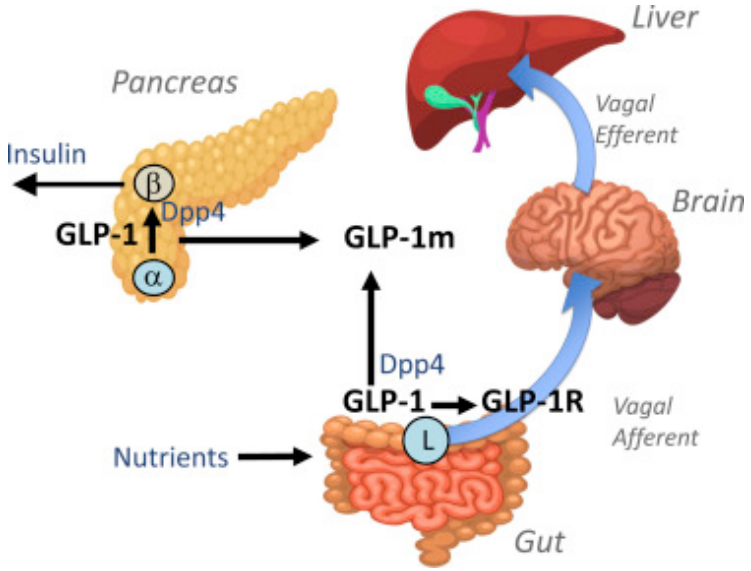

Effect of Linagliptin vs Placebo on Major Cardiovascular Events in Adults With Type 2 Diabetes and High Cardiovascular and Renal Risk

Type 2 diabetes is associated with increased cardiovascular (CV) risk. Prior trials have demonstrated CV safety of 3 dipeptidyl peptidase 4 (DPP-4) inhibitors but have included limited numbers of patients with high CV risk and chronic kidney disease. To evaluate the effect of linagliptin, a selective DPP-4 inhibitor, on CV outcomes and kidney outcomes in patients with type 2 diabetes at high risk of CV and kidney events. Randomized, placebo-controlled, multicenter noninferiority trial conducted from August 2013 to August 2016 at 605 clinic sites in 27 countries among adults with type 2 diabetes, hemoglobin A_{1c} of 6.5% to 10.0%, high CV risk (history of vascular disease and urine-albumin creatinine ratio [UACR] >200 mg/g), and high renal risk (reduced eGFR and micro- or macroalbuminuria). Participants with end-stage renal disease (ESRD) were excluded.

Characteristics	Linagliptin (n = 3494)	Placebo (n = 3485)
Age, y	66.1 (9.1)	65.6 (9.1)
Sex, No. (%)		
Male	2148 (61.5)	2242 (64.3)
Female	1346 (38.5)	1243 (35.7)
Race, No. (%)		
White	2827 (80.9)	2769 (79.5)
Asian	307 (8.8)	333 (9.6)
Black/African American	194 (5.6)	217 (6.2)
Smoking status, No. (%)		
Never smoker	1897 (54.3)	1856 (53.3)
Ex-smoker	1231 (35.2)	1276 (36.6)
Current smoker	362 (10.4)	350 (10.0)
Missing data	4 (0.1)	3 (0.1)
History of heart failure, No. (%)	952 (27.2)	921 (26.4)
Ischemic heart disease, No. (%)	2029 (58.1)	2052 (58.9)
History of hypertension, No. (%)	3171 (90.8)	3178 (91.2)
Atrial fibrillation, No. (%)	319 (9.1)	354 (10.2)
eGFR (MDRD), mL/min/1.73 m^2	54.7 (25.1)	54.5 (24.9)
Body mass index[d]	31.4 (5.3)	31.3 (5.4)
Hemoglobin A_{1c}, %	7.9 (1.0)	8.0 (1.0)
Fasting plasma glucose, mg/dL	151.2 (45.0)	151.2 (45.0)
Diabetes duration, y	15.0 (9.6)	14.5 (9.3)
Systolic blood pressure, mm Hg	140.4 (17.7)	140.6 (18.0)
Diastolic blood pressure, mm Hg	77.8 (10.5)	77.9 (10.4)
Heart rate, /min	69.8 (12.2)	69.8 (12.3)
Total cholesterol, mg/dL	173 (49)	171 (47)
Low-density lipoprotein cholesterol, mg/dL	92 (40)	91 (39)
High-density lipoprotein cholesterol, mg/dL	45 (13)	44 (13)
Triglycerides, mg/dL	190 (136)	187 (130)
≥1 Glucose-lowering medication, No. (%)	3378 (96.7)	3376 (96.9)
Metformin	1881 (53.8)	1927 (55.3)
Sulfonylurea	1102 (31.5)	1140 (32.7)
Insulin	2056 (58.8)	1995 (57.2)

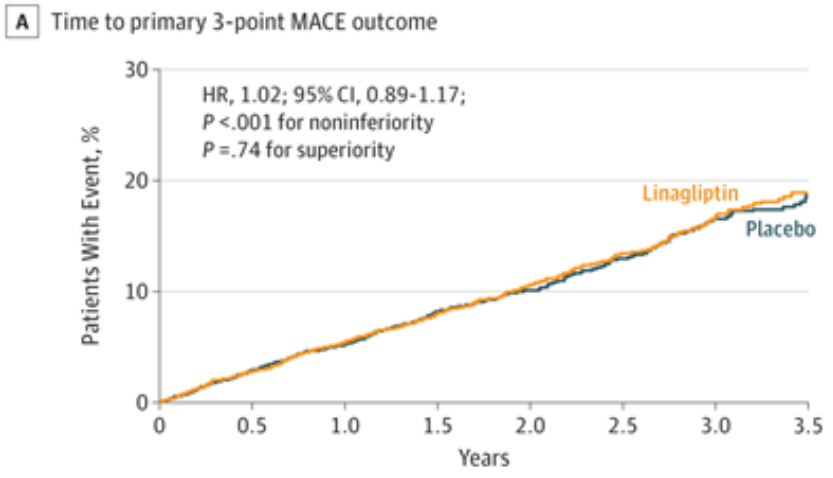
A Time to primary 3-point MACE outcome
HR, 1.02; 95% CI, 0.89-1.17;
P <.001 for noninferiority
P =.74 for superiority
Linagliptin
Placebo
Patients With Event, %
Years
No. of patients
Placebo 3485 3353 3243 2625 1931 1285 758 251
Linagliptin 3494 3373 3254 2634 1972 1306 778 269

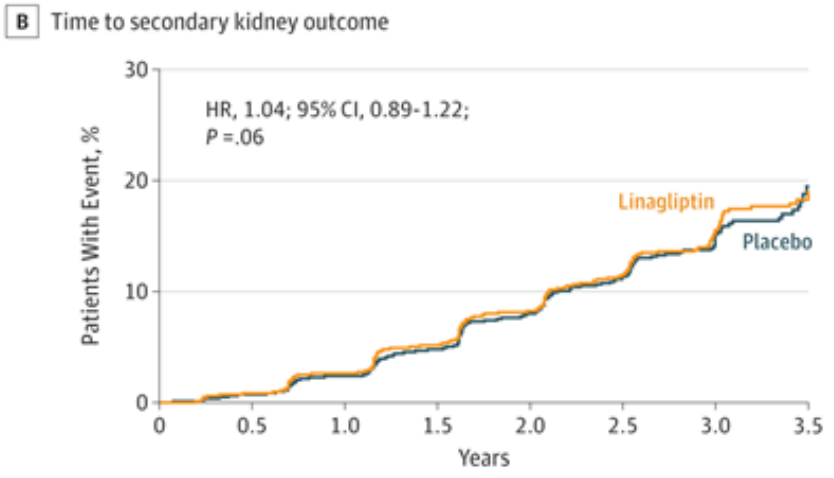
B Time to secondary kidney outcome
HR, 1.04; 95% CI, 0.89-1.22;
P =.06
Linagliptin
Placebo
Patients With Event, %
Years
No. of patients
Placebo 3485 3213 2995 2298 1608 1005 496 103
Linagliptin 3494 3227 3018 2345 1675 1040 518 109

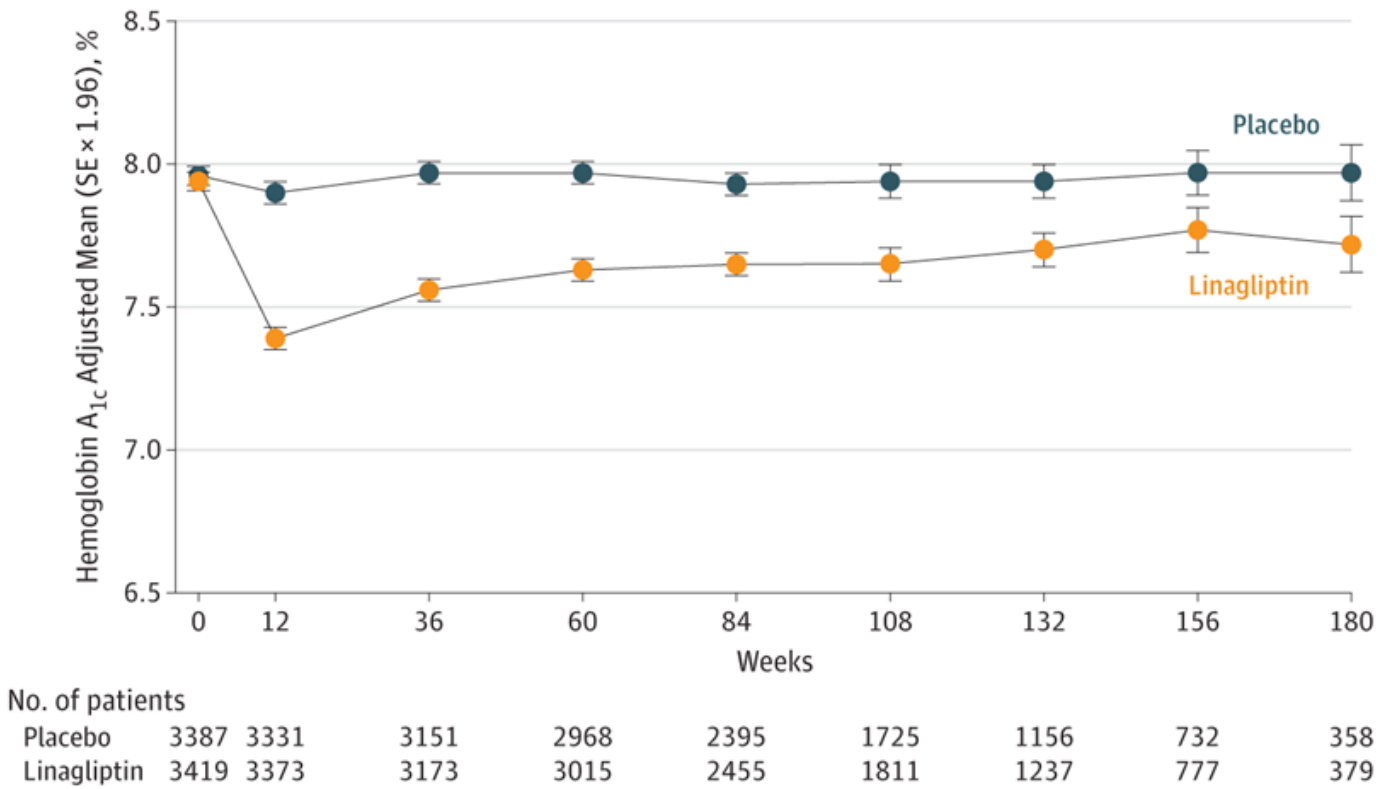
Placebo
Linagliptin
Hemoglobin A1c Adjusted Mean (SE × 1.96), %
Weeks
No. of patients
Placebo 3387 3331 3151 2968 2395 1725 1156 732 358
Linagliptin 3419 3373 3173 3015 2455 1811 1237 777 379

Discussion

In this large, multicenter, randomized clinical trial involving a population of patients with type 2 diabetes at high risk of CV events and with a high prevalence of kidney disease, linagliptin added to usual care was noninferior to placebo added to usual care for the primary outcome of 3-point MACE and did not demonstrate evidence of CV benefit. Similarly, there was no significant benefit of linagliptin compared with placebo for the incidence of the secondary kidney composite outcome. The MACE and composite kidney findings were consistent across all prespecified sensitivity analyses and most subgroups.

In this randomized noninferiority trial that included 6979 patients followed up for a median 2.2 years, use of linagliptin compared with usual care resulted in an incidence of the primary composite outcome (CV death, nonfatal myocardial infarction, or nonfatal stroke) of 12.4% vs 12.1%. The hazard ratio had a 1-sided 97.5% confidence limit of 1.17, which met the criterion for noninferiority (upper confidence limit <1.3).

Among adults with type 2 diabetes and high CV and renal risk, linagliptin added to usual care compared with placebo added to usual care resulted in a noninferior risk of a composite CV outcome over a median 2.2 years.

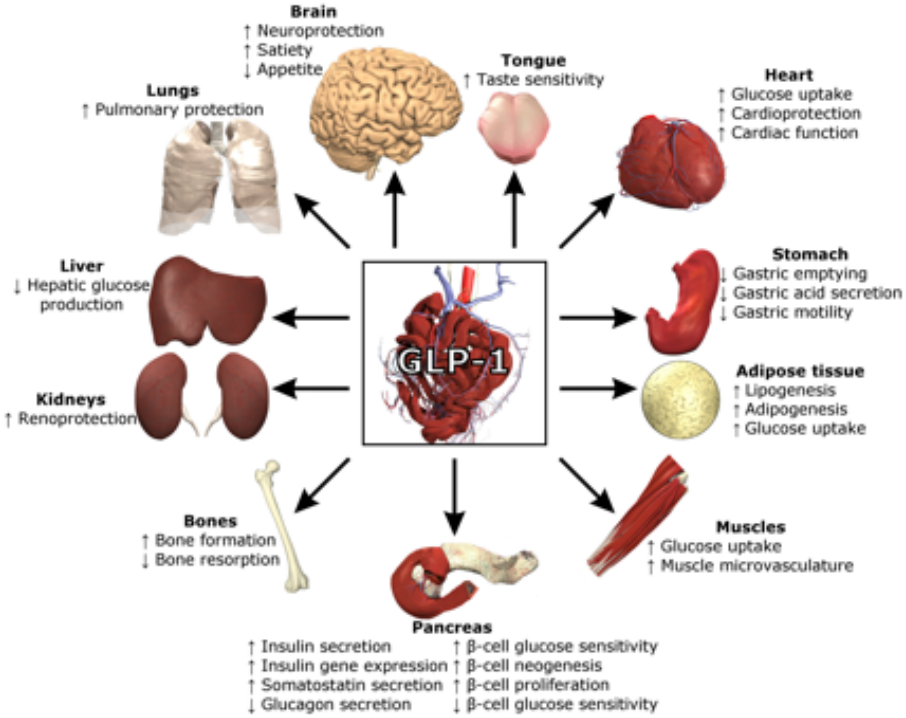

Question of the Week

What is the most appropriate next step for a patient with an extensive history of smoking; a spiculated, 2.5-cm, solitary pulmonary nodule detected by CT scan without evidence of metastatic disease on positron emission tomography and brain MRI; and no weight loss, dyspnea, or chest pain?

- Obtain sputum for acid-fast bacilli stain and culture
- Refer for transbronchial biopsy
- Obtain sputum for cytology
- Refer for surgical excision
- Refer for CT-guided transthoracic biopsy

Your answer is correct.

Obtain sputum for acid-fast bacilli stain and culture
Refer for transbronchial biopsy
Obtain sputum for cytology
Refer for surgical excision
Refer for CT-guided transthoracic biopsy

Key Learning Point View Case Presentation >

A patient with an extensive history of smoking and a 2.5-cm, malignant-appearing, solitary pulmonary nodule detected on CT without evidence of metastatic disease on positron emission tomography and brain MRI should be referred for surgical excision of the nodule, provided that the patient has no contraindication to surgery.

Detailed Feedback

In a patient with an extensive history of smoking, a pulmonary nodule detected on CT is likely to be malignant if it has a spiculated appearance and measures ≥2.3 cm in diameter. According to a risk calculator (http://www.brocku.ca/lung-cancer-risk-calculator), the probability of malignancy in this nodule is at least 70%. If the patient has no contraindication to surgery and there is no evidence of metastatic disease, the most appropriate next step is referral to a thoracic surgeon. Excision of the nodule would enable both treatment and diagnosis of the suspected malignancy.

CT-guided biopsy or transbronchial biopsy of the nodule could yield a diagnosis of cancer, but the nodule would still need to be excised after a positive biopsy. Moreover, when the pre-test probability of malignancy is high, a negative biopsy would not sufficiently rule out malignancy because of the possibility of sampling error, and excision of the nodule would still be recommended.

Incidental Pulmonary Nodules Detected on CT Images

Major recommendations and ratings

- Prior imaging studies should always be reviewed whenever available (grade 1A; strong recommendation; high-quality evidence)
- Solid nodules <6 mm do not require routine follow-up in low-risk patients (grade 1C; strong recommendation).
- For pure ground-glass nodules (GGNs) <6 mm, no routine follow-up is recommended (grade 1B; strong recommendation)
- Some solid nodules <6 mm with suspicious morphology, upper lobe location, or both may pose higher risk and warrant follow-up at 12 months (grade 2A; weak recommendation).
- For solitary solid noncalcified nodules measuring 6 to 8 mm in patients at high risk, an initial follow-up examination is recommended at 6 to 12 months and again at 18 to 24 months (grade 1B; strong recommendation; moderate-quality evidence)
- For solitary solid noncalcified nodules >8 mm in diameter, consider 3-month follow-up, workup with combined positron emission tomography (PET) and CT, tissue sampling, or a combination thereof (grade 1A; strong recommendation; high-quality evidence).

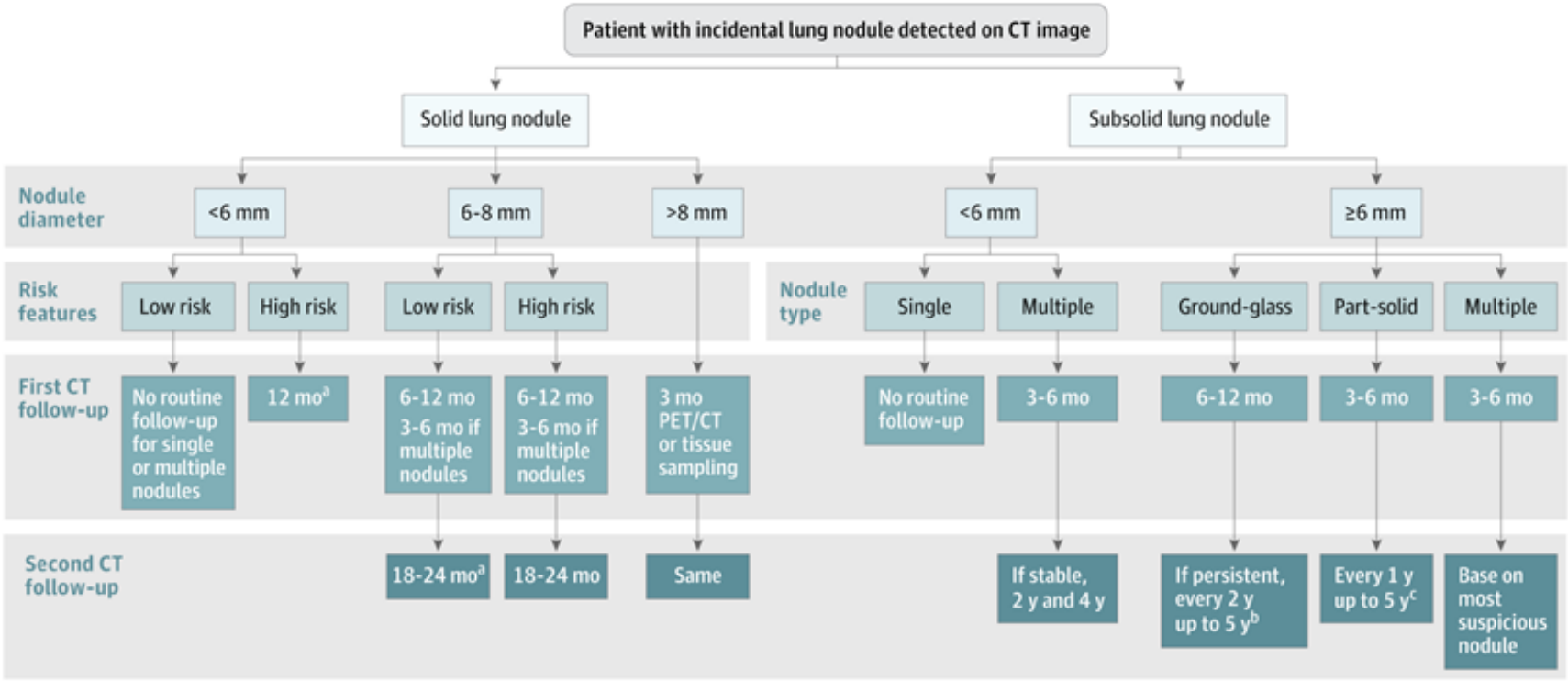

An incidental lung nodule on CT scan can create uncertainty for clinicians and anxiety for patients and families, given that lung cancer is the leading cause of cancer mortality in the United States. Incidental lung nodules are not uncommon. A systematic review of CT screening lung cancer trials noted that a lung nodule was detected in up to 51% of study participants. More than 95% of detected nodules are benign and have a wide variety of causes, including infections, granulomatous disease, hamartomas, arteriovenous malformations, round atelectasis, and lymph nodes. High-risk patient factors include older age and heavy smoking, while high-risk nodule features include larger nodule size, irregular or spiculated margins, and upper lobe location. Low-risk nodules are defined as having an estimated risk of cancer of less than 5% and are associated with young age and less smoking, along with smaller size, regular margins, and location in an area other than the upper lobe. Nodules at intermediate risk have mixed low- and high-risk characteristics, which may include other higher-risk factors such as emphysema and pulmonary fibrosis, positive family history, and known exposure to inhaled carcinogens. For the purposes of the Fleischner recommendation table, nodules with intermediate-risk estimations of 5% to 65% were combined with the high-risk category.

A 37-year-old female patient was referred to the rheumatology department at Treliske Hospital (Truro, UK) in April, 2015, following 8 months of rib pain, initially thought to be costochondritis. She had isolated hypophosphataemia (serum phosphate level 0·50 mmol/L) and a pelvic MRI identified stress fractures. 14 months after her presentation she had a persistently low serum phosphate concentration, with normal parathyroid hormone and serum calcium levels, and a 25(OH) vitamin D concentration of 32ng/mL. It was concluded that she had subclinical vitamin D deficiency, and she was prescribed cholecalciferol 20 000 units per week and Phosphate Sandoz (HK Pharma Ltd, Bedford UK), given as two tablets twice daily. In March, 2016, still symptomatic, she was referred to the UCL Centre for Nephrology (University College London, London, UK) to investigate a possible renal cause for her hypophosphataemia.

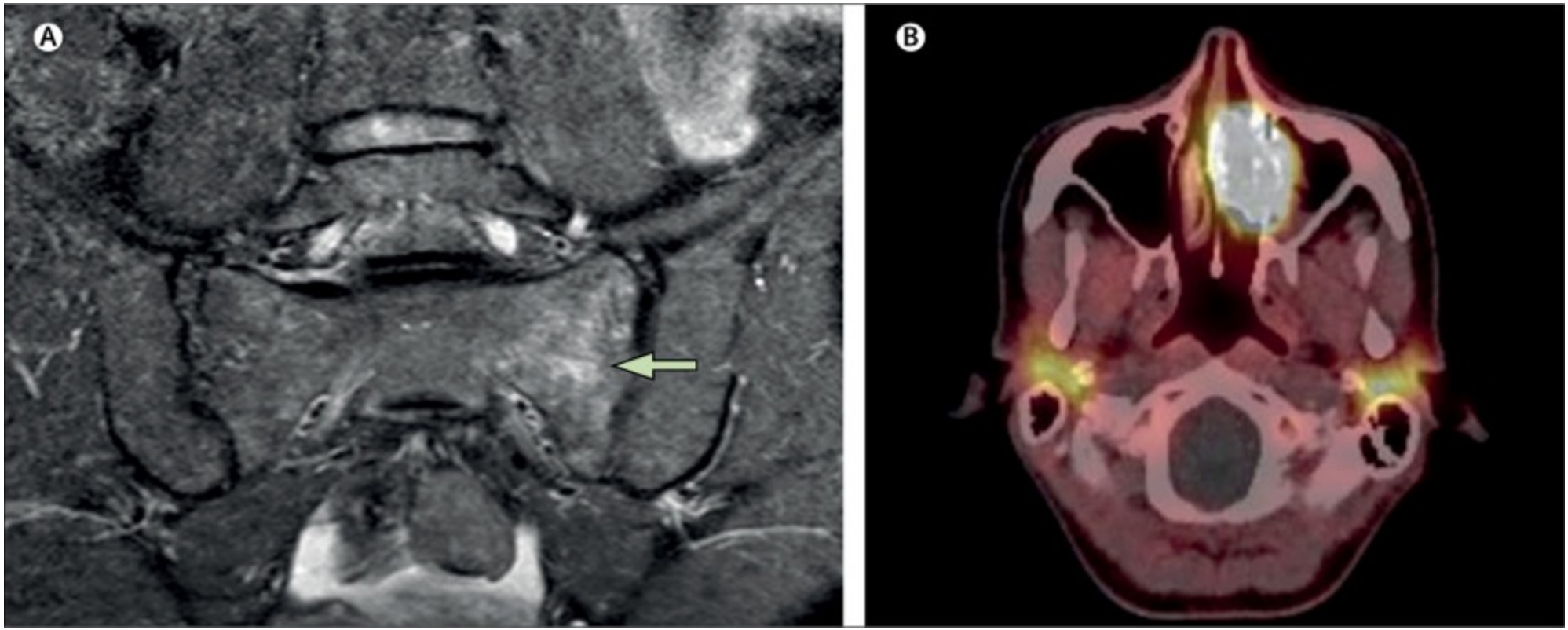

There, her calculated urinary fractional excretion of phosphate was raised at 42%, confirming hyperphosphaturia. Her sex and age weighed against X-linked, autosomal dominant, or recessive hypophosphatemic rickets; and normal excretion of low-molecular-weight protein, urate, and glucose ruled out the renal Fanconi syndrome. Her serum concentration of FGF23 was 180 relative units (RU) per mL (normal range is 0–150 RU/mL). Previous standard practice protocolled a first-line FDG PET/CT scan, which identified a nasal cavity mass that was avid on a subsequent ^{68}Ga DOTATATE PET/CT scan. The tumour was excised and pathology confirmed as sinonasal mucosa with evidence of phosphaturic mesenchymal tumour; her serum phosphate and FCF23 returned to normal following surgery. Oncogenic osteomalacia is a paraneoplastic syndrome usually associated with mesenchymal tumours, although somatic mutations in adenocarcinomas causing this syndrome have been reported. Phosphatonins (eg, FGF23) decrease renal resorption of phosphate, leading to hypophosphataemia, muscle weakness, and osteomalacia. Most such tumours are located in the bone and soft tissue, are solitary, and rarely cause local symptoms, often making the diagnosis long and difficult. Use of radiolabelled somatostatin analogues (such as octreotate, as in a ^{68}GA-DOTATATE scan) is the most sensitive and specific functional imaging. The only definitive management is removal of the phosphaturic mesenchymal tumour; recurrence is rare but has been described in some cases.